THE UNIVERSITY OF CHICAGO

MOLECULAR-LEVEL INTERROGATION AND VISUALIZATION OF HOW CHAPERONES DISPERSE HEAT-INDUCED PROTEIN CONDENSATES

A DISSERTATION SUBMITTED TO
THE FACULTY OF THE DIVISION OF THE BIOLOGICAL SCIENCES
AND THE PRITZKER SCHOOL OF MEDICINE
IN CANDIDACY FOR THE DEGREE OF
DOCTOR OF PHILOSOPHY

INTERDISCIPLINARY SCIENTIST TRAINING PROGRAM:
BIOPHYSICAL SCIENCES

BY

KYLE MATTHEW LIN

CHICAGO, ILLINOIS
AUGUST 2025

Copyright 2025 by Kyle Lin

Abstract

When a cell experiences environmental change, such as heat shock, its molecular landscape transforms. Many proteins reassemble into larger bodies called condensates. Also, specific classes of proteins, called heat shock proteins or molecular chaperones, are produced. An important role of chaperones is to disperse protein condensates as cells adapt to environmental change. However, much remains unknown about condensates themselves, how their dispersal happens, and why only specific types of chaperones support dispersal. In this thesis, I address two main questions: what do condensates and their dispersal look like at the molecular scale; and why do two similar chaperones, Sis1 and Ydj1, have opposing effects on dispersal?

To answer the first question, we used single-molecule microscopy to track individual, dye-labeled poly(A)-binding protein (Pab1) condensates formed during physiological heat shock. We find that condensates are heterogeneous but small entities, which typically contain ~100's of proteins. We observe that condensate dispersal by chaperones is heterogeneous and often incomplete, and we see unexpected effects upon absence of ATP and addition of the chaperone Sse1. These results are among the first direct visualizations of chaperone-mediated condensate dispersal and help build a more complete picture of this molecular process.

To answer the second question, we use biochemical and single-molecule approaches to interrogate Sis1 and Ydj1's divergent behaviors. While Sis1 is essential to dispersal, Ydj1 fails at and even impedes dispersal—yet both chaperones are J-domain proteins that fulfill similar functions: substrate binding, substrate handoff to the chaperone Hsp70, and stimulation of Hsp70 ATP hydrolysis. We observe that both Sis1 and Ydj1 bind condensates, suggesting that the difference lies in coordination with Hsp70. Unexpectedly, mutation of Hsp70's EEVD tail, which should disrupt interaction with Sis1, does not completely prevent dispersal. We further investigate

Sis1 dimerization and Hsp70 ATP hydrolysis as contributors to Sis1 function. These and other results guide us to a more nuanced understanding of how Sis1, Ydj1, and J-domain proteins work in the condensate dispersal context.

Other projects I have pursued include investigating human chaperones and human cell responses to fever temperature; visualizing differences in the condensation of Pab1 from yeast species adapted to different thermal environments; and helping develop a new technology which could advance future single-molecule studies of chaperones and condensates. Together, this thesis provides new insight into the molecular events that transpire when cells respond to heat shock and environmental change and offers promising opportunities for future research.

Contents

List of Figures ..... **vii**

List of Tables ..... **ix**

Acknowledgments ..... **x**

1 | Introduction **1**

1.1 Cells and Their Thermal Environment 1

Why Heat (Shock) Matters: Fever as a Case Study 1

1.2 Molecular-Scale Responses to Heat Shock 3

Biomolecular Condensates (Not Misfolded Aggregates) 3

Molecular Chaperones, Aggregates, and Condensates 4

2 | Visualizing Individual Condensates and their Dispersal **6**

2.1 Introduction 6

Protein Labeling Strategy 7

Design of a Single-Molecule Imaging Setup 8

2.2 Methods 13

Purification of Pab1 13

Purification of Chaperones 15

Measuring Protein Concentration (Bradford) 17

Preparation of Dye Stocks 18

Preparation of Labeled Pab1 18

Degree of Labeling 19
Preparation of Pab1 Condensates 21
Condensate Dispersal: Fluorescence Anisotropy 22
Condensate Dispersal: TSP Assay 23
Passivation of Coverslips with PEG 24
Microscopy 26
Timelapse Microscopy 27
Single-Molecule Data Analysis: Background Subtraction 28
Single-Molecule Data Analysis: Object Identification and Trace Calculation 29
2.3 Results 35
Pab1 is Predominantly Monomeric Prior to Heat Shock 35
Pab1 Condensates are Small and Heterogeneous 36
Highly Labeled Pab1 Condensates Contain ~100's of Molecules 38
Microscopically Observed Pab1 Condensates are Rapidly Dismantled 41
Dispersal is Heterogeneous and Partially ATP-Independent 43
Dispersal of Larger Condensates Is Not Favored, Even with Sse1 45
2.4 Discussion 46
3 | JDPs 59
3.1 Introduction 59
3.2 Methods 63
Plasmids 63
Protein Purification 64

Optimized Preparation of Fluorescently Labeled Proteins 65
Fluorescence Anisotropy-Based Binding Assay 67
Luciferase Reactivation 68
ADP Formation Assay (Ssa2 ATPase Activity) 69
Colocalization Microscopy 69
3.3 Results 70
Functional Expression of Sis1, Ydj1, and Chaperones 70
Functional Expression of Labelable Chaperone Mutants 71
Binding of Pab1 Condensates by Sis1 and Ydj1 72
Interrogation of Molecular Basis of Ydj1 Inhibition 74
Relationship of Hsp70 EEVD to Sis1 Function 76
Dimerization, ATP Hydrolysis, and Sis1 Function 77
3.4 Discussion 80
4 | Beyond Condensate Dispersal 88
4.1 Novel Technology for Multiplexed Biomolecule Detection 88
4.2 Visualizing Differential Condensation of Pab1 from Different Organisms 92
4.3 Human Chaperones and Human Cell Responses to Fever 95
4.4 Conclusion 100
References 101

List of Figures

Figure 2.1, Single-molecule microscope design. 11

Figure 2.2, Schematic of imaging modalities. 12

Figure 2.3, Background subtraction method. 33

Figure 2.4, Example of single-molecule analysis pipeline in use. 34

Figure 2.5, Single-molecule imaging of Pab1 monomers. 49

Figure 2.6, Dispersal of wildtype and labeled condensates. 50

Figure 2.7, Single-molecule imaging of Pab1 condensates. 51

Figure 2.8, Biochemical validation of 100% Pab1 mutant condensates. 52

Figure 2.9, Imaging of highly-labeled condensates. 53

Figure 2.10, Bulk imaging of labeled condensate dispersal at 20 minutes. .54

Figure 2.11, Analysis of single-condensate dispersal traces. 55

Figure 2.12, Size distributions of condensates over time. 56

Figure 2.13, Dispersal outcomes at the single condensate level. 57

Figure 2.14, Relationships between dispersal outcomes and sizes. 58

Figure 3.1, Sis1 and Ydj1 domain architecture and basic functions. 62

Figure 3.2, Functional activities of Sis1 and Ydj1. 82

Figure 3.3, Activities of wildtype and mutant chaperones. 83

Figure 3.4, Binding of Sis1 and Ydj1 to Pab1 condensates. 84

Figure 3.5, Interrogation of Ydj1 inhibition. 85

Figure 3.6, Effect of Hsp70 C-terminus perturbation on dispersal. 86

Figure 3.7, Interrogation of Sis1 function in dispersal. 87

Figure 4.1, Molecular targets for FRETfluor labeling. 91

Figure 4.2, Imaging condensation of Pab1 from different species. 94

Figure 4.3, Human chaperones and cellular responses to heat shock. 98

Figure 4.4, Transcriptional responses of human cells to fever. 99

List of Tables

Table 2.1, Filters and Dichroics. 10

Table 2.2, Default Camera Settings. 27

Table 2.3, Analysis Pipeline Parameters. 32

Table 2.4, Size Estimates of a Typical Pab1 Condensate. 41

Table 3.1, Plasmids. 63

Acknowledgments

I am so grateful to all the individuals who have supported and collaborated with me directly and indirectly in my thesis work; who have trained, taught, mentored, and inspired me over the years; and who have made me who I am today through their presence and influence in my life.

In particular, I want to thank all the members of both of my labs over my five PhD years, including: Diangen (Dana) Lin, Kavya Vaidya, Maya Igarashi**,** Trevor Anderberg**,** Andrés Cook**,** Kepler Domurat-Sousa**,** Sarah Christensen, Ayesha Ejaz, Jiachong Chu, Aria Coraor, Maya McDaniel, Madeline (Maddie) Joseph, Olivia Schaffer, João Shida, George Turner, Roy Hays, Natalie Tsang, Mallie Fitzgerald, Estefania (Stef) Cuevas-Zepeda, Caitlin Wong Hickernell, Leah Chaney Winner, Alyssa Guzman Considine, Karen Velez, Josh Melamed, Dana Christopher, Jeffery Zhang, Madison Nelson, Hendrik Glauninger, Samantha (Sammy) Keyport Kik, Jared Bard, Haneul Yoo, Catherine (Cat) Triandafillou, and Rosalind Pan. You have been incredible colleagues, friends, mentors, and peers. I also want to emphasize the scientific contributions of several individuals: Dana Lin, my primary collaborator in Chapter 2; Stef Cuevas-Zepeda, my primary collaborator in Chapter 3; Haneul Yoo, whose prior work was the scientific foundation for my thesis; and Kavya Vaidya, who is launching new investigations into the condensate-chaperone system described in my thesis. I have been very lucky to work with two exceptionally talented undergraduates, Dana Lin and Josh Melamed. Their undergraduate research inspires me, and I am excited to discover the amazing things they will do in their future careers.

I would like to thank so many people in the larger BMB, PME, MSTP, Pritzker School of Medicine, and Biophysics communities. You make everything that students like me do possible, and you have made my time as a graduate student a truly special experience.

I am especially grateful to my primary research mentors over the years, not only for training and teaching me, but for investing in me as a person and giving me the opportunity to learn, grow, and experience the wonders of science. Each of you—Thomas (Tom) Kleist, Wolf Frommer, Liang Feng, Allan Drummond, and Allison Squires—inspire me, show me what it means to be a scientist and a scientific leader, and have made me the thinker and person I am today.

I want to thank Arianna Stancari for being an incredible partner, for supporting me through the most fun and most challenging times, and for making graduate school a better and more special place. You inspire me as a scientist, musician, partner, and all-around amazing person.

Finally, I want to thank my family for everything, from my earliest years until today. You have given me so much and continue to support and inspire me in so many ways, and I could not have done any of this without you.

1 | Introduction

1.1 Cells and Their Thermal Environment

All life exists in the context of an environmental temperature, and environments change. Animal life is intricately regulated by thermal signals, which can determine seasonal migrations,[1,2] circadian rhythms,[3–5] food seeking,[6,7] sex determination,[8,9] and homeostasis and growth.[10–13] Even within the human or animal body, temperature is strictly regulated, and deviations from the normal often signal disease, illness, or a physiological crisis. Despite the importance of temperature as a biological signal, fundamental questions remain unanswered at the cellular level. How do cells sense and transduce temperature, and to what end? What happens to molecules in cells when the temperature changes, and why? Which molecular-scale responses are helpful or harmful to the cell—and how does the biological context accompanying a temperature change matter?

Why Heat (Shock) Matters: Fever as a Case Study

Cellular- and molecular-scale questions about temperature have been posed at least since the 1960's discovery of the transcriptional heat shock response—that is, the ability of cells to alter their genetic programs in the face of elevated temperature.[14,15] Vast amounts of research and entire new fields of inquiry have arisen in the ensuing decades, in order to understand the relationship between cell biology and temperature. Why does understanding this relationship matter?

Biology itself tells us that temperature is important, even subtle changes of a few degrees Celsius. An illustrative example from the field of medicine is **fever**. The ability of our bodies to raise their temperature during infection and injury has been known (and treated) for thousands of years. The metabolic cost of maintaining a fever is not trivial. For an endotherm such as a human, a fever of 2–3 °C can result in 20% higher bodily energy consumption.[16] Yet organisms across the

animal kingdom routinely pay the metabolic price to increase their temperature during illness—not only endotherms such as mammals and birds,[17–19] but also ectotherms ranging from lizards, scorpions, amphibians, and fish which relocate themselves to warmer environments to achieve "behavioral fever".[18–31] Evolution shows that life cares about being at the right temperature, at the right time.

The importance of fever is clear, both medically and evolutionarily. Yet what fever means to cells biophysically and physiologically, and in what circumstances a host benefits from fever, remain surprisingly murky. One likely function of fever is "thermal restriction", the role of high temperature as a direct defense against pathogens to restrict or prevent their growth.[32] Yet many pathogens such as malaria are resistant to fever temperature and have even evolved their molecular and genetic makeup around fever.[33–35] In these cases, does fever carry a benefit? In fact, animals infected with pathogens derive a striking survival benefit from mounting a febrile response, even when the pathogen grows well at the host's fever temperature.[21,36,37] These studies, as well as more recent cellular immunological studies, show that fever leads to survival benefits which are host-intrinsic and likely involve regulation of the body's own immune cells.[38] Recent studies have unveiled some of the molecular-level responses and actors in immune cells during fever;[39–41] but fundamentally, much remains unknown about how immune cells sense and interpret fever at the molecular and biophysical level.

Thus, elucidating how cells—for instance, host immune cells and pathogens—respond to a physiological increase in temperature has the potential to change our interpretation of even basic, ancient responses of hosts to infection such as fever.

Fever, however, is just one example of physiologically-important heat (shock). Organisms across the tree of life have their own physiologically meaningful heat shocks and environmental

stimuli to which they must respond and adapt. Yet diverse organisms respond in similar ways to sudden elevated temperature. Understanding the intersection of two of these responses is the focus of this thesis.

1.2 Molecular-Scale Responses to Heat Shock

When cells across life encounter a heat shock, two striking events occur. Proteins and RNA molecules reorganize into **biomolecular condensates**, and cells upregulate expression of a subset of proteins called heat shock proteins, or **molecular chaperones**. Why do cells make condensates, and why do cells make chaperones? The answers to these questions have evolved over decades of research and continue to change.

Biomolecular Condensates (Not Misfolded Aggregates)

Biomolecular condensates are non-stoichiometric assemblies of proteins and RNA. There are many types and classifications, some of which (such as the nucleolus) are constitutively present in cells during normal growth, while others form during heat shock and other forms of cellular stress.[42] Stress granules, for example, are microscopically visible accumulations of mRNAs and proteins, such as poly(A)-binding protein and other RNA-binding proteins, which form during heat shock, oxidative stress, nutrient deprivation, and other physiochemical stresses.[43,44]

Why do proteins accumulate in this way in response to heat shock and other stresses? An early interpretation of this phenomenon was that proteins denature when exposed to heat or other changes in their chemical environment, and denatured proteins tend to aggregate. Thus, protein accumulation was thought to be **misfolded protein aggregation**, a proteotoxic crisis for the cell to prevent if possible or else mitigate once it occurs.

This model has since been replaced with a new framework, that of **adaptive condensation**. Some of the key predictions that follow from the misfolded aggregation model include: aggregates

are harmful to the cell, aggregates form by nonspecific denaturation of proteins, and the goal of cells is to clear (or even destroy) aggregates. However, when actual proteins that condense in cells (such as Pab1) have been carefully studied, these predictions have been found not to be the case. With Pab1, condensates are shown to be adaptive not harmful to the cell; condensation occurs via specific, sequential activation of folded domains; and condensates are restored and resolubilized rather than degraded.[45–47] Before these advances in our understanding were made, however, much research had been done on what machinery cells have to clear misfolded aggregates, and how this machinery works. We learned that molecular chaperones, the very proteins cells upregulate during stress, are powerful tools at the cell's disposal to prevent and clear aggregation.[48–50]

Molecular Chaperones, Aggregates, and Condensates

Molecular chaperones, or heat shock proteins, are a set of proteins whose functions involve regulating the state of other proteins: that is, ***chaperoning*** them to fold, refold, assemble, or disassemble properly. Certain isoforms of these proteins are expressed basally to perform functions in protein folding, translocation, endocytosis, and other cellular functions; however, during heat shock or other stresses, their expression is upregulated manyfold, often through inducible isoforms.

Several classes of chaperone have been observed to be necessary for clearance of stress granules *in vivo*: Hsp70, J-domain proteins (JDPs), and Hsp104.[43,51] Moreover, these three classes of protein were shown early on to possess the ability to resolubilize misfolded protein aggregates.[52] Since that early discovery, we have learned a great deal about the action of these chaperone classes, along with a fourth family (the Hsp70 nucleotide exchange factors, sometimes termed Hsp110 or more broadly NEFs), in disaggregation.[48–50,53–55] However, one aspect remained puzzling: the fact that chaperones were strikingly inefficient at what was supposed to be their physiological function. To resolubilize and refold a model misfolded protein such as firefly luciferase (chosen not for its

biological relevance but for its relatively simple activity assay), considerable excess of chaperones were required just to achieve partial disaggregation on an hours timescale.[56]

This mystery was resolved by recent work by Dr. Haneul Yoo and colleagues, who bridged the known dispersal activity of chaperones with the new insight that physiological condensates are distinct entities from misfolded aggregates.[56] When misfolded aggregates were replaced with Pab1 condensates formed under physiological heat shock *in vitro* as the substrate, the dispersal process was strikingly different. Chaperones were effective at dispersing physiological condensates on a minutes timescale, with far lower concentrations of chaperones in the physiological range, and did so completely. Moreover, drastic differences in the way chaperones disperse condensates versus misfolded aggregates began to emerge. Whereas two types of JDP, Sis1 and Ydj1, were known to be synergistic in aggregate dispersal and to be interchangeable in protein refolding contexts, with Ydj1 outperforming Sis1, the opposite was shown with Pab1 condensate dispersal.[53,54,56] Only Sis1 could function in condensate dispersal, while Ydj1 was not only nonfunctional but inhibitory.

From this work, a major theme became clear. Studying the real, endogenous substrates of chaperones formed during physiological heat shock (i.e., condensates) would yield novel, more physiologically relevant insight into the action of chaperones as disaggregases, which could in fact contradict existing models of chaperone function. Moreover, there is much we do not understand about the interaction of chaperones and condensates as molecular actors. My thesis is situated at this intersection and seeks to fill two major gaps in our understanding: what do physiological condensates and their dispersal look like, by direct visualization; and what is the molecular basis for the divergent behaviors of Sis1 and Ydj1? The following two chapters address these two questions and my research contributions to answer them. In the final chapter, I revisit fever and other broader questions in the realm of temperature, chaperones, and condensates.

2 | Visualizing Individual Condensates and their Dispersal

2.1 Introduction

Until now, we have lacked direct visualization of the Pab1 condensate dispersal process, nor have we had a firm grasp of how large these molecular entities are (in terms of molecular number), both initially and over the course of their disassembly. The primary assay used to assess Pab1 dispersal in previous work relied on a Pab1 monomer functional readout, i.e., RNA binding, which reports on the production of free Pab1, not on the nature of the condensates themselves.[56] As far as condensate size, techniques such as Dynamic Light Scattering (DLS) and sedimentation by centrifugation have provided important but limited quantitative insights.[45] DLS is biased toward the largest particles in a heterogeneous, polydisperse mixture, and sedimentation provides only a binary readout of how much protein has exceeded a particular size threshold (i.e., proportion in pellet or supernatant). Thus, we have lacked an exact quantitative description of how big Pab1 condensates really are—how many Pab1 molecules are in a typical condensate formed during physiological heat shock, how heterogeneous condensate size can be, and how condensate sizes dynamically change during dispersal.

Being able to observe condensates directly, particularly those formed under physiological heat shock conditions and amenable to chaperone-mediated dispersal, could provide novel insight into how chaperone-mediated dispersal works and an opportunity to directly test existing models. From previous research, our strong hypothesis is that chaperones, specifically Hsp70, must cluster in close proximity on a condensate to engage the disaggregase Hsp104 and achieve rapid dispersal. Additionally, one of the crucial chaperones for dispersal, Sis1, belongs to a family of chaperones

(the Class B J-domain proteins) thought to interact preferentially with larger substrates (> MDa).[57] Thus, we might expect that a minimum size, and perhaps a minimum surface area, of condensate may be required for efficient dispersal, and that therefore larger condensates disperse more readily, if not exclusively. On the other hand, the dispersal of smaller condensates might be favored, if chaperones primarily bind to the surface of Pab1 condensates, leading to a surface area-limited process. Whether any relationship between condensate size and dispersal outcomes exists has not been easily testable with existing methods.

Single-molecule microscopy offers an avenue for answering such questions directly. By quantifying the brightness of a single Pab1 protein molecule and comparing this signal to that of condensates, one condensate at a time, we can construct a distribution of particle sizes. By tracking the brightness over time of many condensates imaged under the same biochemical conditions, we can directly visualize dispersal dynamics, including whether larger condensates are dispersed more or less readily, and whether any heterogeneities in dispersal between condensates exist.

In order for this approach to be feasible and successful, we required two key elements: (1) a way to render single condensates imageable, and (2) a suitable single-molecule imaging platform. The creation and reasoning behind of both elements are described in the next two subsections.

Protein Labeling Strategy

To measure the number of Pab1 molecules in a condensate, we needed to attach a visible label to Pab1 molecules with a known label-to-protein stoichiometry, such that we could extrapolate Pab1 composition from the amount of label present. There are two common methods for attaching a fluorescent label to proteins: genetic fusion of a label or labeling element, or chemical reaction with a small molecule label. Expression of a fluorescent protein (FP) genetic fusion (for example, Pab1-Clover) has the advantage of exact 1:1 stoichiometry of FP to target

protein, as the label is expressed as part of the same polypeptide chain. However, there are two main disadvantages: (1) many FPs do not have optimal photophysical properties for prolonged and accurate single-molecule imaging (for example, Clover photobleaches rapidly), and (2) the size of many FPs can be large relative to the target protein itself (Clover is nearly half the molecular weight of Pab1). Self-labeling enzymatic technologies, such as SNAP-tag and HaloTag, circumvent the first issue by allowing incorporation of several small molecules as the fluorophore, but these tags are still generally of comparable size to FPs.[58,59]

Instead, we opted for a small molecule chemical labeling approach. The thiol-maleimide chemical reaction is a well-established method for attaching small molecule dyes to sulfhydryl groups on proteins, which specifically occur on cysteine residues. Thus, a protein that has a single exposed cysteine residue can be labeled at that site specifically. Any dye molecule (typically ~1 kDa) or other label, such as biotin, functionalized with a maleimide chemical group (~0.1 kDa) can then be attached at a maximum 1:1 dye-to-protein stoichiometry to the protein of interest.

Starting with a cysteine-less mutant of Pab1, Pab1 C70A/C119A/C368 (gift of Dr. Hendrik Glauninger), I introduced a labeling site at the C-terminus of Pab1 with an A577C mutation. The C-terminal domain of Pab1 is not required for Pab1 condensation, and condensation is primarily driven by the RNA recognition motifs (RRMs), so I reasoned that introducing a label at the C-terminus would not disrupt Pab1's ability to condense.[45]

Design of a Single-Molecule Imaging Setup

To quantify the fluorescent signal from single Pab1 molecules and Pab1 condensates, we needed a microscopy platform which would enable reliable, high signal-to-noise fluorescence imaging of a large (i.e., 100's of molecules or more) field of view. Anticipating future work that

would involve colocalization of condensates with other factors (e.g., chaperones), we also wanted the ability to image in multiple colors and build in additional microscope channels as needed.

We decided to construct our microscope from free optical components, such that we could build in the exact functionalities we required and tailor the instrument to the specific experiments we wanted to conduct. We also decided to make this instrument capable of multiple modes of imaging, including total internal reflection fluorescence (TIRF) microscopy, a highly effective technique for imaging single molecules. In TIRF, the excitation source does not directly pass into the sample and only excites molecules via an evanescent field of ~100 nm depth. Excitation of molecules outside of the focal plane as well as other excitation-dependent sources of background are greatly reduced. However, we also wanted the ability to switch easily into and out of TIRF, as traditional widefield illumination has the ability to excite deeper into the sample volume.

The initial layout for this instrument is illustrated in Figure 2.1, as well as current pictures of the setup. Although various modifications have been added to the setup over time, by other lab members and myself, the core design principles and strategy remain the same. The setup combines 488 nm and 637 nm excitation sources into a single excitation beam for two-color imaging; the setup also separates fluorescence emission into two detection channels which are projected onto a single Photometrics Prime 95B scientific Complementary Metal–Oxide–Semiconductor (sCMOS) pixel array. By projecting both channels onto the same camera, images in both channels can be acquired on the same detection apparatus at the same timepoint.

In order to convert easily between confocal, widefield, and TIRF imaging, we magnetically mounted the Köhler lens on a kinetic stage which can translate the lens across the back focal plane of the microscope objective. In practice, this provides two toggles for the experimenter: (1) switch between widefield and confocal modes by adding or removing the Köhler lens, and (2) continuous

transition between widefield illumination and TIRF. The second transition is accomplished by turning a micrometer which moves the Köhler lens across the back focal plane, thereby changing the angle that light exits the objective. This feature enables not only traditional widefield (i.e., centered on the objective optical axis) and TIRF illumination, but also the intermediate “dirty TIRF” or “Highly Inclined and Laminated Optical sheet” (HILO) approach, where light exits the objective at an angle to reduce background.The exact angle used to produce HILO or TIRF is also tunable to optimize imaging (see Figure 2.2 for a schematic of widefield, HILO, and TIRF).

I designed and built this setup as an early phase of my thesis work; the setup continues to be used for multicolor widefield and TIRF imaging for many applications in our group.

A reference table of the filters and dichroics that I selected can be found below:

Table 2.1, Filters and Dichroics.

Function	**Wavelength(s)**	**Manufacturer**	**Part #**
Beam cube	637 nm	Semrock	FF640-FDi01-25x36
Beam cube	488 nm, 637 nm	Chroma	ZT488/640rpc
Excitation filter	637 nm	Semrock	FF01-637/7-25
Excitation filter	488 nm	Chroma	ZET488/10x
Excitation dichroic	488 nm, 637 nm	Thorlabs	DMSP567
Emission dichroic	488 nm, 637 nm	Chroma	T610lpxr
Emission filter longpass	637 nm	Semrock	BLP01-635R-25
Emission filter bandpass	637 nm	Semrock	FF01-675/67-25
Emission filter longpass	488 nm	Semrock	BLP01-488R-25
Emission filter bandpass	488 nm	Chroma	ET535/70m

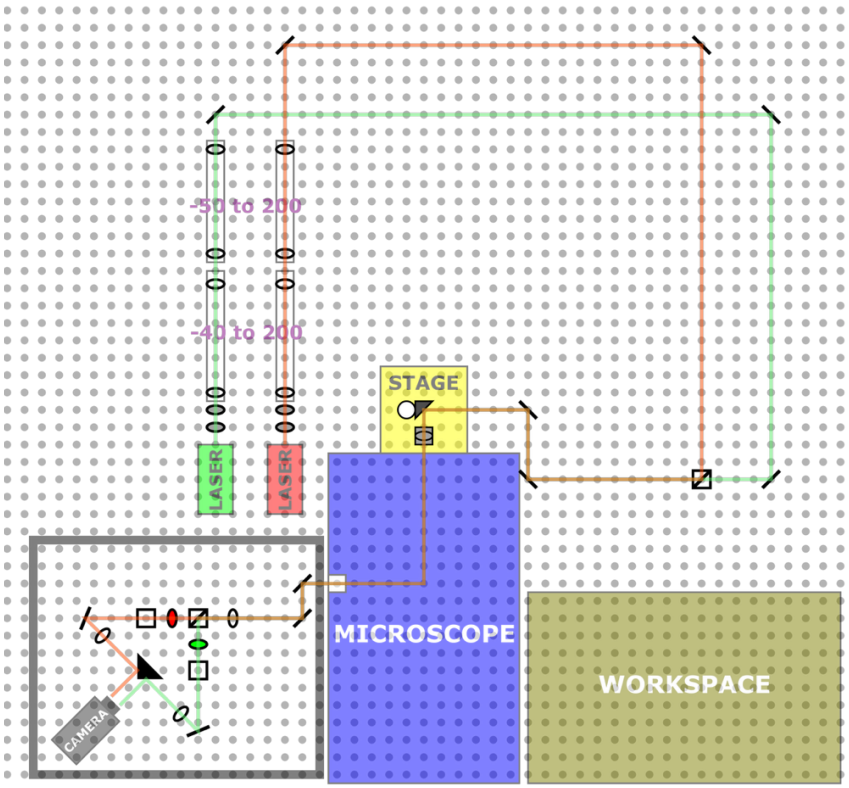

Figure 2.1, Single-molecule microscope design.

Two input beams (from green and red "LASER" boxes) travel through excitation filters and quarter wave plates (gray ovals) to restrict the excitation wavelengths and convert the light from linear to circular polarization. The beams are expanded with telescopes ("−40 to 200", "−50 to 200") to a size that will fill the intended field of view, then transmitted across the optical table with mirrors (black lines) to a dichroic (black box with line) where they are combined into a single optical path. The combined excitation beam is transmitted to a periscope (gray circle and triangle in "STAGE" box), which elevates the beam to the level of the microscope body ("MICROSCOPE"). The periscope and subsequent Köhler lens (gray oval in square) are on a kinetic stage (yellow "STAGE" box), and the Köhler lens is on a magnetic mount. Translation of the stage and presence or absence of the Köhler lens switch between imaging modalities (confocal, widefield, HILO, TIRF). After the Köhler lens, the excitation beam enters the microscope, where it passes through the beam cube and objective to reach the sample. Fluorescence emission as well as scattered or reflected excitation light passes back through the objective and beam cube, then exits the microscope body at the tube lens (white square). The light is then transmitted into a 4f optical system (defined by the lenses depicted as open ovals) in a closed detection box (gray open rectangle). Light is split by the emission dichroic (black box with line), and both excitation light and water Raman scattering are removed by longpass and bandpass emission filter sets (green and red ovals). The separate emission beams are directed onto opposite faces of a right-angle silvered prism (black triangle), which reflects the two emission paths onto parallel, offset trajectories that lead to the pixel array of a single detector ("CAMERA").

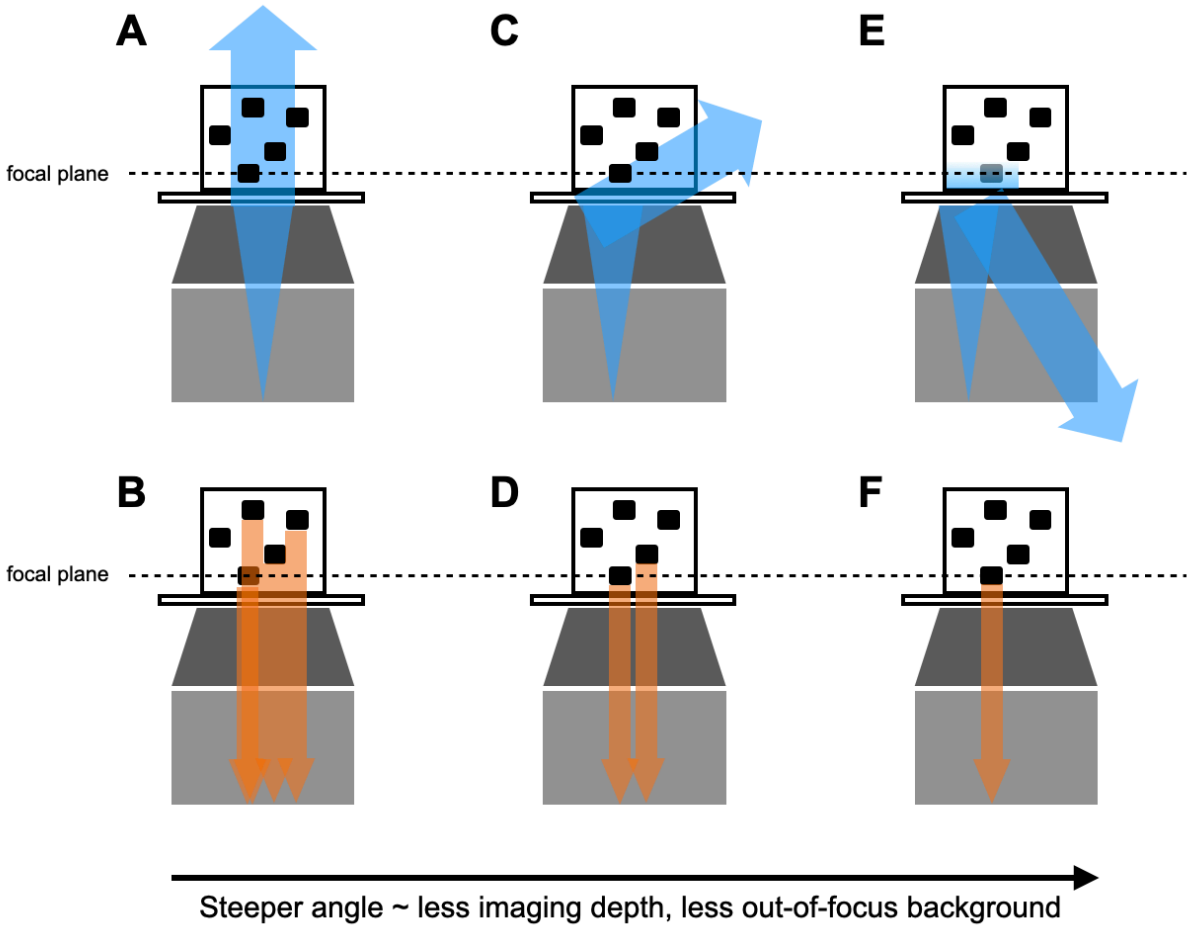

Figure 2.2, Schematic of imaging modalities.

The angle at which light leaves the objective (cartooned in gray) and passes through the coverslip (thin rectangle) into the sample volume (taller box) determines the imaging modality. (A) In traditional widefield imaging, the excitation light (blue beam) passes directly into the sample along the objective's optical axis, leading to excitation of molecules (small black boxes) throughout the sample volume. (B) Particle at all depths, both in and out of the focal plane, emit fluorescence (and/or scatter excitation light) back toward the objective. (C) As the angle at which light leaves the objective is made steeper, less of the sample volume is illuminated. (D) This leads to less out-of-focus light sent back toward the objective, and thus lower background. (E) When the angle is made steep enough to cause total internal reflection, the excitation beam no longer passes into the sample volume and only excites a narrow depth of sample via an evanescent field. (F) The background is lowest in this regime; however, only a shallow depth of sample can be excited.

2.2 Methods

Purification of Pab1

Pab1 purification was based on the protocol described by Yoo et al, with modifications.[60] BL21(DE3) competent *E. coli* (New England Biolabs) were transformed with a Pab1 or Pab1 C70A/C119A/C368A/A577C expression plasmid. Multiple (3 to 10) colonies were picked and used to inoculate a 5 mL overnight starter culture of LB with the appropriate antibiotic (kanamycin). The overnight culture was then used to inoculate the desired quantity of Terrific Broth (TB) with antibiotic (up to 4 L). At an OD of ~0.4 or higher (up to slightly above 1), protein expression was induced with 0.2 mM IPTG for 4–6 hours at 30 °C, or overnight at 18 °C. Cells were separated from medium by centrifugation at 3,000 *g* for 15 minutes at 4 °C, then resuspended in Nickel Binding buffer (150 mM KCl, 20 mM imidazole, 20 mM HEPES, 2.5 mM $MgCl_2$, 1 mM βME, pH 7.3). Cells were either kept on ice for immediate lysis, or were respun at 4,000 *g* for 10 minutes at 4 °C in 50 mL conical tube(s) and flash frozen in liquid nitrogen for storage at −80 °C.

Cells resuspended in Nickel Binding buffer were supplemented with at least 1 Pierce protease inhibitor tablet per 50 mL (for example, 1 tablet for 25 mL buffer added to a 1 L prep, or 2 tablets for 60 mL buffer added to a 4 L prep). Cells were lysed in a 4 °C cold room by sonication (60% amplitude, 5 sec. pulse + 5 sec. wait, 20 min. total sonication) in a 50 mL conical tube or metal bucket immersed in an ice-water bath. The lysate was clarified with two sequential spins, 4,000 *g* for 15 minutes and 30,000 *g* for 20 minutes, both at 4 °C. The clarified lysate was injected onto a Cytiva HisTrap FF 5 mL column (connected to an ÄKTA Pure), and the column was washed with multiple column volumes (CVs) of Nickel Binding buffer until the UV signal stabilized. A 20

mL gradient from 0% to 100% of Nickel Elution buffer (same as Nickel Binding buffer, with 400 mM imidazole) was run, and fractions were collected and pooled.

The collected protein was combined with a ~1 mg aliquot of tobacco etch virus (Tev) protease to remove the 8xHistidine tag. Digestion was performed overnight either at 4 °C while dialyzing (SnakeSkin 10 kDa dialysis tubing) in a bath of ~0.5 L Nickel binding buffer, or at room temperature on a rocker (followed by several-fold dilution into Nickel Binding buffer). The protein was then re-injected onto the HisTrap column to separate the digested protein from the undigested protein, His-tagged Tev protease, and other nickel-binding impurities. This time, the flow-through was collected and saved, and the column was cleaned with several CVs of Nickel Elution buffer.

The sample (flow-through from previous step) was then subjected to multiple rounds of concentration (Amicon Ultra spin concentrators, 30 kDa) and dilution into Q0 or Q50 buffer (0 or 50 mM KCl, 20 mM HEPES, 2.5 mM $MgCl_2$, 1 mM DTT, pH 7.3). (Note: Q0 is more convenient for diluting the protein more quickly, and Pab1 tolerates low salt concentration in my hands; however, other proteins such as Sis1 are more sensitive to low salt concentration and should not be diluted heavily into Q0.) When the KCl concentration was reduced to below ~100 mM, the sample was injected onto a HiTrap Heparin HP 5 mL column. A 30 mL gradient from 0% to 100% of Q1000 buffer (same as Q0 and Q50 buffers, with 1 M KCl) was run, while collecting 1 mL fractions. Pab1-containing fractions were pooled, concentrated, and run on a size exclusion column (Superdex 200 Increase 10/300 GL or Superose 6 Increase 10/300 GL) equilibrated with H150 buffer (150 mM KCl, 20 mM HEPES, 2.5 mM $MgCl_2$, 1 mM DTT, pH 7.3). Fractions were evaluated for purity by denaturing SDS-PAGE gel. Fractions were pooled, concentrated, and flash frozen in liquid nitrogen for storage at −80 °C.

Purification of Chaperones

With the exception of Ssa2, most proteins (in this chapter, Sis1, Sse1, and Hsp104) were purified similarly to Pab1, except a HiTrap Q HP 5 mL anion exchange column was used in place of the HiTrap Heparin HP 5 mL column, and Ulp1 protease was used instead of Tev protease (SUMO cut site). Purification of Ssa2 is described below. Again, protein purification procedures were based on those described in Yoo et al.[60]

For both Ssa2 and Ssa2 C264A/C303N/D555C (which is briefly used in this chapter), the following procedure was used. Rosetta or Rosetta2 (DE3) competent *E. coli* (Novagen, Sigma-Aldrich) were transformed with the appropriate expression plasmid. Multiple (3 to 10) colonies were used to inoculate a 5 mL overnight culture of LB with the appropriate antibiotics (kanamycin and chloramphenicol). The overnight culture was used to inoculate the desired quantity of Terrific Broth (TB) with antibiotic (up to 4 L). At an OD of ~0.4 or higher (up to slightly above 1), protein expression was induced with 0.2 mM IPTG for overnight at 18 °C. Cells were separated from medium by centrifugation at 3,000 *g* for 15 minutes at 4 °C, then resuspended in Hsp70 Nickel Binding buffer (750 mM KCl, 20 mM imidazole, 50 mM HEPES, 1 mM ATP, 5 mM $MgCl_2$, 2 mM βME, 10% glycerol, pH 7.3). Cells were supplemented with 1 Pierce protease inhibitor tablet per ~50 mL total volume, and lysis was immediately performed (without freeze-thaw) at 4 °C by sonication (60% amplitude, 5 second pulse plus 5 second wait time, 20 min. total sonication) in a 50 mL conical tube or metal bucket immersed in an ice-water bath.

The lysate was clarified with two sequential spins, 4,000 *g* for 15 minutes and 30,000 *g* for 20 minutes, both at 4 °C. The clarified lysate was injected onto a Cytiva HisTrap FF 5 mL column (connected to an ÄKTA Pure), and the column was washed with multiple column volumes (CVs) of Nickel Binding buffer until the UV signal stabilized. The column was then washed with multiple

column volumes of High ATP buffer (Hsp70 Nickel Binding buffer mixed with 100 mM ATP stock to a final ATP concentration of 20 mM), and the column was incubated for at least 30 minutes at 20 mM ATP. (Rationale: Incubation with ATP should promote the ATP-bound state of Hsp70 with lower affinity for binding other proteins. Hsp70 protein substrates should be released.)

The column was rewashed with multiple column volumes (CVs) of Nickel Binding buffer. A 20 mL gradient from 0% to 100% of Nickel Elution buffer (same as Nickel Binding buffer, with 400 mM imidazole) was run, and fractions were collected and pooled. The collected protein was combined with a homemade aliquot of Ulp1 protease to remove the 6xHistidine tag. Digestion was performed overnight either at 4 °C while dialyzing (SnakeSkin 10 kDa dialysis tubing) in a bath of ~0.5 L Nickel binding buffer, or at room temperature on a rocker (followed by several-fold dilution into Nickel Binding buffer).

The protein was re-injected onto the HisTrap column to separate digested from undigested protein (as well as His-tagged Ulp1 and other nickel-binding impurities). The flow-through was collected and saved, and the column was cleaned with several CVs of Nickel Elution buffer.

The sample (flow-through from previous step) was then subjected to multiple rounds of concentration (Amicon Ultra spin concentrators, 30 kDa) and dilution into Q0 or Q50 buffer (0 or 50 mM KCl, 20 mM HEPES, 1 mM ATP, 5 mM $MgCl_2$, 0.5 mM EDTA, 2 mM DTT, 10% glycerol, pH 7.3). Note: Given the ability of EDTA to chelate magnesium ions, I tried removing EDTA and $MgCl_2$ separately during different Ssa2 preparations. Neither EDTA nor $MgCl_2$ were found to be individually necessary for successful purification by anion exchange.

When the KCl concentration was reduced to below ~100 mM, the sample was injected onto a HiTrap Heparin HP 5 mL column. A 30 mL gradient from 0% to 100% of Q1000 buffer (same as Q0 and Q50 buffers, with 1 M KCl) was run, while collecting 1 mL fractions. An SDS-PAGE

gel was then typically run to assess which fractions contained protein, as typically a main peak with a right shoulder appears. (Note: In my hands, only the main peak contains protein. The right shoulder may be free ATP, which is anionic and absorbs at 280 nm, but I have not yet tested this hypothesis experimentally. In previous work, it was found that the right shoulder contained protein which was nonfunctional.[60] In either case, only later fractions contain functional Ssa2.)

The selected fractions were pooled and concentrated. Optionally, Ssa2 was then run on a small-scale purification size exclusion column (Superdex 200 Increase 10/300 GL) equilibrated with Hsp70 storage buffer (150 mM KCl, 50 mM HEPES, 1 mM ATP, 2.5 mM $MgCl_2$, 2 mM βME, 10% glycerol, pH 7.3)., and fractions were evaluated for purity by denaturing SDS-PAGE gel. (Note: In the published protocol, size exclusion chromatography was not used.[60] I have found that sizing may help remove RNase activity, likely by removing a minor impurity that has RNase activity. Reducing RNase activity is useful for the fluorescence anisotropy-based dispersal assay, which is RNA-based and affected by RNA degradation.)

Fractions were pooled, concentrated, and flash frozen in liquid nitrogen for storage at −80 °C. If the protein was not sized, exchange into Hsp70 storage buffer was performed before storage.

Measuring Protein Concentration (Bradford)

A 96-well clear flat-bottom plate was loaded with 200 µL Bradford reagent (Quick Start, BioRad) per well. Four standards of bovine serum albumin (BSA) were prepared from a 2 mg/mL stock to concentrations of 0.9, 0.66, 0.43, and 0.2 mg/mL. 4 µL of these standards and the protein sample (diluted to an appropriate concentration) were added to each well, in triplicate. Wells were mixed by multichannel pipettor, and large bubbles were manually removed with pipette tips.

After brief shaking (5 s), absorbance at 590 nm and 450 nm were measured with a Tecan Spark plate reader. A linear fit was determined between the known BSA standard concentrations

and their A_{590} / A_{450} ratios, which (unlike A_{590} alone) is linear with protein concentration.[61] Protein sample concentration was then determined from the linear fit. Measurements were only considered if the average A_{590} / A_{450} of the triplicate measurements fell within the range of the BSA standards.

Preparation of Dye Stocks

Fluorescent dyes functionalized with a maleimide group were dissolved into dimethyl sulfoxide (DMSO) to a final intended concentration of > 1 mM (typically 5 or 10 mM), then aliquoted into single 0.2 mL tubes and stored in a 50 mL conical tube with silica gel desiccant at −80 °C. For fluorescent dyes, the concentration of the stock was empirically determined by making serial dilutions of the dye stock in phosphate buffered saline, pH 7.4 (PBS), then measuring the dye absorbance at the peak absorbance wavelength with a NanoDrop One spectrophotometer. Concentration was calculated by applying Beer's law, the dye's extinction coefficient (ε_{dye}), the standardized NanoDrop pathlength (b) of 1 cm, and the dilution factor (DF).

$$[dye\ stock] = DF \cdot \frac{A_{dye}}{\varepsilon_{dye} \cdot b}$$

Preparation of Labeled Pab1

To prepare Pab1-CF 640R, Pab1 C70A/C119A/C368A/A577C was incubated with 10 mM tris(2-carboxyethyl)phosphine (TCEP) for 45 minutes at room temperature to favor the reduction of cysteines. The sample was then diluted and buffer exchanged into phosphate buffered saline, pH 7.4 (PBS) with a Zeba spin desalting column (7 kDa molecular weight cutoff), and a 20-fold molar ratio of label (CF 640R-maleimide, Biotium) was added. The reaction was incubated at room temperature for 2.5 hours with shaking (300 rpm, Eppendorf ThermoMixer), covered with foil to prevent photobleaching. The dye reaction was clarified by centrifugation (8,000 *g* for 3 minutes); no visible pellet formed. The supernatant was purified with a Zeba spin column (7 kDa), then

further purified and concentrated with two sequential Amicon Ultra spin concentrators (10 kDa molecular weight cutoff). The sample was purified with two additional Zeba spin columns until the second column did not retain visible dye. With the final column, the sample was exchanged into H150 buffer (20 mM HEPES, 150 mM KCl, 2.5 mM $MgCl_2$, 1 mM DTT, pH 7.3). Pab1-CF 640R was aliquoted and flash frozen in liquid nitrogen for storage at −80 °C.

To prepare Pab1-biotin, a similar approach was used, with several minor differences. Pab1 C70A/C119A/C368A/A577C was incubated with 10 mM TCEP for 30 minutes on ice. The sample was buffer exchanged into PBS with Zeba spin columns (40 kDa molecular weight cutoff). A 200-fold molar ratio of biotin (EZ-Link™ Maleimide-PEG2-Biotin, Thermo Fisher) was added from a freshly made solution in PBS, and the reaction was diluted severalfold with additional PBS to 0.5 mL. After 2.75 hours of incubation with shaking at 300 rpm, the sample was buffer exchanged into Condensation buffer (20 mM HEPES, 150 mM KCl, 2.5 mM $MgCl_2$, 1 mM DTT, pH 6.8) with a Zeba spin column. The sample was concentrated (Amicon Ultra, 10 kDa cutoff). A clarifying spin was performed prior to storage and use (8,000 g for 3 minutes); no visible pellet formed. Pab1-biotin was aliquoted and flash frozen in liquid nitrogen for storage at −80 °C.

Degree of Labeling

The degree of labeling for a protein is the molar ratio of label to protein:

$$DOL = \frac{[label]}{[protein]}$$

The concentration of the fluorescent label was determined by absorbance at the dye's peak absorbance wavelength provided by the manufacturer. Using the dye's extinction coefficient at that wavelength (ε_{dye}) and the pathlength (b), the dye concentration can be determined by application of Beer's law:

$$[label] = \frac{A_{dye}}{\varepsilon_{dye} \cdot b}$$

Absorbance measurements were taken on a NanoDrop One spectrophotometer, whose absorbance recordings are standardized to a pathlength of 1 cm.

The concentration of protein was determined in one of two ways: by absorbance at 280 nm (A_{280}), or by the Bradford method (described above). For Pab1, similar results were obtained by either method. To determine protein concentration by A_{280} in the presence of a small molecule dye, the absorbance value must be corrected for the dye's absorbance at 280 nm, typically provided by the manufacturer as a correction factor (CF_{280}) equaling a proportion of the dye's absorbance at its peak absorbance wavelength. Thus,

$$[protein] = \frac{A_{280} - CF_{280} \cdot A_{dye}}{\varepsilon_{protein} \cdot b}$$

The extinction coefficient of Pab1 was estimated using the ProtParam online tool on the Expasy server, assuming the protein is fully reduced.[62]

For a protein such as Pab1 C70A/C119A/C368A/A577C with a single labeling site, assuming no off-target reaction and total removal of free dye, the maximum degree of labeling should be 1, or 100%. Lower degree of labeling could indicate incomplete or inefficient reaction, while higher degree of labeling could indicate incomplete removal of free dye or off-target reaction. For unknown reasons, the labeling efficiency was more frequently around 70% with CF 640R, although other dyes yielded higher degrees of labeling.

This method did not translate to Pab1-biotin, as it relies on characteristic visible absorbance of the label. However, the exact degree of biotin labeling was not important for subsequent experiments, since biotin was not used for molecular counting (thus, the exact amount present did

not matter). Pab1 reactions with biotin were carried out similarly to Pab1 reactions with dye, so a similar degree of labeling would be expected.

Preparation of Pab1 Condensates

Condensate preparation was based on the procedures described by Yoo et al., with some modifications (particularly with respect to duration of heat shock and the introduction of labeled Pab1).[60] A mixture of wildtype Pab1, Pab1 C70A/C119A/C368A/A577C, Pab1-dye, and/or Pab1-biotin was prepared in Condensation buffer (20 mM HEPES, 150 mM KCl, 2.5 mM $MgCl_2$, 1 mM DTT, pH 6.8) such that the total Pab1 concentration equaled 25 μM, and the individual Pab1 constituents were present at the intended proportions. In most cases, a total volume of 600 μL was used, so that a full 500 μL could later be used for FPLC. The mixture was then heat shocked at 42 °C for variable times (typically 30 minutes or 1 hour) in an Eppendorf ThermoMixer. The sample was subjected to a clarifying spin at 8,000 *g* for 3 minutes at room temperature, and the supernatant was removed. (Typically, no pellet or a small pellet was visible, depending on the condition.) The supernatant was then loaded onto a 0.5 mL loop on an ÄKTA Pure system and injected onto a Superose 6 Increase 10/300 GL size exclusion column, equilibrated with H150 buffer (20 mM HEPES, 150 mM KCl, 2.5 mM $MgCl_2$, 1 mM DTT, pH 7.3) at a flow rate of 0.3 mL/min, for approximately 5 loop volumes (or 2.5 mL). The sample was eluted at a flow rate of 0.5 mL/min., and the void fraction (typically at a retention volume ~8 mL for the Superose 6 Increase column) was collected. In some cases, the Pab1 monomer fraction was also recovered. The void fractions with the highest absorbance were pooled, and aliquots were flash frozen in liquid nitrogen then stored at −80 °C. The total Pab1 concentration in the condensates was estimated by comparison to Pab1 standards of 4, 2, 1, and 0.5 μM run on an SDS-PAGE denaturing gel. Yield was typically around 0.5 to 1 μM in terms of Pab1 monomer concentration.

Condensate Dispersal: Fluorescence Anisotropy

The approach of Yoo et al. was used to monitor Pab1 dispersal by fluorescence anisotropy of labeled poly(A) RNA, with modifications. For each experiment, a series of 15 µL reactions were prepared in wells of a black 384-well flat bottom plate (Corning 3575). Dispersal buffer (20 mM HEPES, 150 mM KCl, 2.5 mM $MgCl_2$, 1 mM DTT, 0.02% Triton X-100, 0.5 mg/mL BSA pH 7.3) was used for all applications requiring buffer (blanking, dilution, filling wells to 15 µL, etc.). For all non-condensate common components (typically chaperones, creatine kinase/phosphate, RNase inhibitor, RNA), a master mix was prepared and dispensed to all 0 mM ATP negative control wells. ATP was then supplemented from a 100 mM stock to the remaining master mix to reach a final ATP concentration of 5 mM; the ATP-supplemented master mix was dispensed to all other wells. (Note: the volume of master mix per well increases by 0.75 µL due to the addition of ATP; 0.75 µL of Dispersal buffer was added individually to each 0 mM ATP well to make up for this volume.) Components that were not included in the master mix (e.g., when testing different types of chaperones) were added individually to wells (e.g., from a 5x stock solution prepared in Dispersal buffer). Condensates were added to reactions last and as quickly as possible, usually making up 40% of the reaction volume (6 µL), although this volume varied depending on the concentration of the condensates and how much substrate was desired. The wells were sealed with a strip of film, and the plate was immediately transferred to a Tecan Spark pre-equilibrated to 30 °C.

Fluorescence anisotropy measurements were taken every 20 seconds, blanked against 15 µL of Dispersal buffer. The G-factor was determined for each new plate by testing a sample of free dye in water (blanked with water). The z-position and gain were generally optimized for the first experiment performed on a particular 384-well plate, then these values were reused in subsequent experiments. Analysis was performed in RStudio with code adapted from Dr. Haneul Yoo. Raw

anisotropy values were normalized to the first timepoint of each condition and to the average of the 0 mM ATP negative control wells at each timepoint.

Chaperone concentrations varied by experiment. Fixed concentrations of other reaction components were used: 200 nM A19 RNA modified with 6-carboxyfluorescein (FAM) from IDT, 8 mM creatine phosphate, 1 μM creatine kinase, and 2% (volume/volume) SUPERase·In™ RNase Inhibitor (Thermo Fisher).

Condensate Dispersal: TSP Assay

The protocol here is based on the protocol of Dr. Sammy Keyport Kik, with modifications. Indidivual 15 μL reactions containing chaperones, ATP (0 or 5 mM), ATP regeneration system (8 mM creatine phosphate, 1 μM creatine kinase), and condensates was prepared in a separate 1.5 mL tube. H150 buffer (20 mM HEPES, 150 mM KCl, 2.5 mM $MgCl_2$, 1 mM DTT, pH 7.3) was used as the reaction buffer. Condensates were added last. Reactions were incubated at 30 °C (Eppendorf ThermoMixer). At the end of the reaction, 5 μL was removed ("total" or "T" sample), and 5 μL of 2x Laemmli buffer (Bio-Rad) was added to the "total" sample. The remaining 10 μL reaction was centrifuged at 20,000 *g* for 20 minutes at 4 °C. 5 μL was removed ("supernatant" or "S" sample), and 5 μL of 2x Laemmli buffer was added to the "supernatant" sample. The remaining supernatant was carefully removed, and 40 μL H150 buffer was added (taking care not to resuspend the pellet). The reaction was respun at 20,000 *g* for 20 minutes at 4 °C. The entire supernatant was removed, and the pellet (or "P" sample) was resuspended with 10 μL of 2x Laemmli buffer and vortexed.

Samples were then subjected to denaturation at 95 °C, 10 minutes, and run on an SDS-PAGE gel (Bio-Rad 4–20% Criterion™ TGX™ Precast Midi Protein Gel, 26 well, 15 μl) at 200 V for 40 minutes. The gel was imaged on a ChemiDoc imager (Bio-Rad) using settings for Cy5 (red dye) detection. Band intensities were determined in ImageJ by calculating the mean intensity

of a rectangular selection (of the same shape for all bands) and subtracting the mean intensity of a background selection slightly above each band. The signal of the pellet sample was divided by 2, because the pellet was formed from 10 μL of reaction, whereas the total and supernatant were both 5 μL samples. The proportion of Pab1 in the supernatant or pellet was determined by dividing the signal in the supernatant or pellet by the sum of signal in both samples.

Passivation of Coverslips with PEG

Although passivation of coverslips was ultimately not necessary for most experiments, a protocol for coating coverslips with polyethylene glycol (PEG) and PEG-biotin was optimized for our laboratories' use which was closely adapted from Paul and Myong's published method.[63] Glass coverslips (Epredia or Richard-Allan Scientific) were placed into a ceramic slide boat and briefly plasma cleaned (at least 5 minutes on highest setting). Coverslips were kept in the ceramic slide boat or transferred to a polypropylene slide boat and were fully submerged in a mixture of 150 mL methanol, 2 mL N-(2-Aminoethyl)-3-Aminopropyltrimethoxysilane, and 2 mL glacial acetic acid. After 40 minutes incubation (foil covered in chemical fume hood), the coverslips were removed and rinsed at least three times in ultrapure water (by submerging in a glass container fill with water, then replacing the water). Coverslips were dried with nitrogen air (complete drying not necessary). A PEG treatment chamber was prepared by cleaning an empty pipette tip box and empty insert (with 70% ethanol), partially filling the box with ultrapure water (to increase humidity), placing the insert into the box, and covering the insert with lens paper. Half of the treated coverslips were arranged onto the lens paper surface. A PEG treatment mixture was prepared by mixing a sodium biocarbonate aqueous solution (~84 mg per 10 mL ultrapure water) with PEG-succinimidyl valerate (~5,000 Da molecular weight, Laysan Bio) succinimidyl valerate in a 300 μL:60 mg ratio. Biotin-PEG-succinimidyl valerate was optionally included at a 1:60 ratio with unbiotinylated PEG

(1 mg per 60 mg unbiotinylated PEG). (Note: It is recommended to weigh out the PEG-biotin into a 1.5 mL microcentrifuge tube, then add the appropriate amount of PEG based on the PEG-biotin weight, then pipette in the bicarbonate solution.) The PEG mixture was mixed vigorously by both vortexing and pipetting until PEG was visibly dissolved (may be cloudy). The solution was clarified with by centrifugation (12,000 *g*, 1 min.), and 70 μL was pipetted directly onto coverslips. A second coverslip was then carefully placed (without introducing bubbles) on top of each PEG-treated coverslip, forming coverslip sandwiches. The pipette box was closed and covered in foil. After 3–5 hours, the coverslip sandwiches were separated under a stream of ultrapure water (e.g., direct output of MilliQ system), rinsed, then reorganized onto a slide boat with attention to which side was treated (e.g., by marking one side of the slide boat and placing all coverslips in the same orientation). Half of the coverslips were placed back into the treatment chamber on new lens paper (treated side up). The PEG treatment process was then repeated. (Note: The same bicarbonate stock solution can be reused on the same day, but the PEG mixture should be made fresh, as succinimidyl valerate has a short lifetime in aqueous solution. The bicarbonate stock should be made the day it is used.) After overnight incubation, the coverslips were again separated, thoroughly rinsed with ultrapure water, and placed into a slide boat (with attention to the treated sides). The PEG-coated coverslips were dried gently but thoroughly with nitrogen air and were stored at −20 °C in a slide boat inside a clean box.

For using PEG-coated coverslips, chambers such as CoverWell perfusion chambers (Grace Bio-Labs) did not adhere as well to the PEG-coated surface as to untreated glass. Silicone such as two-component Ecoflex 5 was applied in small amounts (using pipette tips) to seal chambers to the PEG-coated surface. For anchoring, 0.2 mg/mL neutravidin in aqueous solution was applied for several minutes, then was removed prior to adding biotinylated sample (e.g., condensates).

Microscopy

Samples for microscopy were prepared by diluting the appropriate starting sample into H150 Imaging buffer (20 mM HEPES, 150 mM KCl, 2.5 mM $MgCl_2$, 1 mM DTT, pH 7.3), which was additionally filtered through a 0.02 μm syringe filter to remove particulate contaminants which could have fluorescent signal. Imaging buffer may optionally be supplemented with 3 mM Trolox and/or an oxygen-scavenging system (e.g., 60 nM protocatechuate-3,4-dioxygenase and 2.6 mM protocatechuic acid) to improve dye photostability. Although these components were used in other experiments not shown here, they were not used to obtain the data in this chapter.

The appropriate sample dilution was determined empirically for each sample. Condensates typically required on the order of ~100-fold dilution, while uncondensed samples were typically imaged at a concentration of below 1 nM (i.e., 1000's or more-fold dilution). 50 μL of the appropriately diluted sample was transferred to a CoverWell 0.9 mm depth perfusion chamber (Grace Bio-Labs) adhered to a freshly (i.e., same-day) plasma cleaned glass coverslip (Epredia or Richard-Allan Scientific). Same-day plasma cleaning is important both for eliminating fluorescent contamination and for ensuring the perfusion chamber adheres well to the glass (as fresh plasma cleaning alters the charge and chemical groups on the glass surface).

Single-molecule microscopy was performed on the custom imaging setup described above (see "Design of a Single-Molecule Imaging Setup" in Section 2.1 for details). In brief, samples were excited with 637 nm illumination (OBIS LX, Coherent) on an Olympus IX71 microscopy body with a 1.42 numerical aperture, infinity-corrected oil-immersion objective (Olympus PlanApo N 60x), and images were acquired with a Photometrics Prime 95B sCMOS detector.

The following camera settings were used for optimal single-molecule imaging.

Table 2.2, Default Camera Settings.

Bit depth	12-bit (or 16-bit for very bright samples)
Gain	3 (most sensitive), or 1-HDR at 16-bit depth
Clear dark counts	Never (do not clear; fastest acquisition)
Auto speckle correction	No (do not apply corrections)
Fan speed	High
Metadata	Yes (save metadata)

Timelapse Microscopy

Timelapse videos of condensate dispersal were taken by Diangen Lin on the same imaging setup described in the previous section, with the addition of an extra component in the excitation optical path: a camera-controlled shutter (ThorLabs SHB05T). A mixture of condensates and all other components (chaperones, ATP, and/or creatine kinase/phosphate depending on the condition) were prepared in a 1.5 mL tube, using Dispersal Imaging buffer (20 mM HEPES, 150 mM KCl, 2.5 mM $MgCl_2$, 1 mM DTT, 0.5 mg/mL BSA, pH 7.3) for dilutions and for completing the 50 µL reaction volume. The following concentrations of reagents were used: 0.5 µM Sis1 dimer (1 µM monomer), 1 µM Ssa2, 0.1 µM Hsp104 hexamer (0.6 µM hexamer), 50 nM Sse1, 8 mM creatine phosphate, 1 µM creatine kinase, 5 mM ATP, and 0.2% condensates (volume/volume). The mixture was immediately transferred to an imaging chamber (plasma cleaned coverslip and perfusion chamber, as described in previous section) and placed on the microscope objective. The sample was focused as quickly as possible, the focus was secured with the tension knob, and a timelapse series of 121 frames at 10 second intervals was acquired (20 minutes total), such that the shutter only allowed excitation light to reach the sample during acquisition of frames. Default camera settings were used (Table 2.2, 12-bit depth), and 2 mW output power of 637 nm illumination was

used (~2 W × cm^{-2} at the objective). This approach was effective at preventing photobleaching of condensates (no more than a few percent of the initial signal, as shown in Figure 2.13).

Focus drift was occasionally an issue during acquisition. Videos with substantial drift were not considered for subsequent analysis.

Single-Molecule Data Analysis: Background Subtraction

Video analysis was performed in Python with Anaconda (Jupyter notebooks). The first step of analysis was background subtraction, for which I devised a median-of-last-frames method. The rationale is that multiple images of a single sample (at different fields of view) will share a common background pattern (consisting of out-of-focus fluorescence, debris on optical components, scattered light, etc.), but they will have different constellations of objects of interest (e.g., single molecules or condensates). Since objects of interest occupy a small fraction of the total area (if imaged at an appropriate density), a median projection across all images will retain the common background pattern but will omit specific objects that appear in only one of the particular images. This concept is illustrated in Figure 2.3.

Thus, for a particular set of videos—that is, videos taken of the same sample, using the same hardware and optical path (camera settings, laser power, specific microscope alignment and configuration)—a background image can be calculated by taking the last frame of each video and computing a median projection (finding the median value at every pixel across all last frames). In many cases, using this method effectively zeros out the background and allows for single molecule brightnesses to be calculated by simple summing of background-subtracted pixels, without further corrections. An example of this background subtraction method applied to real data is included in Figure 2.3. This approach is most effective with large sets of videos (~10 or more), but it can be used for smaller video sets. If too few videos are used, and/or if the density of objects in each video

is too high, objects will begin to appear in the median projection, and the median projection will no longer accurately represent the background pattern alone.

A different approach was used for the single condensate timelapse dispersal data in Figures 2.11–14, due in part to the low number of videos per video set. Instead of a median projection, a minimum projection was used. A minimum projection minimizes the chance that an object will be projected into the background array (for example, if there are three videos in a set, and two happen to contain an object at the same position). Moreover, a minimum projection was calculated for every frame (i.e., every timepoint), instead of only at the last frame. Thus, an entire background video was assembled, and the background video was subtracted (frame-by-frame) from each video. Making a background video (with frame-specific background) is not necessary if the background pattern remains constant frame-to-frame. However, for these timelapse data, the background did not necessarily remain constant, and new objects noticeably appeared in videos over time. Thus, a more rigorous, frame-by-frame background subtraction approach was warranted.

Single-Molecule Data Analysis: Object Identification and Trace Calculation

Video analysis was performed in Python with Anaconda (Jupyter notebooks). I developed a custom analysis pipeline to extract single molecule data from background-subtracted videos. Some example outputs at different steps in this pipeline are shown in Figure 2.4. Conceptually, the pipeline consists of four general stages: **test image selection**, **object detection**, **object sizing and elimination**, and **trace calculation**. There is an optional feature to **check for maxed out pixels**.

Test image selection: A test image is obtained, in which objects will be identified. Based on user input, the test image can be either a quantile projection in time of a video or a specific frame of the video. (For example, objects could be identified in the 90th percentile of a video, i.e. objects that appear at any time for at least 10% of the time; objects could be identified in the first

frame of a video, i.e., only objects that are initially present). Based on user input, the test image is also cropped to a specific area of interest.

Object detection: A binary mask is applied to the test image, with the masking threshold determined by user input (**mask_threshold** parameter). Image segmentation is then performed on the binarized image to group adjacent pixels that are brighter than the threshold into single objects. Any objects with fewer pixels than a user-specified threshold (**smallobj_threshold** parameter) are removed from consideration. For each remaining object, the center of mass and sum signal from all pixels are both calculated. The list of objects is sorted from highest to lowest sum signal (such that priority is given to the brightest objects in the next stage of analysis).

Object sizing and elimination: The effective footprint or size of each object, in order of brightness, is determined. Additionally, if objects fail to meet specific criteria, they are removed from consideration. The borders of a square box (3x3 pixels) is drawn around the center of mass of an object. This box is then expanded in all directions, one pixel at a time, until the median signal at the box's borders decreases to the level of a user-defined threshold (**sizing_threshold** parameter, typically set to be half of **mask_threshold**). Objects will be discarded during this sizing step for several reasons:

- Any part of the box extends beyond the boundaries of the image (i.e., the object is too close to the image edge)
- Any part of the box overlaps with another object's territory (with priority effectively given to brighter objects)
- The final box size is below a user-specific threshold (**sizing_min**)

Once the object's box stops expanding (and if it meets the above criteria), this box is saved as the object's effective territory, which other objects may not encroach upon.

For large objects that reach a user-specified size limit (**sizing_max**), one of two treatments is used, based on user preference. Either the box size is capped at the **sizing_max** parameter, or the irregular shape from image segmentation in the previous step is used instead of the box. (The irregular shape may better approximate the footprint of a large object than a square.)

Trace calculation: For each object that passes all criteria and receives a finalized territory (usually a square box of variable size), the signal from all pixels in the object's territory is summed at every frame of the video. These signals are saved as the single-molecule trace for that object. All objects' traces are plotted as subfigures of a large panel, numbered such that their locations can be referenced on an output map of all final objects (see Figure 2.4 for an example). Changepoint detection is performed for each trace using a linearly penalized segmentation (Pelt) method with a radial basis function (rbf) model, via the ruptures Python library developed by Truong et al.[64] The linear penalty applied is a user-input parameter, **level_penalty**. For each level detected (i.e., each section of trace between changepoints), the mean and standard deviation is plotted on the trace.

Check for maxed out pixels: Optionally, objects that contain a maxed out pixel (i.e., a value at the maximum value that can be recorded) in any frame are removed from consideration. Enforcing this criterion is advisable when the exact signal from an object is important (for example, when trying to estimate the true brightness of an object).

The key analysis parameters, the value(s) used for analysis, and their conceptual meaning are described in the following table. (There are additional parameters not described here that are not conceptually important for analysis, such as the size of a pixel, the output directory, etc.)

Table 2.3, Analysis Pipeline Parameters.

Parameter	Value(s) Used	Meaning
spotfind_method	'frame'	Find objects in a specific frame of the video
spotfind_param	1	Find objects in the first frame of the video
checkmax	True	Eliminate objects containing a mixed out pixel
maxpixel	4095 or 65535	Max pixel value, depending on bit depth
level_penalty	5	Penalty used for level finding (higher = fewer levels)
mask_threshold	variable	Cutoff used for binary mask (lower = more objects)
smallobj_threshold	4	Remove objects with fewer than this number of pixels
sizing_threshold	½ mask_threshold	Cutoff used to determine size/edges of an object
sizing_min	2	Minimum object size (2 = 5×5 pixel box)
sizing_max	7	Maximum allowed box size (7 = 15×15 pixel box)
shapeswitch	True	For large objects, use segmented shape (not box)

Follow-up analysis and graphing were also performed in Python with Anaconda (Jupyter notebooks), using the output trace data from this analysis pipeline.

For finding and plotting down step sizes in a particular dataset, the ruptures-based linearly penalized segmentation (Pelt) method was used, with penalty = 5. For each trace, the difference in means between adjacent levels was found and used as the step size. (Only decreasing or "down" steps were considered in the subsequent analysis.)

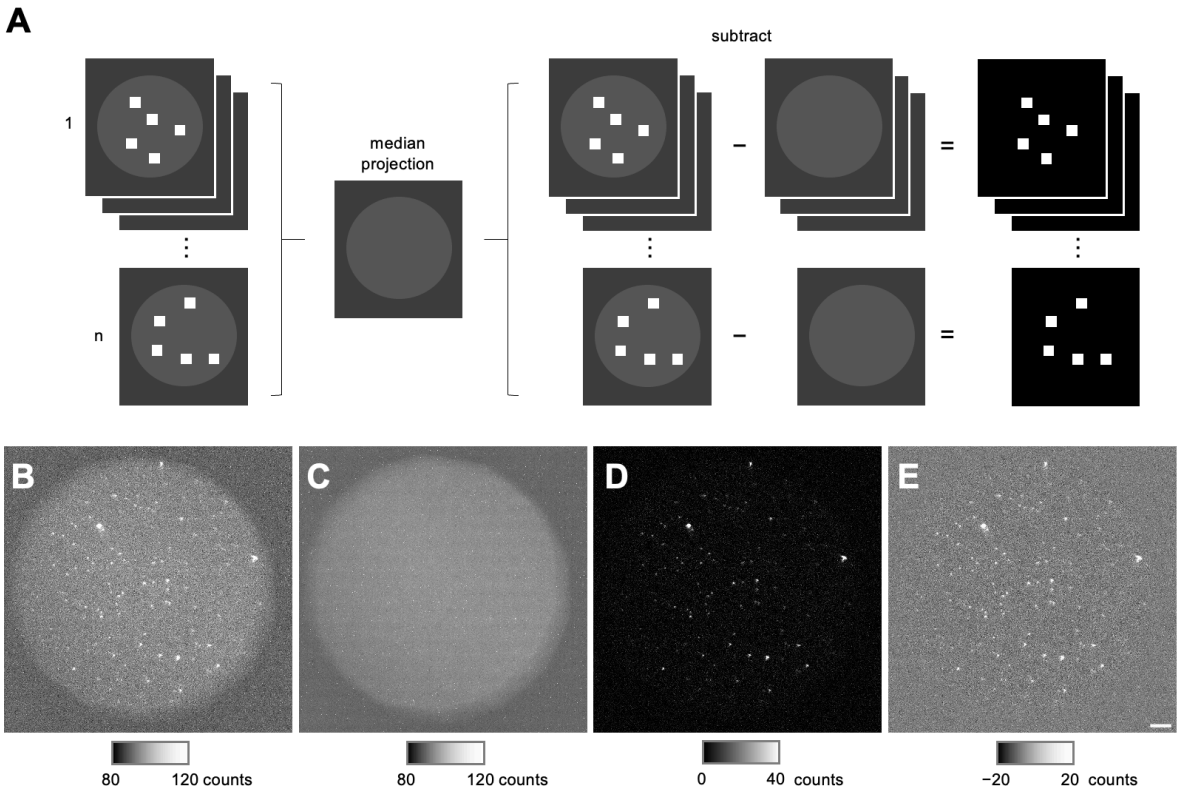

Figure 2.3, Background subtraction method.

(A) Schematic of the median projection approach, in which objects that appear in a single video are removed, while features of the field of view that are constant are retained. (B) Image without background subtraction. (C) Background obtained by the median-of-last-frames approach. (D) Background subtracted image, with the scaling set so that 0 counts is completely dark. (E) The same background subtracted image, with scaling including negative values to illustrate the zeroing of the background level.

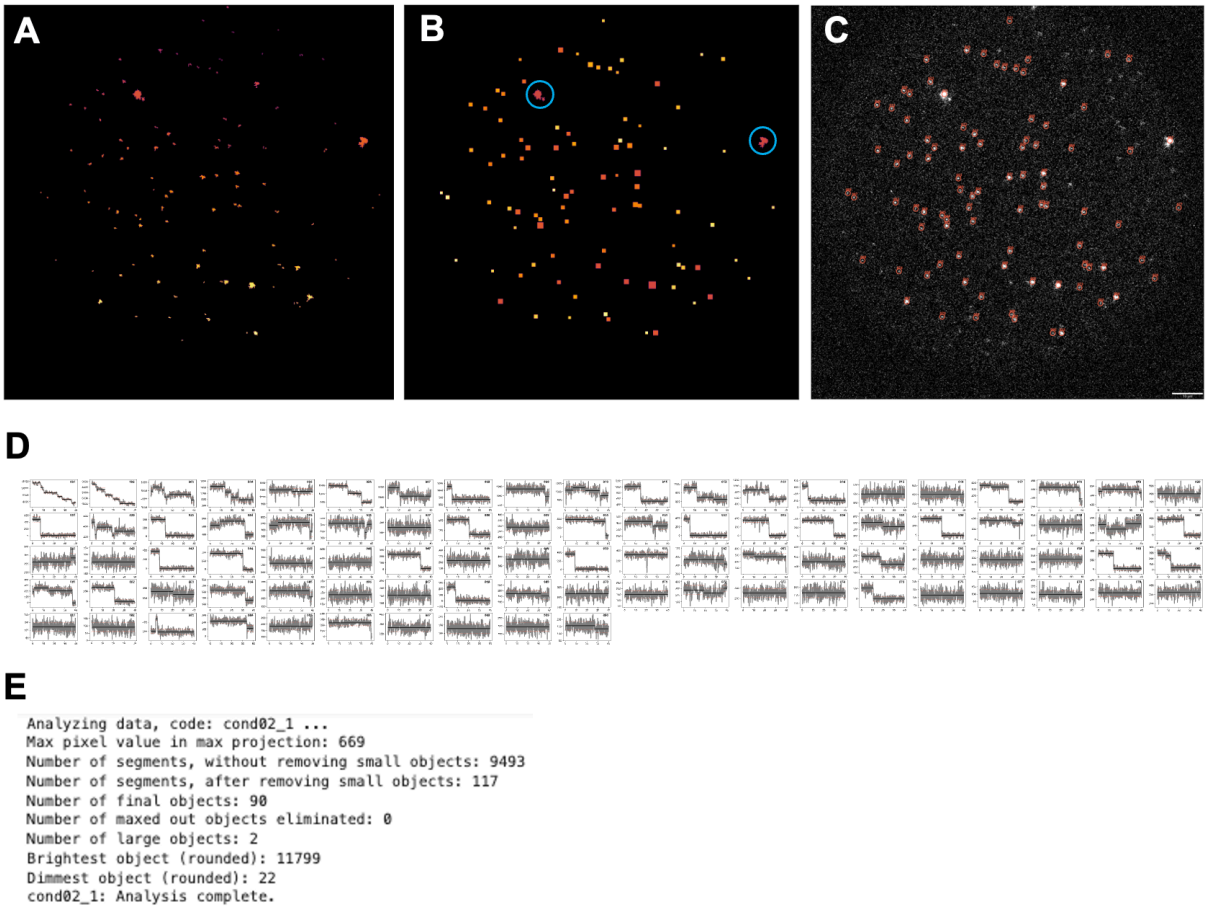

Figure 2.4, Example of single-molecule analysis pipeline in use.

(A) Segmentation of an example test image, post-binary masking. Color indicates ranked priority of the segments, based on brightness. (B) Final territories assigned to different objects of interest, which vary based on the empirical footprint of the object in the image. Blue circles indicate two objects which were large enough to be given an irregular segmented area (matching that in panel A) instead of a square box area. Color indicates ranked priority of the segments, based on brightness. (C) Actual image used for finding objects, with circles and number codes annotated in an automated fashion for each identified object, in order of brightness. Scale bar, 10 microns. (D) Menagerie of single-molecule traces automatically calculated and plotted for every object of interest. (E) Example live output from the analysis code in Python, displaying key information about the sample (the maximum pixel value in the raw data, the number of objects found, etc.)

2.3 Results

Pab1 is Predominantly Monomeric Prior to Heat Shock

In order to investigate Pab1 condensates, we first needed to understand the single-molecule imaging characteristics of uncondensed, labeled Pab1. Using our custom TIRF microscopy setup, I recorded videos of free CF 640R dye molecules and Pab1-CF 640R at a ~70% degree of labeling. I then used a self-written custom video analysis pipeline, which performs background estimation and subtraction, image segmentation, object identification based on user input, and extraction of single-molecule information such as single-molecule traces over time (i.e., object brightness over time). This analysis process is described above in Methods, "Single-Molecule Video Analysis". Examples of the background subtraction process and subsequent analysis steps are illustrated in **Error! Reference source not found.** and 2.4, respectively. In the fully processed videos and data, both free dye and labeled Pab1 exhibited the expected single-molecule behavior, such as stable "on" signal levels and stepwise (in many cases, single-step) blinking and photobleaching (Figure 2.5, A–H).

By pooling data from many single instances of free dye and labeled Pab1, we constructed initial brightness distributions for both samples. The labeled Pab1 distribution closely overlapped with the free dye distribution, consistent with Pab1 being predominantly monomeric. Larger species such as dimers were occasionally present, as evidenced by two-step photobleaching traces and a slight enrichment of labeled Pab1 over free dye at higher gray count levels (Figure 2.5, G and I). This is consistent with Pab1's reported ability to self-associate and multimerize (Figure 2.5, E–I).[65] However, since monomers were the most abundant species observed, we subsequently refer to this sample as "Pab1 monomers", and its size distribution as the "Pab1 monomer distribution".

Using the Pab1 monomer data, I estimated the brightness of a single labeled Pab1 by measuring down steps (e.g., photobleaching increments) in the single-molecule traces, binning the step sizes, and determining the most populated bin (i.e., mode of histogram). This approach yielded a brightness level of 231 gray counts. With this value in hand, we were then able to proceed with measuring the brightness of Pab1 condensates.

Pab1 Condensates are Small and Heterogeneous

To study condensates, I sought to generate labeled condensates that closely approximated wildtype Pab1 condensates (i.e., mostly wildtype Pab1 composition and only a low percentage of label present). To make these condensates, I heat shocked a mixture of 80% wildtype Pab1, 10% Pab1-biotin, and 10% Pab1-CF 640R at a ~70% final degree of labeling (thus, overall dye-to-total-Pab1 proportion of 0.07), at 42 °C for 30 minutes. (Pab1-biotin was included so that condensates could be anchored to an imaging chamber via neutravidin if needed; this procedure was ultimately not necessary.) This Pab1 mixture condensed more readily than wildtype Pab1, which required heat shock at 42 °C for 1 hour to undergo a similar degree of condensation. Despite this difference, both labeled and unlabeled condensates dispersed similarly under the same biochemical conditions (Figure 2.6). Thus, we were confident we had produced a dispersible, mostly wildtype yet imageable condensate sample formed by physiological heat shock (yeast induce a robust heat shock response at 42 °C yet can tolerate several degrees higher temperature, as well as prolonged heat shock > 30 minutes at 42 °C).[66,67]

I imaged and analyzed these condensates under the same conditions used to image and analyze Pab1 monomers. As expected, the sample contained large clusters of fluorophores, but many objects were much smaller, exhibiting single-step photophysical behavior and the brightness of only one or two dyes (Figure 2.7, A–D). A fluorescent monomer could reflect a true Pab1

monomer, or it could reflect a condensate which only acquired a single labeled Pab1. Since we separated condensates from physical Pab1 monomers by size exclusion chromatography, we suspected that many of the fluorescent monomers were in fact condensates of mostly dark Pab1.

To determine how prevalent fluorescent monomers were relative to larger clusters, I pooled the initial brightnesses of all objects identified and normalized to the predetermined brightness level of a Pab1 monomer. This brightness level was similar to the most frequent down step size observed in the condensate traces (Figure 2.7, D). This normalization revealed that the vast majority of the condensate data resembled the Pab1 monomer data (Figure 2.7, E). However, a long tail was present in the distribution extending to > 100 labeled Pab1's per cluster, which was absent from the Pab1 monomer distribution (Figure 2.7, E–F). Although large objects occurred infrequently, they potentially represented a substantial fraction of the total Pab1 content. Indeed, the cumulative distribution function of Pab1 content across all objects revealed that around 20% of the labeled Pab1 resided in objects of monomer or less brightness, while around half of labeled Pab1 resided in clusters of > 39 labels. When scaled to the labeling ratio (~0.07), this number of labels corresponds to around ~540 total Pab1 molecules—our first rough estimate of the size of a typical Pab1 condensate (combined weight of ~36 MDa, which is ~11 ribosomes).

To support this estimate, I redid the analysis to exclude monomer-like objects whose true molecular size we could not determine. I increased the binary masking threshold from a low value (intended to pick up dim objects) to the brightness of a single labeled Pab1 (see Methods, "Single-Molecule Data Analysis: Object Identification and Trace Calculation" for an explanation of this parameter). By making the identification of objects more stringent, I extracted only large clusters of ~10 or more dyes from the data, whose brightness distribution was well separated from that of Pab1 monomers (Figure 2.7, H). These condensates spanned over an order of magnitude of size,

ranging from 100's to 1000's of total Pab1 molecules (Figure 2.7, H). In the condensate-only distribution, a typical condensate (i.e., midpoint in terms of Pab1 content) was ~1000 proteins large, or between 60–70 MDa (Figure 2.7, I). This estimate is likely an overestimate, due to purposeful exclusion of objects containing one or a few labels, but also represent a more reliable analysis for the same reason.

Highly Labeled Pab1 Condensates Contain ~100's of Molecules

A size of ~1000 or fewer Pab1 molecules per condensate was smaller than we expected. The prevalence of entities with only one or a few labels, likely due to the generally small sizes of condensates, also posed an unexpected challenge in analysis. We decided to move to a condensate sample with a much higher labeling percentage.

We made condensates composed completely of Pab1 C70A/C119A/C368A/A577C labeled with CF 640R at ~70% labeling efficiency, using a heat shock of 42 °C for 20 minutes. This heat shock is slightly shorter in duration than what was previously used, although it matches the original heat shock condition published in Yoo et al. where Pab1 condensate dispersibility was reported.[56])

Since these condensates no longer contained wildtype Pab1, we did several experiments to test if they were comparable to wildtype Pab1 condensates. We confirmed that the mutant Pab1 binds RNA similarly to wildtype Pab1 (Figure 2.8, A). We also confirmed that condensates composed entirely of mutant Pab1 dispersed similarly to wildtype Pab1 condensates, using RNA binding (labeled RNA fluorescence anisotropy) as the functional readout (Figure 2.8, B). Next, we tested the dispersal of the new Pab1-CF 640R condensates. The total Pab1 in the new condensates was too low to use the fluorescence anisotropy assay. Instead, we used a centrifugation-based "TSP" (total-supernatant-pellet) assay to assess how much labeled Pab1 remained pelletable upon addition of chaperones and ATP. The labeled Pab1 was mostly pelleted in both the new condensates

("high label") and the previous, low labeling ratio condensate sample ("low label"), with almost 100% of the Pab1-CF 640R in the pellet in the high label sample (Figure 2.8, C–D).

Unexpectedly, the proportion of Pab1-CF 640R in the pellet (pPel) decreased for both samples upon addition of chaperones without ATP (Figure 2.8, C–D). Importantly, the pPel reflects the amount of Pab1 that is insoluble, not the amount of Pab1 that is fully dispersed into functional monomers. Fluorescence anisotropy experiments using RNA binding as a functional readout have shown that ATP is necessary for complete dispersal of Pab1.[56] Therefore, the ATP-independent loss of pPel may reflect a previously-unappreciated fragmentation stage of dispersal, in which larger condensates may be converted into smaller, non-pelletable condensates by chaperones independent of ATP. Nevertheless, as expected, the pPel of both samples further dropped upon addition of ATP, suggesting that highly-labeled condensates are in fact dispersible in a chaperone-dependent, ATP-dependent manner ((Figure 2.8, C–D). With these results in hand, we were confident that we had produced highly-labeled condensates which were formed via physiological heat shock and retained key qualitative characteristics of wildtype and low labeling ratio condensates.

We imaged and analyzed these condensates to determine their size distribution. The entities observed in this sample were highly heterogenous in size, spanning multiple orders of magnitude of brightness (Figure 2.9, A). Due to the high brightness of many condensates, images were taken at a higher bit depth and lower gain than previous images, so that the brightest condensates could be accurately measured. A Pab1 monomer distribution was remeasured under these new imaging conditions, the signal of a monomer was redetermined, and the distribution of condensate sizes (in terms of number of labels) was produced with this new information. Comparison to the Pab1 monomer distribution revealed that the 70% labeled condensate sample contained a considerable proportion of monomers and small oligomers (Figure 2.9, B). Since most of the Pab1 is labeled, it

seems likely that condensate samples contain a real population of monomers and small oligomeric assemblies. However, a considerable amount of the labeled Pab1 exists in assemblies of ~10 or more labels, which are nearly absent from the Pab1 monomer distribution (Figure 2.9, C).

Scaling the condensate size distribution to number of Pab1 proteins and to the amount of Pab1 present in each object revealed that around half of the Pab1 resides in clusters of more than 192 Pab1 molecules, and that only a small percentage of Pab1 is actually monomeric (Figure 2.9, D). This estimate of ~200 molecules (slightly > 10 MDa) is smaller than the previous estimates but within the same order of magnitude (~100's of molecules per condensate). (The heat shock used on this sample was also shorter in duration.)

As was done with the low labeling ratio sample, the single-molecule analysis was repeated using higher thresholds (masking threshold at the level of a Pab1 monomer). This approach once again was successful at isolating clusters of multiple dyes in the data, while excluding monomeric material (Figure 2.9, E–F). Isolating clusters more clearly revealed the range of condensate sizes, which was highly heterogenous and spanned two orders of magnitude (Figure 2.9, E). Scaling the distribution to number of Pab1 proteins and amount of Pab1 present in each object showed that of Pab1 that is clustered, around half resides in clusters of more than 272 Pab1 molecules (Figure 2.9, G). This figure for the size of a typical condensate corresponds to ~17 MDa or ~5 ribosomes.

A summary of the four estimates of condensate size, the sample type, and how the analysis was performed is provided in the table below. Estimates of "Ribosomal Equivalent" size are given in terms of number of ribosomes equaling the same weight, assuming a yeast ribosomal weight of approximately 3.3 MDa.[68,69]

Table 2.4, Size Estimates of a Typical Pab1 Condensate.

Estimate (number of Pab1 proteins)	Weight (MDa)	Ribosomal Equivalent	Sample Type	Analysis Method (i.e., which objects are considered in the analysis)
557	36	11	7% labeled	Account for all objects
1048	67	20	7% labeled	Only consider clusters/condensates
192	12	4	70% labeled	Account for all objects
272	**17**	**5**	**70% labeled**	**Only consider clusters/condensates**

The final estimate is bolded as the preferred estimate, for the following reasons. (1) It was obtained using the highly-labeled sample, meaning that numbers of dyes could more confidently be extrapolated to numbers of proteins. (2) It only considered objects which were clusters of many dyes and excluded fluorescent monomers. Although the existence of fluorescent monomers in the condensate samples is an important finding, these species only constitute a minor percentage of the total Pab1 and (for the highly-labeled sample) likely do not represent true condensed material, in the sense of actual assemblies of multiple molecules.

Microscopically Observed Pab1 Condensates are Rapidly Dismantled

We next turned to Pab1 dispersal. Previous bulk biochemical experiments showed that three chaperones (Sis1, Hsp70, and Hsp104) and ATP are necessary to restore Pab1's RNA binding activity once condensed, and that this recovery of Pab1 occurs within ~20 minutes. Little is known about the dynamics of individual condensates during this dispersal process—how does the size of condensates change over the course of dispersal, and do condensates of all sizes disperse similarly? The same bulk biochemical rate and completeness of dispersal might be explained by very different molecular scenarios: (1) all condensates disperse as one population over the entire time course of dispersal; (2) only large condensates are dispersed efficiently, but they contain most of Pab1; (3) only smaller condensates are dispersed efficiently, but they contain most of Pab1; (4) initiation of dispersal on any single condensate is stochastic and infrequent, but dispersal proceeds rapidly once

initiated. Visualizing the dispersal process directly could allow us to distinguish between these possibilities and understand the dynamics and underlying mechanisms of condensate dispersal.

To visualize condensate dispersal, we returned to the sparsely-labeled condensates (with ~7% dye content), since these condensates contained mostly wildtype Pab1 and were dispersed similarly to wildtype condensates (Figure 2.6). To investigate dispersal dynamics, we decided to focus on four conditions: (1) complete reaction mix containing condensates, the chaperones Sis1, Hsp104, and Ssa2 (one of the yeast Hsp70's), ATP, and creatine kinase and phosphate; (2) reaction lacking ATP; (3) reaction lacking ATP and chaperones; and (4) complete reaction mix plus Sse1, a chaperone nonessential for dispersal. Sse1 is an Hsp70 nucleotide exchange factor (NEF) which in low amounts boosts the rate of Pab1 condensate dispersal; it is also known to facilitate protein disaggregation both *in vivo* and *in vitro*.[56,70,71] In the human system, the NEF has been proposed to improve chaperone-mediated dispersal of amyloid fibrils by favoring clustering or close packing of Hsp70 on the substrate; how Sse1 improves Pab1 dispersal mechanistically remains unclear.[72]

To evaluate dispersal under these four conditions, I imaged each mixture after 20 minutes of incubation at room temperature, and I compared the results to data from condensates in buffer alone. I evaluated the extent of dispersal by calculating the proportion of fluorescent signal present within clusters of more than five dyes' brightness, termed pClustered (Figure 2.10). As expected, the pClustered of condensates alone was not significantly different from condensates with the ATP regeneration system alone or with chaperones and ATP regeneration (but no ATP). Furthermore, the pClustered of the complete reaction mixtures, both with and without Sse1, were significantly different and close to zero (mean value ~0.1). Thus, we verified by direct microscopy that dispersal of large clusters of Pab1 is near-complete after 20 minutes of incubation, with or without Sse1.

Dispersal is Heterogeneous and Partially ATP-Independent

This experiment was an important proof-of-concept that we could image dispersal directly and produce results that are qualitatively consistent with previous biochemical findings. However, these data only provided a snapshot of the distribution of Pab1 at a specific time point (20 minutes), without providing insight into dynamics at the single-condensate level. To visualize the dispersal of individual condensates, Diangen Lin devised an approach to acquire timelapse videos of single condensates with camera-synchronized, shuttered sample illumination (see Methods, "Timelapse Microscopy"). This method drastically reduced photobleaching of condensates to a few percent over 20 minutes of imaging, such that loss of fluorescence signal beyond this low level could be interpreted as Pab1 dispersal. Using this approach, Diangen conducted timelapse experiments on condensates under the four conditions of interest, on which I conducted single molecule analyses.

To extract single-condensate dispersal data from the videos, there were two main obstacles. First, most of the objects present in the sparsely-labeled condensate sample are small (one or two dyes), meaning that their dispersal cannot be meaningfully measured. To filter out these objects, I found the brightness of a dye monomer in the no-dispersal, "basal" condition (only condensates and ATP regeneration system, without ATP or chaperones); I then chose analysis settings that only detected objects brighter than three dyes' signal (Figure 2.11, A–B). Second, condensates that do not remain stable and well-separated from others (that is, if they move, disappear, or merge with or are covered by another condensate) would not provide an easily-interpretable signal trace. To account for these possibilities, I checked the single-condensate traces for frame-to-frame shifts of more than half the starting signal of the trace, and removed any such trace from further analysis. The traces which were filtered out are highlighted in Figure 2.11, C–F.

With the curated single-condensate data, I then examined dispersal by comparing the initial distribution of condensate sizes to different timepoints for each condition (Figure 2.12). The size distributions of the basal condition and the chaperone-only condition (no ATP) did not significantly change at any timepoint tested, including at 20 minutes (Figure 2.12, A–B). However, the reactions with ATP both showed significant changes midway through dispersal (at 8 minutes without Sse1, and at 12 minutes with Sse1). Notably, in both cases, the entire size distribution seemed to shift *en masse* to lower sizes, suggesting that condensates were dispersing together as a population, rather than a particular size regime dispersing selectively, or single condensates dispersing stochastically (Figure 2.12, C–D).

To confirm this interpretation, I plotted the signal traces of individual condensates for each condition. The basal condition remained stable throughout the course of dispersal, with only a few percent decrease in the mean trace, attributable to photobleaching (Figure 2.13, A). Unexpectedly, adding chaperones without ATP led to a small but striking downward deflection of the condensate traces, suggesting that there is in fact ATP-independent dispersal occurring (Figure 2.13, B). This observation is consistent with the TSP experiment showing ATP-independent loss of Pab1 pelleting in the presence of chaperones (Figure 2.8). Adding ATP with chaperones led to slightly greater, yet still incomplete, dispersal, with noticeably greater variability at the single-condensate level (Figure 2.13, C). Addition of Sse1 led to the greatest mean dispersal and the greatest heterogeneity, with a single trace achieving complete dispersal, many traces achieving partial dispersal, and a few traces which did not disperse at all (Figure 2.13, D). Quantification of the apparent mean dispersal under each condition showed that addition of chaperones, ATP, and Sse1 each led to significant increases in the extent of dispersal, starting from similar initial size distributions of condensates (Figure 2.13, E–G). Combined, these data show that dispersal of condensates is frequently incomplete at

the single condensate level, is partially ATP-independent, and is increasingly heterogenous as the degree of dispersal increases (with sequential addition of chaperones, ATP, and Sse1).

Dispersal of Larger Condensates Is Not Favored, Even with Sse1

Finally, I examined the relationship between condensate size and dispersal outcomes. The biochemical data on Pab1 dispersal are consistent with a model in which Hsp70 must cluster onto condensates to recruit Hsp104.[56] This model is also consistent with the proposed mechanism of Hsp104 activation by multiple Hsp70's, as well as the idea that Hsp70 clustering is important for protein disaggregation in other context (such as amyloid dispersal).[72,73] The exact binding sites of Hsp70 on the Pab1 condensate are not known. However, it is plausible that below a minimum size (i.e., below a certain maximum occupancy of Hsp70), a condensate cannot be effectively dispersed. Moreover, NEFs such as Sse1 likely facilitate dispersal by enriching the clustering of Hsp70.[72] If this model is correct, then we might expect Sse1 to enhance dispersal of larger condensates (which have a greater capacity for Hsp70 binding and clustering) than smaller condensates.

With the hypothesis that larger condensates may disperse better, especially in the presence of Sse1, I plotted the relationship between initial condensate size (in terms of Pab1 number) and the apparent dispersal of a condensate (Figure 2.14). In contradiction to this hypothesis, none of the three conditions showing dispersal (with chaperones alone, with ATP, and with Sse1) showed a positive relationship between size and dispersal. In fact, dispersal with Sse1 showed a slight (r^2 = 0.11) negative correlation between size and dispersal, and apparent dispersal above 50% was not observed in condensates of ~1000 Pab1 proteins or larger (Figure 2.14, D). Thus, dispersal does not appear to improve with increasing condensate size under any condition tested, and most of all in the presence of Sse1.

2.4 Discussion

In this chapter, we have visualized Pab1 condensates at the single-molecule level for the first time and quantified their size in molecular number. We have also observed condensate dispersal at the single-condensate level. Although single-molecule studies have been pioneered on unfolded and aggregated proteins as chaperone substrates, parallel single-molecule investigations have been lacking on condensates as physiological, heat-induced substrates of chaperones.[74,75]

An important insight gained from this work is a ballpark reference for the size of a model condensate formed by a physiological heat shock, as well as a quantitative appreciation for the degree of heterogeneity of sizes that form. Condensates tend to be ~100's of molecules big, with a lowest estimate (from these data) at slightly under 200 proteins, and the largest estimate at ~1000. (Importantly, these estimates are merely reference points and should not be interpreted as the size of most condensates. The term "typical condensate" as used in this chapter means "a condensate at the midpoint of the cumulative distribution of protein in the sample," or in layperson's terms, a midsize condensate.)

This size regime informs us as to the length scale of the molecular problem chaperones are dealing with. A condensate of ~200 molecules might be approximated as a cube with around five molecules to a side, or tens of nanometers. Depending on the steric footprint of chaperones, there may only be room for a few chaperones to bind at a time, and competition for binding (for instance, between functional Sis1 and inhibitory Ydj1) at a single site could have implications for whether a condensate disperses. JDP and Hsp70 bind to amyloid fibrils at 1:10 and 1:2 stoichiometries with substrate.[72] If these stoichiometries roughly carry over to Pab1 condensates, this might be equivalent to a single JDP occupying one side of a five-molecule cube.

From observing condensate dispersal directly, we learned that condensate dispersal is often incomplete when observed directly. However, extensive previous work has shown that Pab1 dispersal is complete in biochemical assays.[56] This discrepancy could involve idiosyncrasies of the imaging approach used (charge or chemical properties of the chamber surface, or an impairment of dispersal due to landing on the chamber surface, for example). This discrepancy could also reflect true incompleteness of dispersal, which could not have been detected without a direct, microscopic window into condensate dispersal. Understanding what is causing this discrepancy is a potential area of follow-up investigation.

Directly viewing condensate dispersal has also led to interesting insights into the stages or possible types of dispersal that occur. There is a clear effect on condensate size of adding chaperones, even in the absence of ATP. From functional assays, we know that ATP is required to restore Pab1's RNA binding activity (or, in other words, return it fully to a folded monomeric state). Thus, there may be a stage of fragmentation of large condensates, which is insufficient to restore Pab1's RNA binding, but is a mode or early stage of disaggregation. Entropic pulling, simply by concentrating Hsp70 on a substrate, is thought to underlie chaperone-mediated amyloid fibril dispersal and may also carry over to Pab1 condensates.[56,72] A version of this process might not require ATP, but only sufficient chaperone binding; it is also known not to require Hsp104.

This entropic puling process is thought to rely on the activity of an Hsp70 NEF to help cluster Hsp70, by removing lone, unclustered Hsp70 molecules from the substrate.[72] Given this model, it would seem likely that an NEF (such as Sse1) would enhance the dispersal of larger substrates, upon which Hsp70 can be clustered. However, such an effect was not observed in our data. Why Sse1 enhances condensate dispersal, whether it does so for the same reasons why NEF

enhances dispersal of other substrates, and where Sse1 is acting (on which condensates, and at what stage(s) of the dispersal process) are intriguing areas for future work.

Continuing single-molecule investigations of condensates and their dispersal has the potential to continue to reveal new insight in this molecular process. Visualizing the effects of specific JDPs, for example, could greatly inform out understanding of their function. Does dispersal of all condensates slow equally in the presence of Ydj1, or are certain sizes or types of condensates differentially affected? Which condensates do Sis1, Ydj1, Hsp70, and Hsp104 prefer to bind during dispersal? These and other molecular-scale questions will hopefully be answered by future studies.

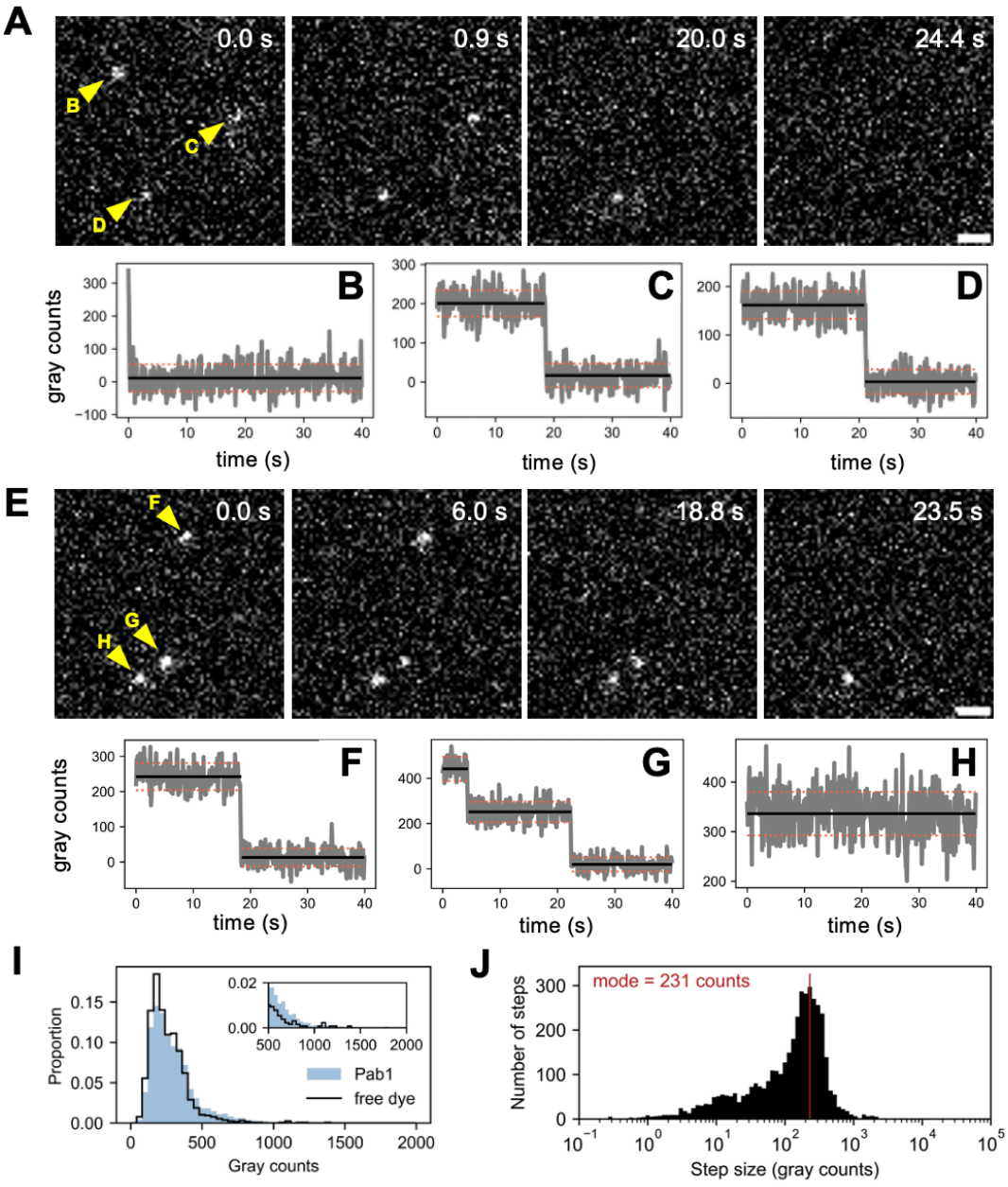

Figure 2.5, Single-molecule imaging of Pab1 monomers.

(A) Example frames of a free dye video. Scale bar, 2 microns. (B–D) Single-molecule traces of objects in panel A. (E) Example frames of a Pab1-CF 640R video. Scale bar, 2 microns. (F–H) Single-molecule traces of objects in panel A. (I) Pab1 versus free dye brightness distributions. (J) Pab1 distribution of downward step sizes in the levels found by changepoint detection, with the mode bin annotated in red.

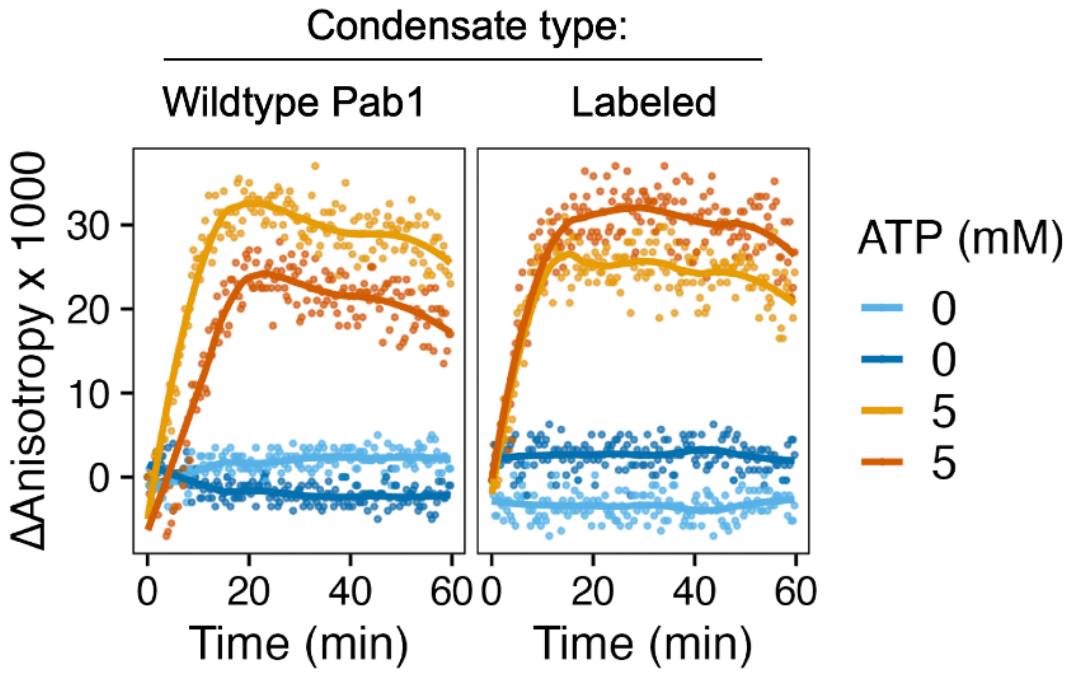

Figure 2.6, Dispersal of wildtype and labeled condensates.

Dispersal of wildtype Pab1 condensates was compared to dispersal of 7% CF 640R, 10% Pab1-biotin labeled condensates. Chaperone concentrations: 0.5 μM Sis1 dimer (1 μM monomer), 1 μM Ssa2, 0.1 μM Hsp104 hexamer (0.6 μM hexamer).

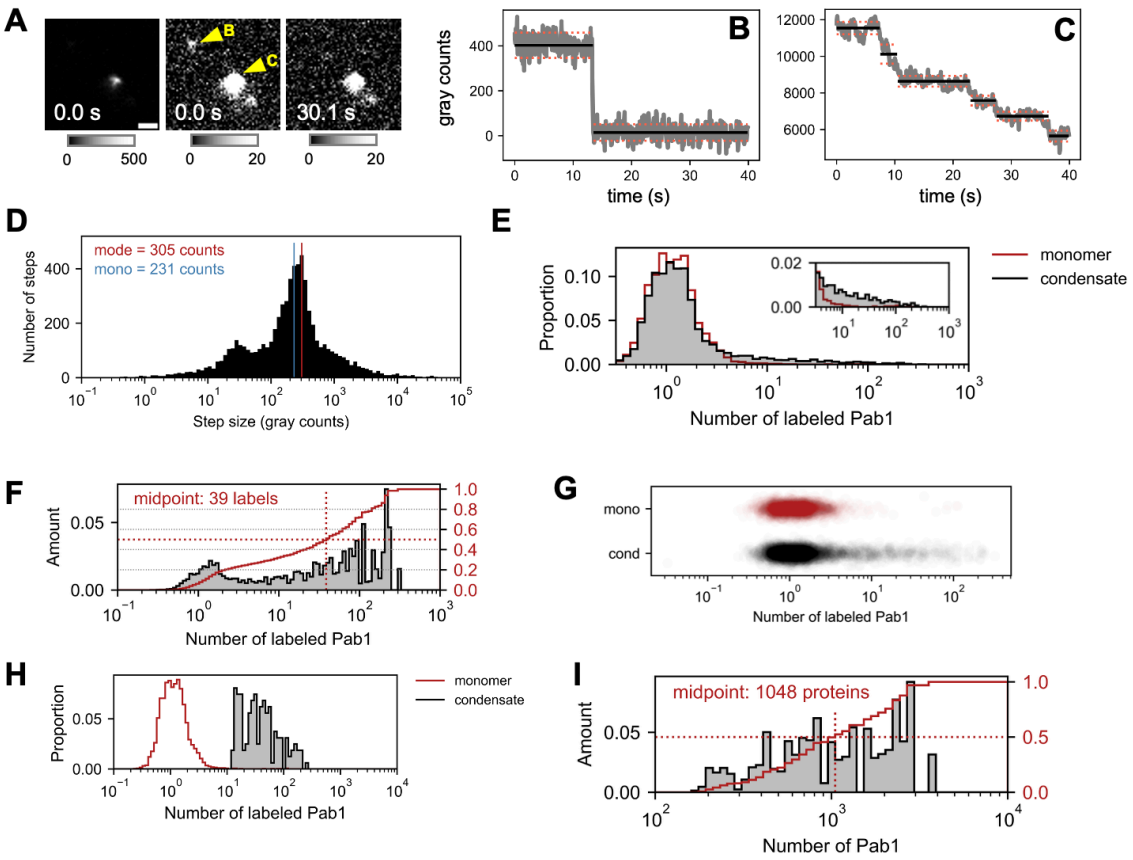

Figure 2.7, Single-molecule imaging of Pab1 condensates.

(A) Example frames of a video of Pab1 condensates. Left and center are same image at different scaling. Scale bar, 2 microns. (B–C) Single-molecule traces of the objects in panel A. (D) Distribution of downward step sizes in the levels found by changepoint detection, with comparison of the mode step size in the condensate data (red) to the previous signal level found in the monomer data (blue). (E) Condensate size distribution normalized to number of fluorescent labels, with the Pab1 monomer distribution in red for reference. (F) Condensate size distribution, weighted by amount of labeled Pab1 present in each bin, with cumulative distribution function in red. (G) Condensate versus monomer size distributions plotted as a scatter plot. (H) Condensate size distribution recalculated with higher detection thresholds in analysis, normalized to number of fluorescent labels, with the Pab1 monomer distribution in red for reference. (I) Recalculated condensate size distribution in terms of estimated Pab1 number, weighted by amount of Pab1 present in each bin, with cumulative distribution function in red.

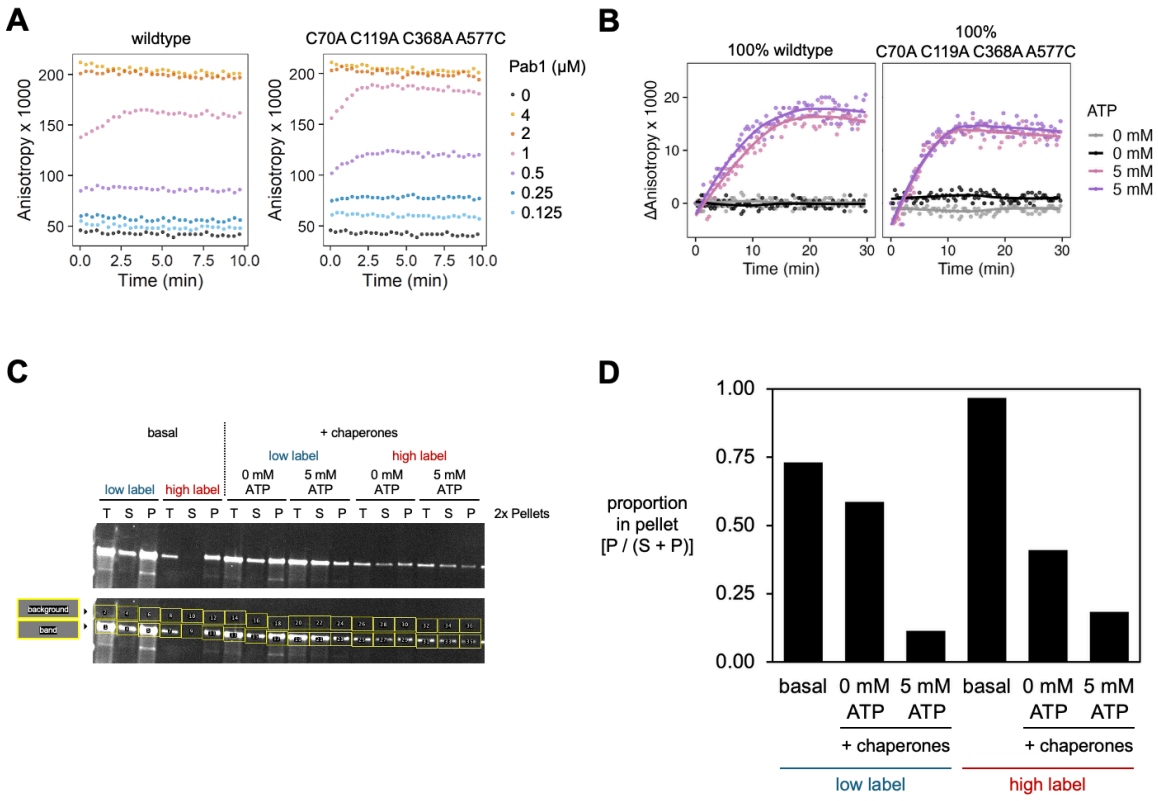

Figure 2.8, Biochemical validation of 100% Pab1 mutant condensates.

(A) Binding of Pab1 or Pab1 C70A C119A C368A A577C to 200 nM fluorescently labeled FAM-A19 RNA. (B) Dispersal of 100% wildtype or 100% Pab1 mutant condensates via fluorescence anisotropy assay. Chaperone concentrations: 0.5 μM Sis1 G210C dimer (1 μM monomer), 1 μM Ssa2 C264A C303N D555C, 0.1 μM Hsp104 hexamer (0.6 μM hexamer), 50 nM Sse1. (C) SDS-PAGE gel of dispersal of 10% Pab1-biotin ~7% Pab1-CF 640R (low label) and ~70% Pab1-CF 640R condensates by TSP assay. Image shown is taken in a red fluorescence channel. Lower panel shows the same image, annotated with regions of interest quantified to obtain panel D. (D) Quantification of panel C, showing proportion in pellet.

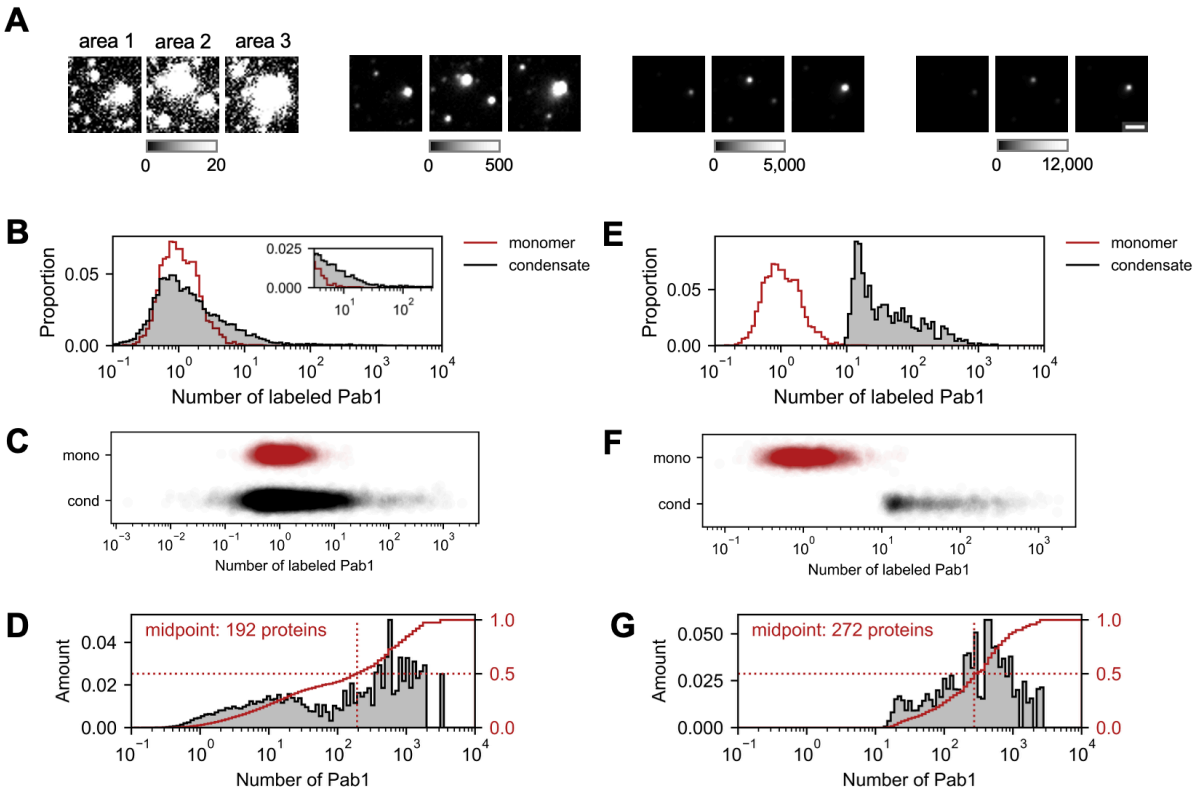

Figure 2.9, Imaging of highly-labeled condensates.

(A) Example images of three fields of view of condensates. Scaling is reshown at four different colorbars of intensities to highlight the difference in brightness (in arbitrary units) of side-by-side condensates. Scalebar, 2 microns. (B) Condensate size distribution normalized to number of fluorescent labels, with the Pab1 monomer distribution in red for reference. (C) Distributions replotted as a scatter plot. (D) Condensate size distribution in terms of Pab1 number, weighted by amount of Pab1 present in each bin, with cumulative distribution function in red. (E–G) Matching plots to panels B–D, after reanalysis using higher object identification thresholds in analysis to exclude fluorescent monomers.

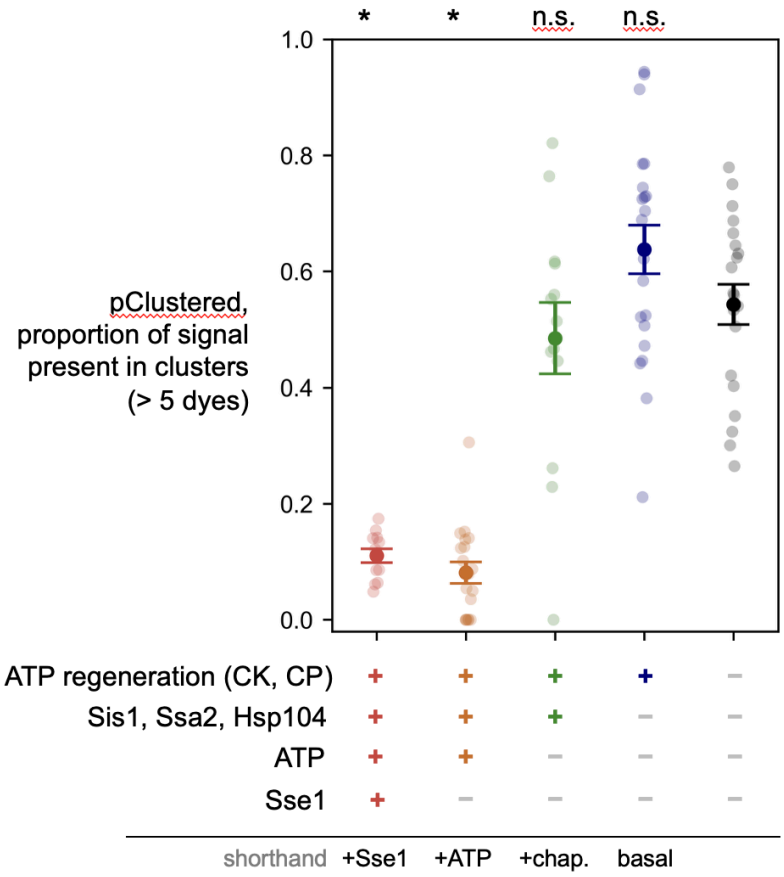

Figure 2.10, Bulk imaging of labeled condensate dispersal at 20 minutes.

Chaperone concentrations: 0.5 μM Sis1 dimer (1 μM monomer), 1 μM Ssa2, 0.1 μM Hsp104 hexamer (0.6 μM hexamer), 50 nM Sse1.

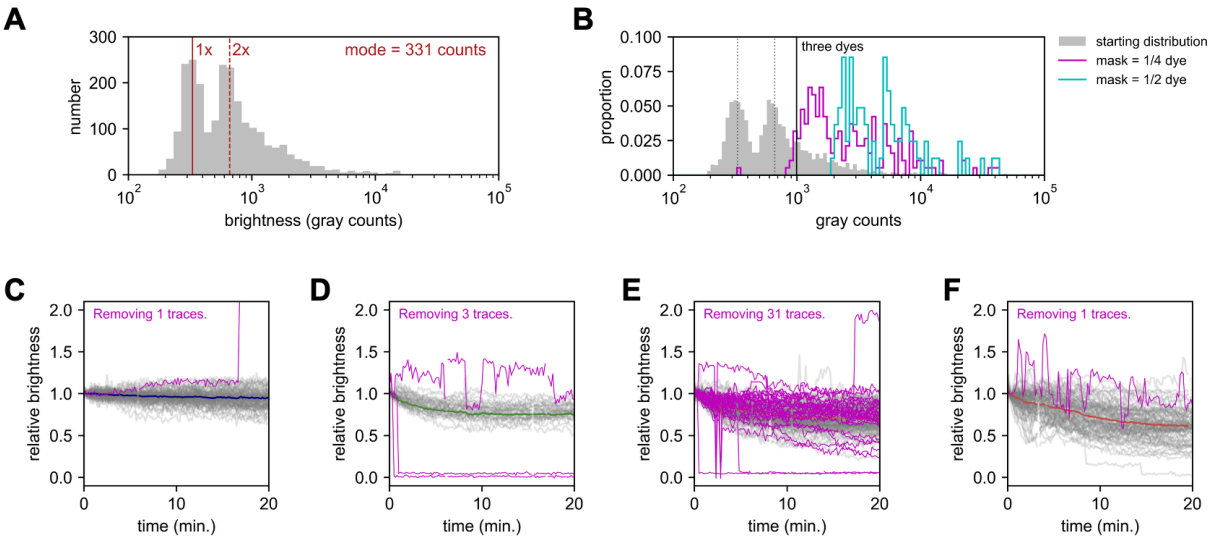

Figure 2.11, Analysis of single-condensate dispersal traces.

(A) Distribution of initial brightnesses of objects found in the basal condensate condition (creatine kinase and phosphate only). Mode bin annotated in red as the brightness of a single label; brightness of a dimer also annotated with dashed line. (B) Size distributions found in the basal condensate condition with object identification reperformed, using thresholds based on the brightness of 0.25 labels or 0.5 labels. The brightness of three labels is shown as a solid line, and the brightness of one and two labels is shown with dotted lines. The original distribution is shown in gray. (C–F) All single-condensate traces found in each of the four conditions (basal, plus chaperones, plus chaperones/ATP, plus chaperones/ATP/Sse1) using the 0.5x label object identification thresholds. Eliminated traces (due to signal fluctuations of more than 0.5x initial intensity in a single frame) are shown in magenta.

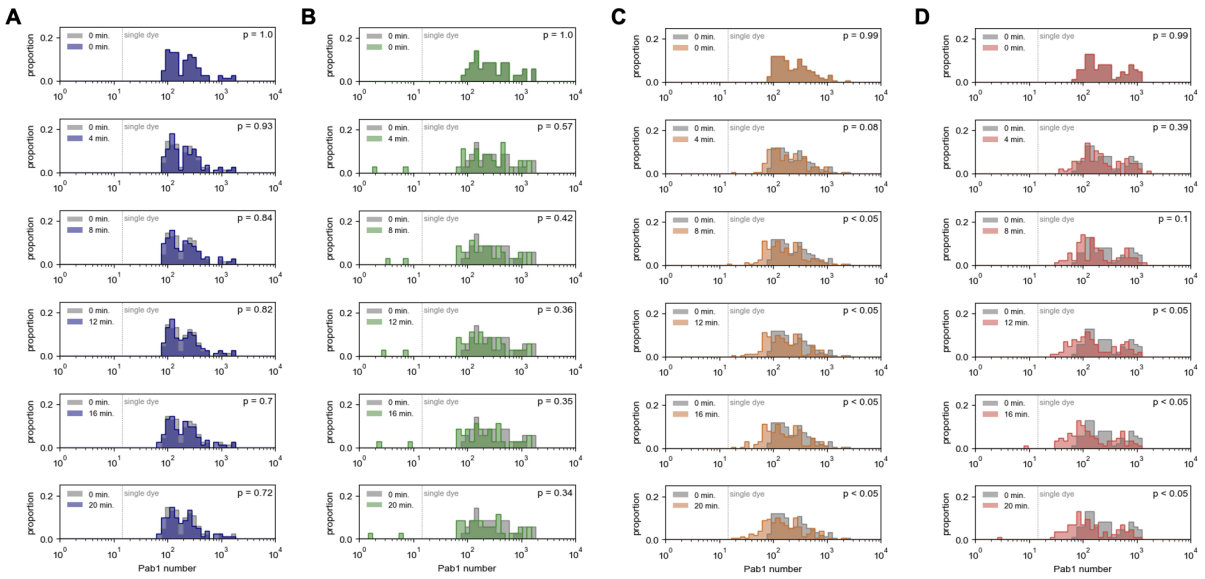

Figure 2.12, Size distributions of condensates over time.

(A) Basal condition (creatine kinase/phosphate ATP regeneration system only). (B) Condensates with ATP regeneration and Sis1, Ssa2, and Hsp104. (C) Condensates with ATP regeneration, chaperones, and 5 mM ATP. (D) Condensates with ATP regeneration, chaperones including Sse1, and 5 mM ATP.

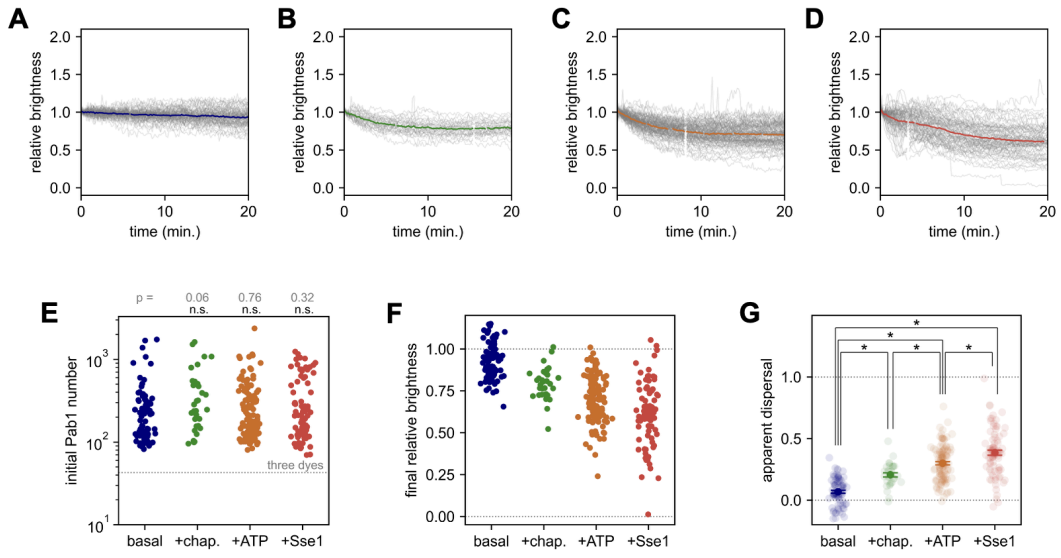

Figure 2.13, Dispersal outcomes at the single condensate level.

(A–D) Single-condensate traces under the four dispersal conditions: (A) Basal condition (creatine kinase/phosphate ATP regeneration system only). (B) Condensates with ATP regeneration and Sis1, Ssa2, and Hsp104. (C) Condensates with ATP regeneration, chaperones, and 5 mM ATP. (D) Condensates with ATP regeneration, chaperones including Sse1, and 5 mM ATP. (E) Distributions of initial sizes of condensates in each condition in terms of Pab1 number, with the results of independent T-tests against the basal condition annotated. Signal level of three labels is annotated in gray. (F) Dispersal outcomes at 20 minutes, in terms of final relative brightness. Reference lines at 0 and 1 shown. (G) Data in panel F converted into apparent dispersal at 20 minutes. References lines at 0 and 1 shown. Means and standard errors of the means plotted with high alpha, and individual condensates plotted with low alpha. Results of independent T-tests shown with stars indicating significance.

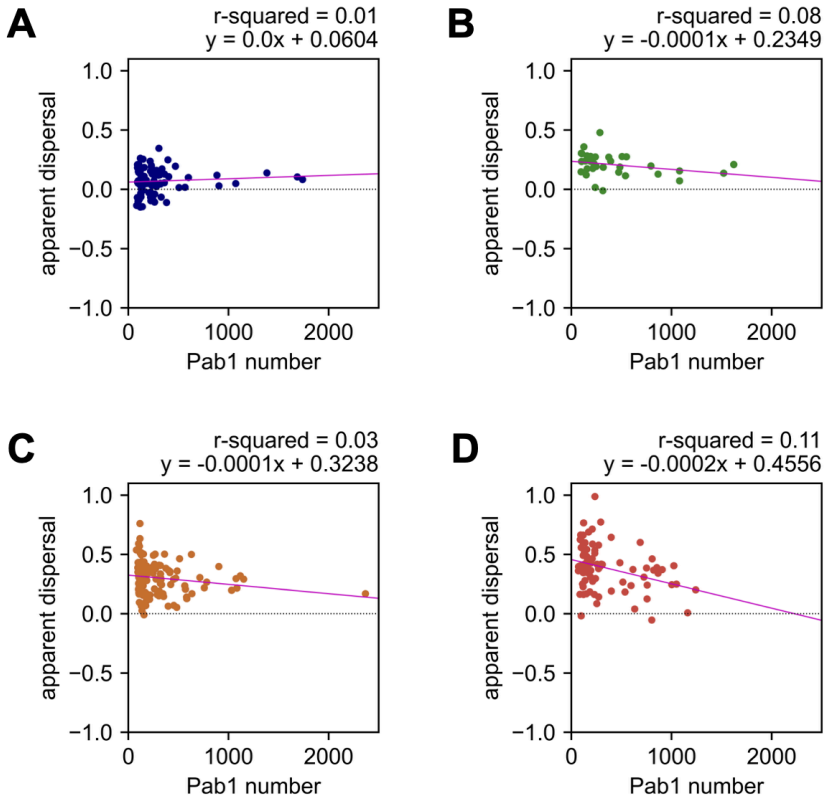

Figure 2.14, Relationships between dispersal outcomes and sizes.

(A) Basal condition (creatine kinase/phosphate ATP regeneration system only). (B) Condensates with ATP regeneration and Sis1, Ssa2, and Hsp104. (C) Condensates with ATP regeneration, chaperones, and 5 mM ATP. (D) Condensates with ATP regeneration, chaperones including Sse1, and 5 mM ATP.

3 | JDPs

3.1 Introduction

One of the striking features of Pab1 condensate dispersal is how J-domain proteins (JDPs) are involved, specifically Sis1 and Ydj1. JDPs are a diverse family of chaperones, whose primary function is to catalyze the ATPase activity of Hsp70 via binding of their J-domain to the nucleotide binding domain of Hsp70. Both Sis1 and Ydj1 share this molecular function, as well as a common overall domain architecture: a dimerization domain, two client binding domains (also termed C-terminal domains or CTDI and CTDII) on each monomer, and a J-domain on each monomer linked to CTDI by a flexible "GF" or "GF/GM" region, named for their amino acid content (Figure 3.1). In yeast cells, Ydj1 and Sis1 are the two chief JDPs (~41,000 and 28,000 proteins per cell) and are thought to perform generalist functions in guiding Hsp70 to various protein clients.[76] In the reactivation of misfolded luciferase, both Sis1 and Ydj1 are functional, with Ydj1 possessing greater activity than Sis1.[54] However, in the dispersal of Pab1 condensates, only Sis1 is functional, while Ydj1 is not only nonfunctional but inhibitory.[56]

Dissecting the molecular basis of this divergent behavior—why Sis1 functions, why Ydj1 fails to function, and more broadly what confers dispersal function or inhibitory activity to a JDP—could help us understand the physiological roles of different JDPs in cellular responses to heat shock, as well as how JDPs fundamentally work.

The functional difference between Sis1 and Ydj1 in condensate dispersal highlights a broader discussion in the chaperone field around class-specific JDP behaviors. That is, Class B JDPs (which include Sis1) have been increasingly observed to possess a unique ability to disperse large protein assemblies (amyloid fibrils, large aggregates), which is not shared by Class A JDPs

(such as Ydj1).[53,57,77,78] This difference is puzzling, as both Class A and B JDPs possess domains for client binding and stimulation of ATP hydrolysis in a similar arrangement, and are thus thought to participate in the same three-step cycle which transfer a substrate to Hsp70: (1) client binding, (2) handoff of client to Hsp70, and (3) stimulation of ATP hydrolysis which converts Hsp70 into its tight-binding form and completes the handoff process (Figure 3.2). What about this process differs in Sis1 and other Class B JDPs to enable their specialized function in the dispersal of large protein assemblies?

Regulation of Class B JDPs by the C-terminal EEVD of Hsp70 has emerged as a leading explanation. In certain Class B JDPs, such as Sis1 and human DNAJB1, the client binding domain CTDI binds directly to the EEVD tail of Hsp70.[77,79–81] This binding is able to unlock the J-domain from a basally repressed state into an Hsp70-activating state; moreover, this binding occurs at a substrate binding cleft and can thus compete directly with substrate.[77,80] Thus, in Sis1 and Class B JDPs, the client handoff and Hsp70 stimulation steps are coordinated through EEVD binding. Class A JDPs such as Ydj1 are not regulated in this way, and their chaperone activities are largely EEVD-independent (although it has been reported that they can bind EEVD).[77,78,81,82] In contrast, Sis1 and DNAJB1's chaperone functions are generally impaired in the absence of EEVD.

However, we are still far from a satisfying molecular picture of how Sis1 or other Class B JDPs catalyze disaggregation. Why conceptually would interaction with the EEVD tail confer the ability to disperse—and is the EEVD tail truly the key difference underlying function in dispersal? Why would Ydj1, which has a constitutively active J-domain (and so does not even need EEVD binding to become unrepressed), not be able to perform the functions of a JDP which is repressed until it binds Hsp70? One promising model is that Sis1 relies on the EEVD tail to catalyze the substrate handoff step via direct competition with substrate, and a similar mechanism does not

exist in Ydj1 (Figure 3.3). Thus, Sis1 can properly transfer its client (such as a condensate) to Hsp70, while Ydj1 cannot. Yet even this explanation seems incomplete. Why would Ydj1 not be impaired in other functions which presumably require substrate handoff to Hsp70?

There is even disagreement in the field about whether JDPs should be thought of as Class A and B, as the behaviors of JDPs within the same class are often hetergeneous.[83] Whether the EEVD binding mechanism is a shared trait of all Class B JDPs, and whether insights we have learned about other EEVD-binding JDPs (or even Sis1 itself in other contexts) will carry over to Sis1-mediated condensate dispersal, have not been shown.

In this work, I sought to shed light on the unique functions of Sis1 and Ydj1 in condensate dispersal, a relatively new and unstudied function of JDPs. First, I sought to distinguish at what step(s) of the JDP cycle Sis1 and Ydj1 differed, starting with substrate binding. Then, I took a more granular, detailed approach to dissecting the roles of EEVD and specific JDP domains in dispersal. By unraveling the nuances of Sis1 and Ydj1 action in condensate dispersal, I hoped to provide new insight not only into how these specific proteins function, but also into broader discussions of how JDPs work, how they should be classified, and what makes them functionally different.

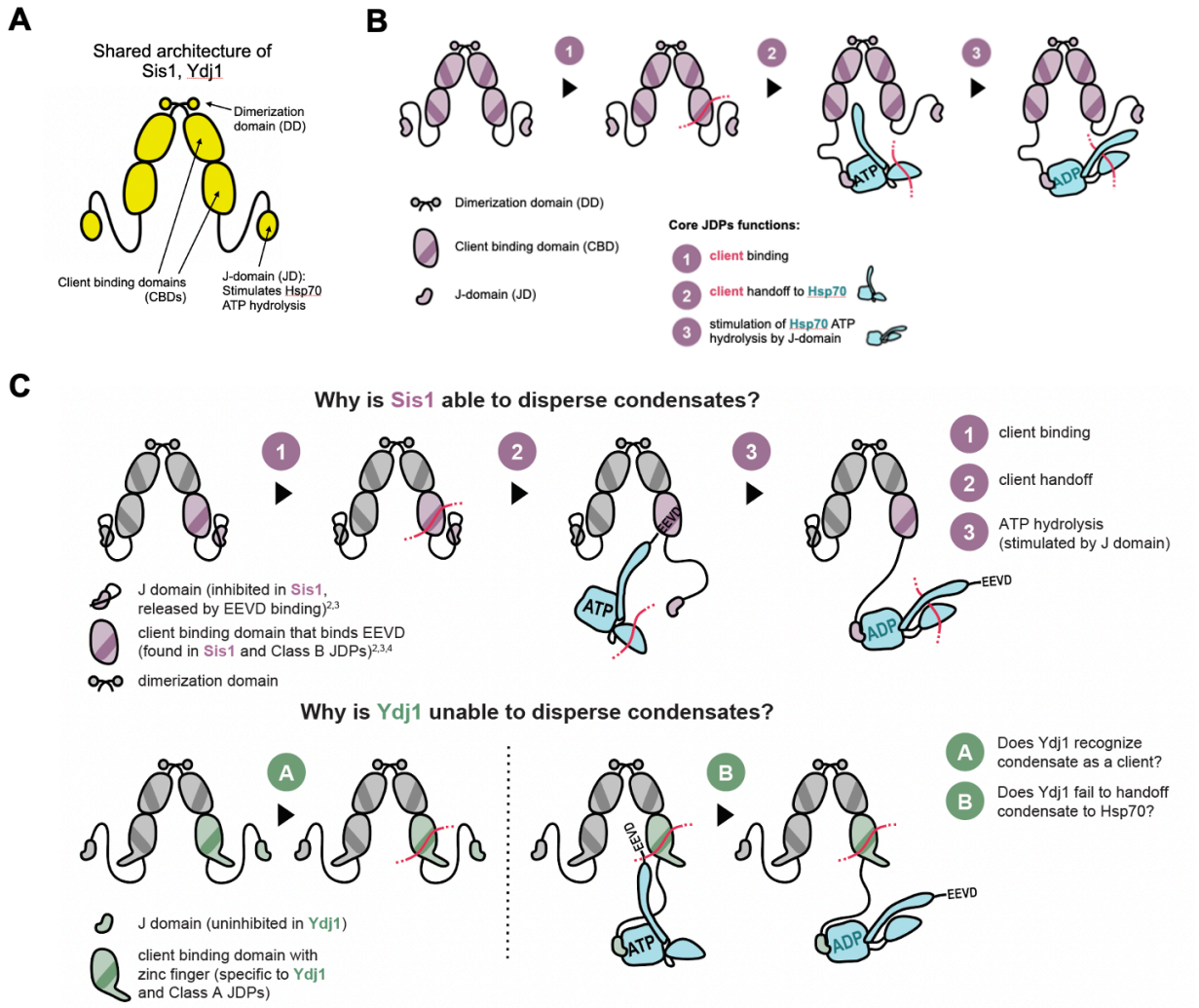

Figure 3.1, Sis1 and Ydj1 domain architecture and basic functions.

(A) General architecture shared by Sis1 and Ydj1. (B) General molecular functions of J-domain proteins in coordinating with substrate and Hsp70. (C) Schematic of Sis1- and Ydj1-specific molecular features, as well as key questions around their function in condensate dispersal.

3.2 Methods

Many of the methods in the previous chapter (Chapter 2) were also used in this chapter. However, some protocols were modified, and some new protocols were developed and introduced.

Plasmids

Cloning was perfomed via blunt-end ligation with Q5 polymerase and KLD enzyme mix or via Gibson assembly (New England Biolabs). Primers were ordered from Integrated DNA Technologies, Inc. Whole-plasmid sequencing was performed by Plasmidsaurus Inc.

A list of plasmids used in and/or generated for this work is provided below.

Table 3.1, Plasmids.

Plasmid	Source	Identifier
8xHis-(TevC)-Pab1 in pET28 backbone	Riback, Katanski et. al. 2017[45]	pJAR006
8xHis-(TevC)-Pab1 C70A C119A C368A in pET28 backbone	Dr. Hendrik Glauninger	pHG5
8xHis-(TevC)-Pab1 C70A C119A C368A A577C in pET28 backbone	This work	pKL031
6xHis-(SUMO)-Ssa2 in pET28 backbone	Yoo et al. 2022[56]	pHY024
6xHis-(SUMO)-*Photinus pyralis* luciferase in pET28 backbone	Yoo et al. 2022[56]	pHY045
6xHis-(SUMO)-Sse1 in pET28 backbone	Yoo et al. 2022[56]	pEP053
6xHis-(SUMO)-Hsp104 in pET28 backbone	Yoo et al. 2022[56]	pEP055
6xHis-(SUMO)-Ydj1 in pET28 backbone	Yoo et al. 2022[56]	pEP056
6xHis-(SUMO)-Sis1 in pET28 backbone	Yoo et al. 2022[56]	pEP057
6xHis-(SUMO)-Hsp26 in pET28 backbone	Yoo et al. 2022[56]	pEP059
6xHis-(SUMO)-Sis1 G210C in pET28 backbone	This work	pKL026
6xHis-(SUMO)-Ydj1 C29A C370F in pET28 backbone	This work	pKL034
6xHis-(SUMO)-Ssa2 C264A C303N D555C in pET28 backbone	This work	pKL050
6xHis-(SUMO)-Sis1 G210C ΔDD in pET28 backbone	This work	pKL068
6xHis-(SUMO)-Ydj1 ΔN C370F in pET28 backbone	This work	pKL073

6xHis-(SUMO)-Ssa2 C264A C303N D555C ΔGPTVEEVD in pET28 backbone	This work	pKL071
6xHis-(SUMO)-Sis1 CTDI C78 in pET28 backbone	This work	pKL083
6xHis-(SUMO)-Sis1 CTDII C78 in pET28 backbone	This work	pKL085
6xHis-(SUMO)-Ssa2 C264A C303N D555C GWLYEIS in pET28 backbone	This work	pKL089
6xHis-(SUMO)-Ssa2 T201A C264A C303N D555C in pET28 backbone	This work	pKL091

- Sis1 G210C ΔDD: A stop codon was introduced into Sis1 G210C at residue position 338.
- Ydj1 ΔN C370F: The first 101 amino acids were removed from the Ydj1 C29A C370F construct (sequence starts at G102).
- Ssa2 C264A C303N D555C ΔGPTVEEVD: A stop codon was introduced at residue position 632, such that the last eight residues (GPTVEEVD) were removed.
- Sis1 CTDI C78: Residues 180–256 of Sis1 were introduced, followed by a nonnative C-terminal cysteine (C78).
- Sis1 CTDII C78: Residues 260–336 of Sis1 were introduced, followed by a nonnative C-terminal cysteine (C78).
- Ssa2 C264A C303N D555C GWLYEIS: The last eight residues of Ssa2 (GPTVEEVD) were replaced with GWLYEIS.

Protein Purification

Protein purification was performed as stated in Section 2.2, “Purification of Chaperones”. Additional proteins that were not purified in the previous chapter include firefly luciferase, Hsp26, Ydj1, and various mutants and truncations of Sis1, Ydj1, and Ssa2. Proteins were typically expressed in BL21(DE3) cells, and expression was induced at 30 °C for 4–6 hours. To improve expression of some constructs, Rosetta (DE3) or Rosetta2 (DE3) cells were used, and/or induction

at 18 °C overnight. For some proteins, size exclusion was not performed if the purity was sufficient after the anion exchange step.

For the client binding domains of Sis1, which are net positively charged following removal of the 6xHis-SUMO tag, cation exchange instead of anion exchange was performed, with a HiTrap SP HP 5 mL column. A similar procedure was followed as with the Q column (including similar buffers). Due to their small size (< 10 kDa), these constructs were concentrated using 3 kDa cutoff spin concentrators. The identities of the constructs were verified by mass spectrometry performed by Estefania Cuevas-Zepeda in the laboratory of Dr. Tobin Sosnick.

Concentrations of proteins were determined by absorbance at 280 nm and/or by Bradford assay (see Section 2.2, "Measuring Protein Concentration (Bradford)"). For many proteins, such as Pab1 and Sis1, either method yielded similar results. However, for ATP-binding proteins, such as Ssa2, measurement by Bradford was necessary, because ATP bound to the protein itself caused additional absorbance at 280 nm which could not be accounted for, even with blanking against ATP-containing buffer.

Optimized Preparation of Fluorescently Labeled Proteins

Labeling of proteins (chaperone cysteine mutants and Pab1 C70A/C119A/C368A/A577C) with maleimide-functionalized dyes was performed in similar fashion to Section 2.2, "Preparation of Fluorescently Labeled Pab1". However, to improve labeling efficiency and protein yield, as well as to accommodate different scales of reaction, the protocol was optimized and generalized:

Proteins (generally, mutant proteins with a single accessible cysteine) were incubated with 10 mM tris(2-carboxyethyl)phosphine (TCEP) for at least 30 minutes (on ice or room temperature) to favor the reduction of cysteines. The sample was then buffer exchanged into phosphate buffered saline, pH 7.4 (PBS) with a Zeba spin desalting column (7 kDa cutoff). Additional PBS was added

to 1 mL, and a 20-fold molar ratio of label (CF 640R-maleimide, CF 488A-maleimide, ATTO 643-maleimide) was added. The reaction was incubated at room temperature overnight on a rocker, covered with foil to prevent photobleaching (the proteins used for labeling in this chapter tolerated long incubation at room temperature). To quench unreacted free label, 5 mM dithiothreitol (DTT) was added, and the sample was incubated for at least 30 additional minutes. The sample was then subjected to serial concentration-and-dilution cycles, in which the sample was spin concentrated (Amicon Ultra 4 mL spin concentrators of appropriate molecular weight cutoff) to remove free label, then additional PBS (~3 mL) was added to dilute the remaining free label. (In two rounds of five-fold concentration and re-dilution, assuming 100% protein labeling efficiency, the ratio of free dye to protein-bound dye can be reduced from 19:1 to < 1:1.) Then, the sample was buffer exchanged (Zeba spin column) into the desired storage buffer (usually, the same buffer the protein was originally stored in). Control experiments in which free dye (without protein) was purified by this procedure showed that this method was effective at removing free dye.

In developing this protocol, various alternative procedures were tried. Fast protein liquid chromatography (FPLC) was the most effective technique for separating labeled protein from free dye in a single step (ÄKTA Pure system, Superose 6 increase 10/300 GL size exclusion column); however, this treatment also led to loss of total yield and substantial dilution of the sample, so the serial concentration-and-dilution approach described above was preferable. A lower concentration of TCEP (5 mM) and shorter reaction times (e.g., 2.5 hours at room temperature with shaking at 300 rpm) were also effective at labeling proteins, but side-by-side comparisons of final labeling efficiency and yield have not been done.

Fluorescence Anisotropy-Based Binding Assay

An analogous approach to experiments by Faust, Abayev-Avraham et al. on human proteins was devised to measure protein-protein binding, although the specific details differ.[77]

Labeled Protein A was diluted to 1 μM of fluorescent label, using H150 buffer (20 mM HEPES, 150 mM KCl, 2.5 mM $MgCl_2$, 1 mM DTT, pH 7.3). 3 μL of this stock was pipetted well-by-well into a black 384-well flat bottom plate (Corning 3575) to achieve a final concentration of 200 nM (in a 15 μL reaction volume). The binding partner Protein B was diluted to 125 μM (1.25x stock) with H150 buffer. In the case of Pab1, this protein was either left at room temperature (no heat shock) or heat shocked at 46 °C for 5 minutes. Both samples were then iced to end the heat shock. The 125 μM stock was serially diluted (3-fold), then 12 μL of each dilution was pipetted into individual wells. The plate was sealed and moved to a Tecan Spark pre-equilibrated to 30 °C. Fluorescence anisotropy measurements were taken for at least 1 hour with at least one measurement per minute, blanked against 15 μL of H150 buffer. The G-factor was determined for each new plate by testing a sample of free dye in water (blanked with water). For analysis, only timepoints after 30 minutes of incubation were considered and averaged, as the signal often required several minutes to stabilize.

Data was fit in RStudio to a simple one-site binding equation described by Jarmoskaite et al. for a "binding" regime where [Protein A] << K_D, which explicitly accounts for bound protein.[84]

$$p_{bound} = \frac{([A]_{total} + [B]_{total} + K_D) - \sqrt{([A]_{total} + [B]_{total} + K_D)^2 - 4 \cdot [A]_{total} \cdot [B]_{total}}}{2 \cdot [A]_{total}}$$

Since the output of the assay is fluorescence anisotropy, not proportion of protein bound, the following assumption was made to convert from proportion bound to anisotropy, where *signal* is the anisotropy recorded, *max* is the maximum possible anisotropy, and *min* is the minimum:

$$signal = p_{bound} \cdot (max - min) + min$$

The concentration of A was set to 200 nM, the minimum anisotropy was set to the average anisotropy at the lowest concentration of substrate (400 nM), and the K_D and maximum anisotropy were both left unconstrained (since binding curves did not always plateau at maximum binding).

Luciferase Reactivation

Luciferase reactivation was tested similarly to Yoo et al., with modifications.[56] *Photinus pyralis* firefly luciferase (FLuc) was mixed with Hsp26 in one of two ways:

- 2 μM FLuc, 10 μM Hsp26 in Condensation buffer (20 mM HEPES, 150 mM KCl, 2.5 mM $MgCl_2$, 1 mM DTT, pH 6.8)
- 33.8 nM FLuc, 169 nM Hsp26 in Mild Aggregation buffer (25 mM HEPES, 50 mM KCl, 0.1 mM EDTA, 1 mM DTT, pH 7.3)

The mixture was heat shocked at 42 °C for 20 minutes, then cooled on ice. The substrate was diluted to a final concentration of 20 nM luciferase in a reaction containing chaperones at the desired concentrations, 5 mM ATP, 8 mM creatine phosphate, and 1 μM creatine kinase in H150 buffer (20 mM HEPES, 150 mM KCl, 2.5 mM $MgCl_2$, 1 mM DTT, pH 7.3). The reactions were incubated at 30 °C in an Eppendorf Thermomixer. At the start of each incubation and at each time point, 1.5 μL of each reaction was combined in a white flat bottom 384-well plate (Corning 3574) with 13.5 μL of a 1:8 mixture of ONE-Glo™ EX Reagent (Promega) and water to achieve 10-fold dilutions of both reaction and ONE-Glo™ EX Reagent (volume/volume). The plate was transferred to a Tecan Spark plate reader and shaken for 5 seconds. Luminescence was recorded after a three minute wait period with an integration time of 1 second.

ADP Formation Assay (Ssa2 ATPase Activity)

To test the ATPase activity of Ssa2, the formation of ADP was measured with an ADP-Glo™ Kinase Assay (Promega). Individual 5 μL reactions were assembled in a white flat bottom 384-well plate (Corning 3574) to final concentrations of 4 μM of Ssa2 (or buffer), 4 μM of J-domain protein (or buffer) by monomer concentration, and (if substrate was included) 4 μM of Pab1 heat shocked at 46 °C for 5 minutes. Reactions were sealed with film and incubated in a Tecan Spark plate reader pre-equilibrated to 30 °C for 1 hour. The film was removed, and the reactions were quenched with 5 μL of ADP-Glo™ Reagent. After at least 40 minutes of incubation at room temperature, 10 μL of Detection Reagent were added. After at least 1 hour of incubation at room temperature, luminescence was recorded in a Tecan Spark plate reader with an integration time of 1 second. Four ADP/ATP standards were used to find the linear relationship between ADP concentration and luminescence: 80%, 60%, 40%, and 20% (volume/volume) 1 mM ADP, where the remaining volume is 1 mM ATP. The standards were made as 5 μL samples and incubated with ADP-Glo™ and Detection Reagents in parallel with other samples.

Colocalization Microscopy

Two-color microscopy was performed on the same TIRF microscopy setup as before, with dual 637 nm and 488 nm excitation lasers (Coherent, OBIS LX 140 mW and OBIS LS 150 mW, respectively). Preincubated labeled chaperone or free dye with Pab1-ATTO 643 condensates were diluted and transferred to an imaging chamber, as before. Fields of view were brought into focus with minimal 637 nm excitation; then the excitation was shuttered, and both lasers were set to a high laser power. Starting with no excitation reaching the sample, a video acquisition was begun, then the excitation shutter was opened during the acquisition to visualize the sample with as little photobleaching as possible. The initial dark frames of the video were removed in postprocessing.

Background subtraction and object identification were implemented similarly to Section 2.2, “Single-Molecule Analysis: Background Subtraction” and “Single-Molecule Analysis: Object Identification and Trace Calculation”. Object identification was performed only in the condensate (637 nm) channel; then signal traces were calculated for both channels at each location. To evaluate colocalization at the single-condensate level, a custom function (**colocalizer**) was implemented to determine which objects contained simultaneous signal in both channels in the first 10 frames of imaging. This function takes the two-channel trace data, finds levels via changepoint detection (as described previously for one-channel data), finds which levels in each trace are significantly above zero (based on a certain number of standard deviations from the mean signal of the level, for these data two standard deviations), then determines whether there is overlapping positive signal in both channels for a minimum number of frames (for these data, 3 frames). The proportion of all objects meeting these criteria in a certain video was used as the proportion colocalization for that video.

To perform the control grid analysis, an arbitrary grid of 81 locations was setup in the video field of view (regardless of the location of objects in the condensate channel). Then the proportion of locations specifically having significant positive signal in the 488 nm channel was determined (again disregarding the 637 nm channel).

3.3 Results

Functional Expression of Sis1, Ydj1, and Chaperones

My first step in this work was to ensure that I could express Sis1, Ydj1, and other proteins functionally, and that I could recapitulate the known behaviors of the chaperones with my own purified proteins. Indeed, using my preparations of Sis1, Ssa2, Hsp104, and Sse1, I observed robust condensate dispersal using fluorescence anisotropy-based assay published by Yoo et al (Figure 3.2, A).[60] Both Sis1 and Ydj1 are known to have protein refolding activity, specifically in recovery of

misfolded firefly luciferase.[53,54,56,75,82] Since Ydj1 is inhibitory in condensate dispersal, luciferase refolding is an important test of positive function of Ydj1. Using luciferase exposed to mild heat shock (pH 7.3, 42 °C for 20 minutes, 33.8 nM luciferase) in the presence of Hsp26, I verified that both Ydj1 and Sis1 can collaborate with Ssa2 in the reactivation of luciferase (Figure 3.2, B). I also observed the highest luminescence in the presence of both Ydj1 and Sis1, a previously observed result.[53,56] Using luciferase heat shocked under more severe conditions (pH 6.8, 42 °C for 20 minutes, higher salt concentration, 2 μM luciferase), which caused detectable aggregation of luciferase by TSP, I also recapitulated Sis1's known ability to disperse large aggregates better than Ydj1 (Figure 3.2, C–D).[53] With these results, I was confident that I had produced Sis1, Ydj1, and other chaperones which could function as expected, and that I then had a foundation upon which I could begin perturbing chaperone function.

Functional Expression of Labelable Chaperone Mutants

In order to interrogate Sis1 and Ydj1's behaviors, such as binding to condensates and/or Hsp70, I mutated Sis1, Ydj1, and Ssa2 to have a single accessible cysteine which could be fluorescently labeldd. I introduced a single cysteine in Sis1's CTDI at a location shown to be nondisruptive in the homologous human JDP DNAJB1.[72] (Sis1 has no native cysteines.) I removed two of Ydj1's three non-zinc finger cysteines (C29A C370F), leaving the final native cysteine (C406) in place as the labeling site. C406 is part of the C-terminal CASQ motif, which is farnesylated *in vivo* to anchor a subpopulation of Ydj1 to the membrane of the endoplasmic reticulum.[85] Farnesylation is not essential for Ydj1's *in vitro* refolding activity and inhibition of condensate dispersal, since *E. coli* expression systems do not farnesylate. Mutation of C406 has also been shown not to disrupt Ydj1's ability to reactivate luciferase.[86] For these reasons, I reasoned that C406S might serve as a suitable labeling site. Finally, I removed two of the three native

cysteines in Ssa2 (C264A C303N). (C15 is a highly-conserved, internal cysteine which was not necessary to remove when labeling human Hsp70, HSPA8.[72]) I introduced a nonnative cysteine at a loop in the alpha helical lid region (D555C), a site which was nondisruptive in HSPA8.[72] These constructs all expressed well in *E. coli*, and they all reacted with dyes with high efficiency.

With these constructs in hand, I sought to test whether they function similarly to the wildtype proteins. Indeed, Ydj1 C264A C303N inhibited condensate dispersal in a concentration-dependent manner and appeared to fully block dispersal at ~2 μM dimer (Figure 3.3, A–B). Sis1 G210C also enabled dispersal similarly to wildtype Sis1, even at a concentration of 125 nM dimer (Figure 3.3, C). I further confirmed that fluorescently labeled Sis1 and Ssa2 can substitute for wildtype Sis1 and Ssa2 in condensate dispersal reactions (Figure 3.3, D). Finally, using an ADP formation assay, I confirmed that both Ssa2 and Ssa2 C264A C303N D555C have comparable ATPase activity, which is stimulated by either JDP (Figure 3.3, E). Both Sis1 G210C and Ydj1 C29A C370F have similar abilities to promote Ssa2 ATPase activity as wildtype Sis1 and Ydj1 (Figure 3.3, F). These results demonstrated that we had the ability to label and visualize our key chaperones of interest while retaining their biochemical functions.

Binding of Pab1 Condensates by Sis1 and Ydj1

Sis1 and Ydj1 are both JDPs which can perform substrate binding, substrate handoff to Hsp70, and stimulation of Hsp70 ATP hydrolysis (Figure 3.1). We reasoned that only Sis1 performs all there of core functions in the context of condensate dispersal, while at least one of these basic activities is impaired in Ydj1. Our first hypothesis was that Sis1 and Ydj1 differ in their ability to bind condensates as substrates. That is, Sis1 functions by binding condensates and then transferring the condensate to Hsp70. If Ydj1 cannot bind the condensate in the first place, it cannot transfer it to Hsp70 and therefore cannot catalyze dispersal. In this model, Ydj1's inhibitory activities must

occur without condensate involvement—for example, unproductive cycling of Hsp70's ATPase activity, with or without another substrate (such as free Pab1 monomers). We termed this model an "off-substrate model" of Ydj1 inhibition, because Ydj1 acts independently of the condensate substrate.

To test the off-substrate model, we sought to determine directly if Sis1 and Ydj1 can bind substrate. Even though we strongly expected Sis1 to bind condensates, it has not been previously shown if either Sis1 or Ydj1 recognizes Pab1 condensates, nor have any specific binding sites been identified. We used fluorescently labeled Sis1-CF 488A and Ydj1-CF 488A to conduct bulk Pab1 binding experiments via fluorescence anisotropy. As expected, neither Sis1 nor Ydj1 bound well to non-heat shocked Pab1, with apparent K_D's of ~400 and ~80 μM, respectively (Figure 3.4, A–B). To our surprise, both Sis1 and Ydj1 bound to heat shocked Pab1 with similar apparent K_D's of 13 and 17 μM, respectively (Figure 3.4, A–C).

These results strongly suggest that both Sis1 and Ydj1 can bind condensates. However, the interpretation of these results is clouded by the fact that the heat shocked Pab1 contains a mixture of condensates and monomers, as we lack a method to purify condensed Pab1 from monomers at high concentrations. To verify that both Sis1 and Ydj1 are in fact binding condensates, we took a single-molecule imaging approach to visualize individual condensates and confirm if Sis1 and/or Ydj1 bound to them. Indeed, both Sis1-CF 488A and Ydj1-CF 488A colocalized similarly to fluorescently-labeled condensates, while free CF 488A did not bind (Figure 3.4, D–E). Ydj1 had an even higher raw proportion of colocalization than Sis1, although this difference disappeared upon correction in the analysis for random chance landing events (Figure 3.4, E). The combination of single-condensate imaging with bulk binding experiments demonstrated that both Sis1 and Ydj1 recognize condensates as substrates.

Interrogation of Molecular Basis of Ydj1 Inhibition

The result that Ydj1 binds to condensates suggested that an off-substrate model of Ydj1 inhibition may not be correct. However, Ydj1 binding does not rule out such a model. That is, Ydj1 could bind condensates with neutral effect, while its inhibitory activities take place off-substrate (or equally on- and off-substrate, independent of condensate binding state). We reasoned that the most likely way this could occur is if Ydj1 stimulates the ATPase activity of Hsp70 when Ydj1 is not condensate-bound, such that Hsp70 is unproductively cycled into its closed conformation (ADP-bound) without having a condensate to bind. Although Hsp70 is thought to hydrolyze ATP optimally in the presence of a bound substrate (not merely with JDP alone), Ydj1 and Sis1 both drastically increase (~order of magnitude) the ATPase rate of Hsp70 at μM concentrations of JDP and Hsp70, even in the absence of substrate.[54,55,87] Thus, such a model was conceptually plausible.

A key prediction of this off-substrate model is that adding enough Hsp70 into the reaction should overcome Ydj1 inhibition. That is, if Ydj1's effect is to remove a fraction of Hsp70 from the active pool, increasing the available pool of Hsp70 should counteract this effect. We therefore tested this prediction by performing condensate dispersal in the presence of Ydj1 while titrating increasing amounts of Ssa2. In the presence of 0.4 μM Ydj1 dimer, which was sufficient to slow dispersal, increasing Ssa2 up to 1.4 μM did not recover the speed of dispersal (Figure 3.5, A–B). Instead, there seemed to be no effect on dispersal rate and a negative effect on the final change of anisotropy reached at high Ssa2 concentration. This latter effect on the final signal was also seen in the absence of Ydj1 and may be the result of RNase contamination in the Ssa2 prep, which can lower the fluorescence anisotropy (Figure 3.5, B). Regardless of the reason for this latter effect, these data combined with the previous binding experiments suggest that an off-substrate model for Ydj1 inhibition is unlikely.

We therefore considered potential "on-substrate" models for Ydj1 inhibition. In general, an on-substrate model of inhibition would involve Ydj1 binding to condensate but not performing its downstream functions correctly—that is, handing off the condensate to Hsp70 and stimulating the ATPase activity of Hsp70 to stabilize it on the condensate. In the simplest version of this model, Ydj1's sole activity is substrate binding. Ydj1 competes for access to condensate with Sis1, but it does not do anything else. Thus, Ydj1 slows dispersal directly through its substrate binding and not through its other molecular functions (J-domain interaction with Hsp70, etc.)

To test this simple, binding-mediated version of on-substrate inhibition, I created a Ydj1 mutant construct (in the cysteine mutant background) which lacked the N-terminal J-domain and GF region (Ydj1 ΔN C370F). Residue 102 was chosen as the start site, because the first 101 amino acids are not necessary for Ydj1 to complex with model peptide substrates, and all of the canonical substrate binding domains (CTDI, zinc finger domain, and CTDII) are C-terminal of this position. Even though this Ydj1 construct contains all canonical substrate binding domains, lacking only the J-domain and unstructured GF region, it failed to inhibit condensate dispersal even at 4 μM dimer concentration, whereas full-length Ydj1 C29A C370F robustly blocked dispersal at 2 μM (Figure 3.5, C). To our surprise, fluorescently-labeled Ydj1 ΔN C370F also failed to bind heat shocked Pab1, even at 100 μM Pab1 (Figure 3.5, D).

These results neither confirm nor rule out a simple, binding-mediated model of on-substrate inhibition, since Ydj1 ΔN C370F did not bind substrate. However, they provide other, unexpected insights into the molecular basis of Ydj1 inhibition. First, *Ydj1 requires its J-domain and GF region to inhibit condensate dispersal*. Second, the J-domain and GF region may be necessary for Ydj1 to bind condensates. How these domains are involved is unclear, and whether these domains alone have binding activity independent of the CTDs and zinc finger domain has not been tested. Yet the

fact that these domains have any role in substrate recognition is an intriguing and unexpected finding, as the J-domain's primary role is thought to be interaction with Hsp70.

Relationship of Hsp70 EEVD to Sis1 Function

So far, we determined that Ydj1 likely inhibits dispersal via an on-substrate mechanism, and that Ydj1 binds condensates similarly to Sis1. Moreover, these findings illustrated that binding alone is not enough to confer activity to a JDP such as Ydj1. Additional activities must be necessary to make a JDP functional in dispersal. These activities likely involve the JDP's direct interactions with Hsp70: substrate handoff to Hsp70 and stimulation of ATP hydrolysis. In Sis1 and other Class B JDPs, both of these steps are linked to a special interaction with Hsp70's C-terminal EEVD tail. By directly binding to CTDI, the Hsp70 EEVD motif directly competes for the substrate binding site on that CTD and drives the J-domain from a locked to an unlocked conformation that can more readily activate Hsp70 ATP hydrolysis.[77,80] Deletion of the EEVD motif specifically impairs Sis1's ability to recover misfolded proteins, while leaving Ydj1's ability unaffected.[78,82] Thus, it seemed highly likely that the ability of Sis1 to coordinate with Hsp70 in condensate dispersal would require the Sis1-EEVD interaction.

To test this hypothesis, I created an Ssa2 construct lacking all eight C-terminal residues (GPTVEEVD) shown to form an anti-parallel strand within the CTDI beta barrel.[79] Additionally, I created a second construct in which the GPTVEEVD tail was replaced by a Ydj1 model binding peptide, GWLYEIS. The GWLYEIS peptide binds in a similar fashion to Ydj1 as GPTVEEVD binds to Sis1, and GWLYEIS competes with luciferase as a Ydj1 substrate.[79,88] By switching the tail of Hsp70 from a Sis1-interacting peptide to a Ydj1-interacting peptide, we reasoned that the activities of the JDPs might be partially or fully swapped. Since Ydj1 and other Class A JDPs have a constitutively unlocked J-domain, they do not require EEVD binding specifically to activate their

function in ATP hydrolysis. Thus, an Hsp70-GWLYEIS might be able to coordinate with Ydj1 similarly to Hsp70-EEVD with Sis1.

In agreement with previous studies of Ssa1 ΔEEVD, I found that Ssa2 C264A C303N D555C ΔGPTVEEVD only coordinates with Ydj1 in reactivating misfolded luciferase, while the full-length Ssa2 C264A C303N D555C functions with either Sis1 or Ydj1 (Figure 3.6, A).[78,82] I next turned to condensate dispersal. At low concentrations of chaperones (0.5 μM Ssa2, 0.25 μM Sis1 dimer, 100 nM Hsp104 hexamer, 50 nM Sse1), the GPTVEEVD tail was necessary for dispersal (Figure 3.6, B). However, by titrating the concentration of Ssa2 higher (up to 2 μM), the activity of the tailless mutant was brought to normal levels (Figure 3.6, C). The activity of Ssa2-GWLYEIS was even more robust, having similar activity to Ssa2 C264A C303N D555C at 1 μM Ssa2 (a typical concentration used for *in vitro* condensate dispersal, and much lower than cellular concentration). Moreover, neither Ssa2-ΔGPTVEEVD nor Ssa2-GWLYEIS functioned with Ydj1, and both retained activity with Sis1 only (Figure 3.6, D). From these data, we concluded that the well-established EEVD interaction with Sis1, thought to be central to the function of Class B JDPs, is not necessary for the dispersal of Pab1 condensates.

Dimerization, ATP Hydrolysis, and Sis1 Function

If the EEVD tail of Hsp70 is not required for Sis1 to function in dispersal, then what is required for Sis1 to function? The EEVD tail should coordinate both substrate handoff and J-domain activity by binding CTDI; perhaps one of these functions is not necessary for dispersal. Another possibility is that substrate binding and handoff does not occur at CTDI, but at CTDII. It is not known which domain(s) Sis1 or Ydj1 uses to bind condensates. To test whether either or both CTDs bind heat shocked Pab1, I generated single CTD constructs, each with a C-terminal cysteine labeling site. Estafania Cuevas-Zepeda verified the identity of these constructs by mass

spectrometry, as there was not a clear functional readout to validate these constructs. Neither CTDI nor CTDII were able to bind heat shocked Pab1, except marginally in the case of CTDII at the highest concentrations tested (Figure 3.7, A). This negative result does not rule out the possibility that CTDI and/or CTDII are used in substrate binding, but it does suggest that neither CTD alone is sufficient to confer binding ability.

The binding mode(s) of Sis1 (i.e., which domain(s) of Sis1 are involved) on physiological stress-induced substrates such as condensates are not well understood. From these data, it seems likely that Sis1 needs to engage multiple binding sites; however, these binding sites could be a pair of specific CTDs on the Sis1 dimer (both CTDI's, for example), or binding could be intrinsic to the Sis1 monomer (CTDI + CTDII). To distinguish between these modes of binding, I generated a dimerization-deficient Sis1 (with the labelable G210C mutation) by introducing a stop codon at residue 338, thereby removing the dimerization domain (DD). I tested whether labeled Sis1 ΔDD-CF488A could bind to heat shocked Pab1. The apparent binding affinity was weaker than Sis1's (36 vs. 13 μM), but there was clear binding of Sis1 ΔDD to heat shocked Pab1 (Figure 3.7, B). We concluded that the Sis1 monomer contains the necessary components to bind condensates, but that binding is enhanced in the full dimer context.

Although Sis1 ΔDD demonstrated substrate binding, it was unclear if it would also retain dispersal activity. Truncation of Sis1 at this site severely impairs its ability to restore luciferase, but its ATPase stimulation activity and *in vivo* coordination with Hsp70 are both reported to be preserved.[89,90] Comparison of Sis1 ΔDD to Sis1 wildtype and G210C revealed a defect in monomeric Sis1's ability to support dispersal at lower concentrations of Sis1, although near-wildtype activity was obtained at high concentration (Figure 3.7, C–D).

Why is Sis1 ΔDD not as effective in supporting dispersal? The reason for monomeric Sis1's defect could be one of two possibilities: (1) the slightly weaker binding affinity is enough to impair Sis1 function, or (2) monomeric Sis1 is deficient in another core JDP activity, such as handoff or J-domain activity. Indeed, in my hands, the Sis1 ΔDD was defective in stimulating ATP hydrolysis, in contrast to a previous report (Figure 3.3, F).[89] However, it is possible that stimulation of ATP hydrolysis is not essential to Sis1's function in the context of condensate dispersal, and that simply binding to and coordination with Hsp70 is sufficient. The fact that Sis1 does not require the EEVD tail of Hsp70, which unlocks the J-domain, supports this hypothesis.

To test this hypothesis, I perturbed Hsp70's ATP hydrolysis in one of two ways: with the chemical inhibitor VER-155008, and with a T201A mutation to Ssa2. VER-155008 is an ATP-competitive inhibitor of Hsp70's which traps Hsp70 into an intermediate conformation and prevents it from properly cycling.[91] T201A is a well-studied mutation to Hsp70 which reduces its ATPase rate (bacterial DnaK and yeast Ssa1) and blocks ATPase stimulation by either Sis1 or Ydj1 (Ssa1).[87,92] Indeed, in my hands, the T201 mutation impairs the ability of Sis1 and Ydj1 to stimulate Ssa2 ATP hydrolysis (Figure 3.3, E). Although both perturbations affect ATP hydrolysis, they had different consequences for condensate dispersal. VER-155008 partially inhibited dispersal, both the initial rate and final level of anisotropy, but it failed to fully prevent dispersal at the highest concentration tested, 50 μM (Figure 3.7, E). VER-155008 has sub-μM binding affinity for Hsp70 and impairs cell growth with single-μM IC50.[91,93,94] In contrast, preventing Sis1 from stimulating ATPase activity with the T201A mutation completely blocked dispersal (Figure 3.7, F). These two results together suggest that both Ssa2 ATP hydrolysis and Sis1's ability to stimulate it are crucial to the dispersal process.

3.4 Discussion

What makes Sis1 function, and what makes Ydj1 nonfunctional and inhibitory? In this work, I determined that Sis1 and Ydj1 do not differ in the initial recognition of substrate, but must differ in their downstream interactions with Hsp70. However, to our surprise, this difference was not solely caused by EEVD binding. Although removal of EEVD binding did have an effect on Sis1's ability to disperse condensates, it was easily remedied by simple addition of more EEVD-less Hsp70. This finding contrasts sharply with other studies of both Sis1 and other Class B JDPs, where EEVD binding was necessary for amyloid dispersal and misfolded aggregate dispersal.[77,78] Thus, condensates as physiological, heat-induced, endogenous substrates have continued to yield new, unexpected insights into how chaperones function. These results raise the question of whether EEVD binding should be considered the defining functional characteristic of Class B JDPs, and whether Class B and other JDPs possess other, not yet appreciated modes of regulation. Moreover, substitution of the EEVD tail with a model Ydj1 peptide failed to confer activity to Ydj1. This result suggests that a lack of Hsp70 tail binding may not be the reason Ydj1 fails at dispersal.

Finally, we have gained considerable insight into what does make Sis1 function. The canonical client binding domains of Sis1 do not appear to be the functional units of condensate binding. Instead, the monomer of Sis1 (lacking only the dimerization domain) appears to be the functional unit of Sis1 for both condensate binding and dispersal. Yet its activity is still impaired compared to dimeric Sis1. These findings suggest interesting models for how Sis1 binds condensates as substrates. If Sis1 interacts with substrate through some combination of its CTDs, several modes of binding are possible: single CTDI binding, single CTDII binding, CTDI and CTDII binding on the same monomer, or various cross-dimer binding configurations (Figure 3.7, G). Single CTD binding is unlikely given our binding experiments with isolated CTDs. Single

monomer binding is possible, as evidenced by monomeric Sis1's ability to bind heat shocked Pab1. However, this binding was weaker than dimeric Sis1's, and more importantly, the monomer did not support dispersal as well. Even more puzzling is that CTDI alone had no detectable substrate binding, and CTDII's binding was barely detectable. The combination of these two domains alone seem unlikely to account for monomeric Sis1's ~36 μM apparent binding affinity. Two conclusions seem likely: that Sis1 uses domains other than its canonical client binding domains to bind client (perhaps its GF/GM regions), and that productive binding of Sis1 during dispersal might involve cross-dimer engagement of substrate. Both of these possibilities warrant future investigation.

In summary, the work I have done in this chapter has provided new insight into what makes Sis1 functional and what makes Ydj1 nonfunctional and inhibitory during dispersal of Pab1 condensates as physiological substrates.

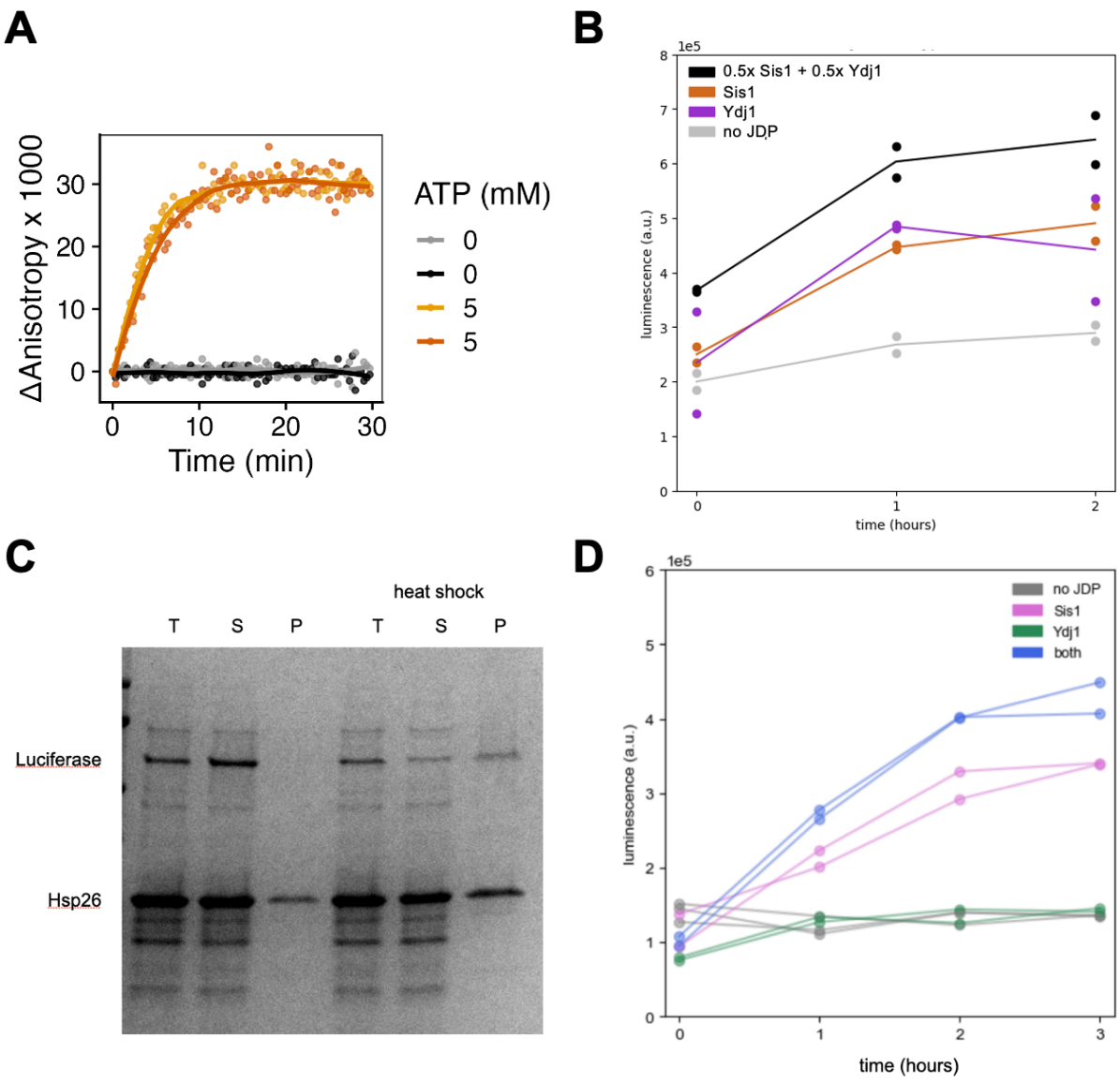

Figure 3.2, Functional activities of Sis1 and Ydj1.

(A) Anisotropy-based Pab1 condensate dispersal assay, with Sis1, Ssa2, Hsp104, and Sse1. (B) Reactivation of heat shocked firefly luciferase by 0.75 μM Ssa2, 0.75 μM Hsp104 hexamer, 38 nM Sse1, and 0.25 μM total dimer concentration of the specified J-domain protein(s). (C) SDS-PAGE gel of TSP experiment on luciferase heat shocked with Hsp26 under a more severe aggregation condition. (D) Reactivation of more severely aggregated firefly luciferase by 0.75 μM Ssa2, 0.75 μM Hsp104 hexamer, 38 nM Sse1, and 0.25 μM total dimer concentration of the specified J-domain protein.

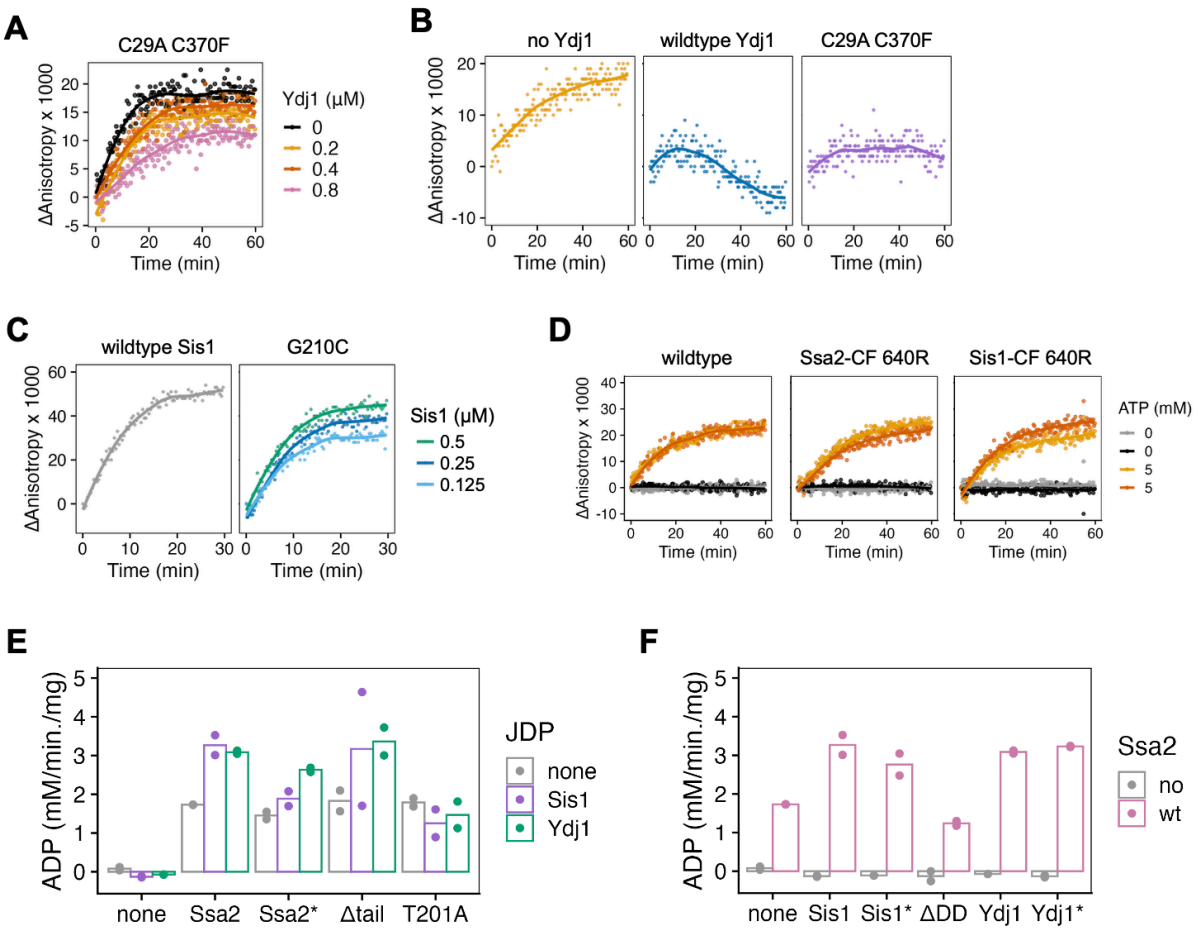

Figure 3.3, Activities of wildtype and mutant chaperones.

(A) Effect of increasing Ydj1 C29A C370F on Pab1 condensate dispersal by Sis1, Ssa2, Hsp104, and Sse1. (B) Comparison of 2 μM Ydj1 wildtype and C29A C370F in the inhibition of condensate dispersal with 50 nM Hsp104 hexamer, 0.5 μM Ssa2, and 250 nM Sis1 dimer. (C) Comparison of Sis1 wildtype (0.5 μM dimer) and G210C in condensate dispersal with 100 nM Hsp104 hexamer, 1 μM Ssa2, and 50 nM Sse1. (D) Comparison of condensate dispersal by 100 nM Hsp104 hexamer, 50 nM Sse1, and 250 nM dimer of wildtype Sis1, 1 μM Ssa2; wildtype Sis1, Ssa2-CF 640R; or Sis1-CF 640R and wildtype Ssa2. (E) ADP formation measured at 1 hour in the presence of 4 μM (by monomer concentration) of each of the specific chaperones. The stars indicate single-accessible-cysteine mutants of the proteins.

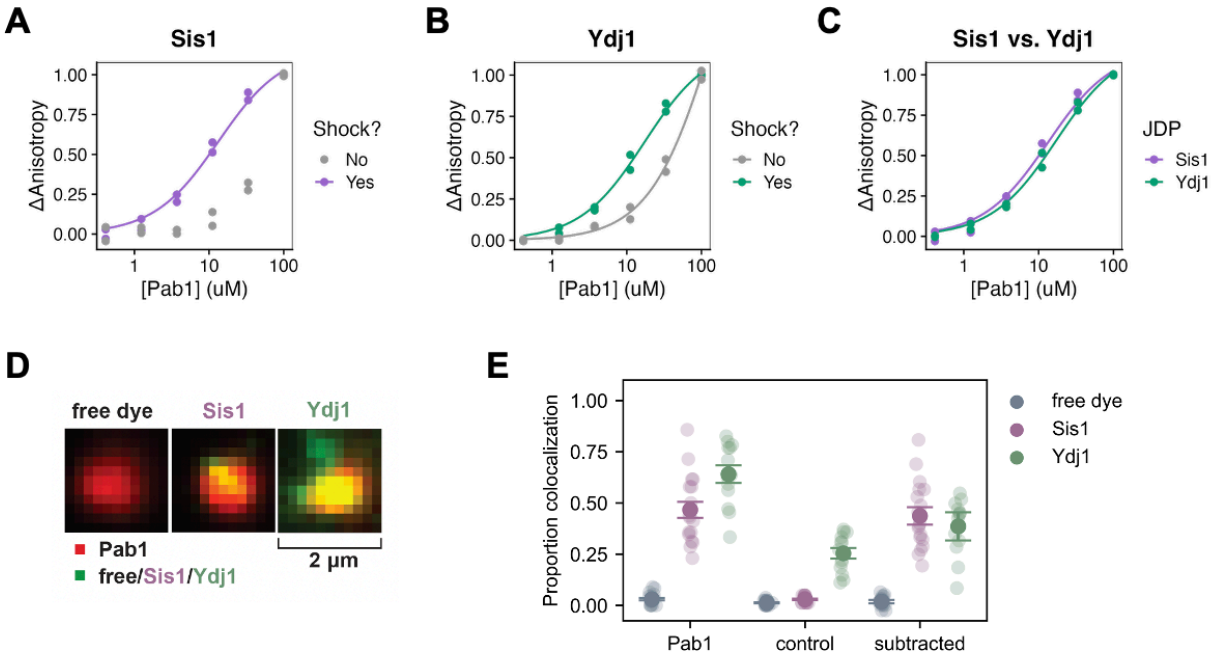

Figure 3.4, Binding of Sis1 and Ydj1 to Pab1 condensates.

(A) Binding of 200 nM Sis1-CF 488A (by label concentration) to Pab1 with or without heat shock at 46 °C for 5 minutes at 125 μM, with fits to a one-site binding equation. (B) Binding of 200 nM Ydj1-CF 488A (by label concentration) to Pab1 with or without heat shock at 46 °C for 5 minutes at 125 μM, with fits to a one-site binding equation. Fit was not obtained for Sis1 binding, no heat shock. (C) Comparison of Sis1 and Ydj1, heat shocked Pab1 data from panels A and B. (D) Example single-molecule images of Pab1-ATTO 643 condensates (red) and free dye, Sis1-CF 488A, or Ydj1-CF 488A. (E) Proportion of condensates with 488 nm channel colocalization ("Pab1"), likelihood of detected 488 nm signal by chance, using a control grid of arbitrary locations ("control"), and the subtracted proportions of colocalization as the final analysis ("subtracted"). High alpha dots and error bars represent the mean and standard error of the mean; low alpha dots represent individual videos.

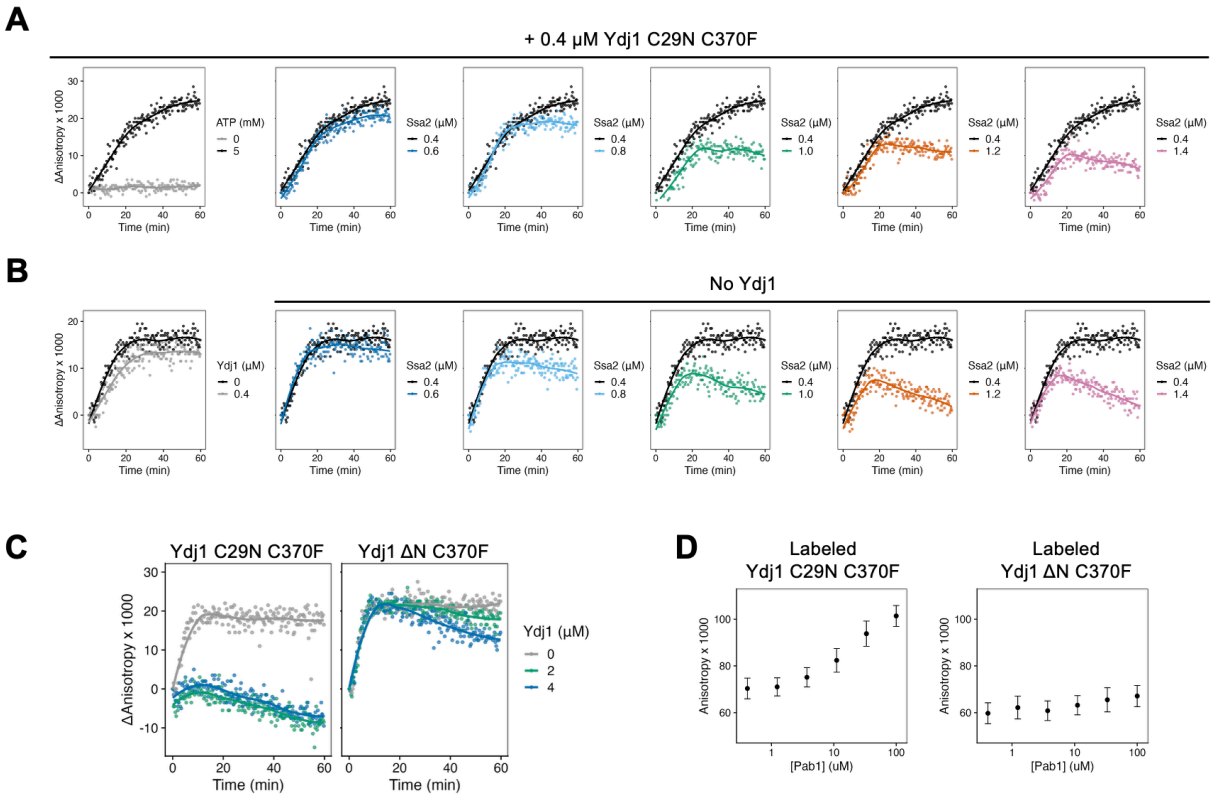

Figure 3.5, Interrogation of Ydj1 inhibition.

(A) Dispersal with the specified ATP concentration (and 0.4 μM Ssa2 C264A C303N D555C), or the specified Ssa2 concentration (and 5 mM ATP), in the presence of 0.4 μM Ydj1 C29N C370F dimer, with 200 nM Hsp104 hexamer, 40 nM Sse1, and 200 nM Sis1 G210C dimer. (B) Dispersal with the specified Ydj1 C29N C370F concentration (and 0.4 μM Ssa2 C264A C303N D555C), or the specified Ssa2 concentration and no Ydj1. (C) Dispersal in the presence of the specified concentrations of the specific Ydj1 mutant, with 0.5 μM Ssa2, 0.25 μM Sis1 dimer, 100 nM Hsp104 hexamer, and 50 nM Sse1. (D) Binding assays of 200 nM CF 488A-labeled Ydj1 mutant (by label concentration) to Pab1 heat shocked at 46 °C for 5 minutes at 125 μM, Error bars represent the standard deviation in measurements taken over an hour time course.

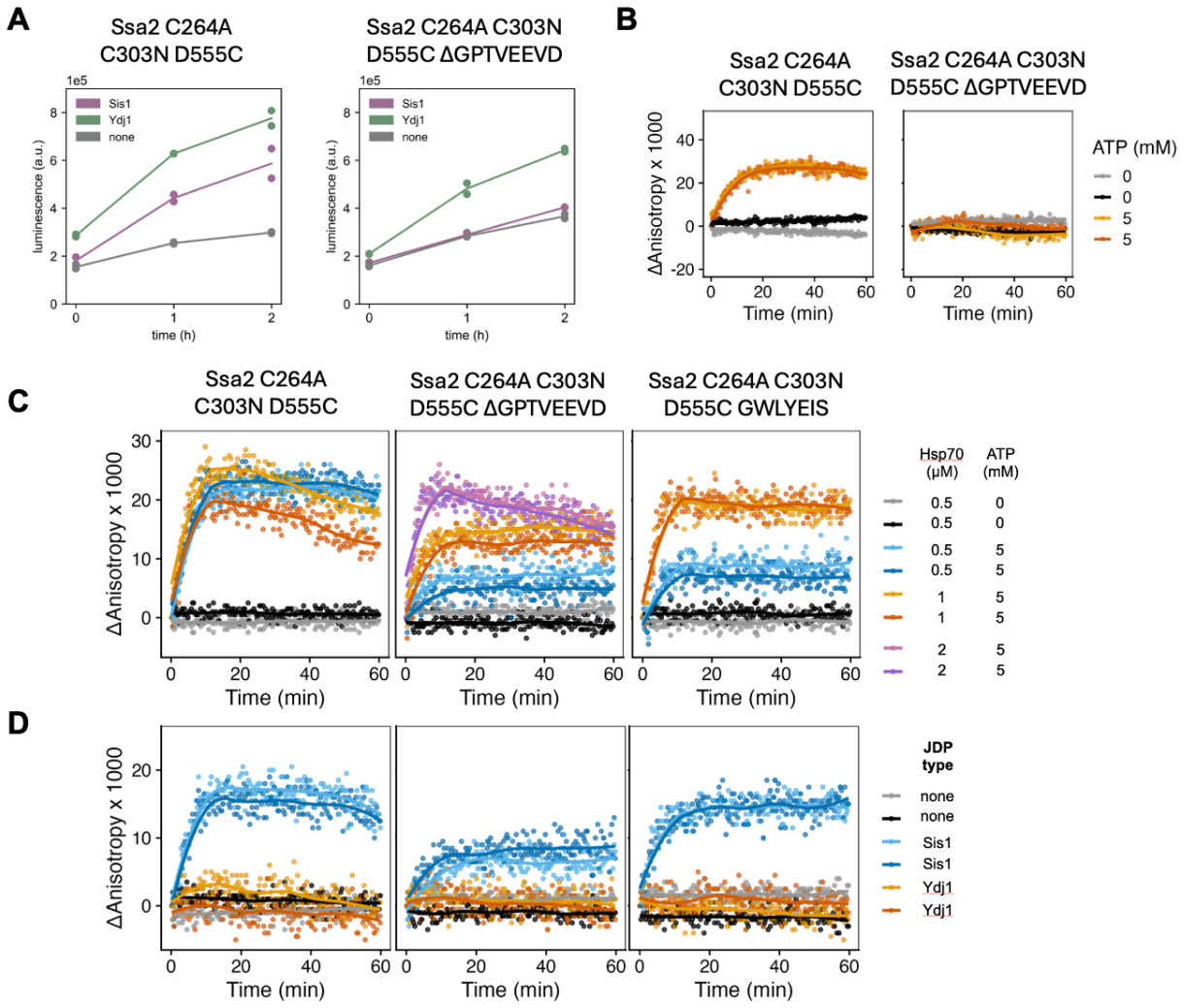

Figure 3.6, Effect of Hsp70 C-terminus perturbation on dispersal.

(A) Reactivation of heat shocked firefly luciferase by 0.75 μM indicated mutant of Ssa2, 0.75 μM Hsp104 hexamer, 38 nM Sse1, and 0.25 μM total dimer concentration of the indicated J-domain protein. (B) Pab1 dispersal by the indicated Ssa2 mutant (0.5 μM), 0.25 μM Sis1 dimer, 100 nM Hsp104 hexamer, and 50 nM Sse1. (C) Pab1 dispersal by the indicated Ssa2 mutant at the indicated concentration, 0.25 μM Sis1 dimer, 100 nM Hsp104 hexamer, and 50 nM Sse1. (D) Pab1 dispersal by the indicated Ssa2 mutant (1 μM), 0.25 μM dimer concentration of the indicated J-domain protein, 100 nM Hsp104 hexamer, and 50 nM Sse1.

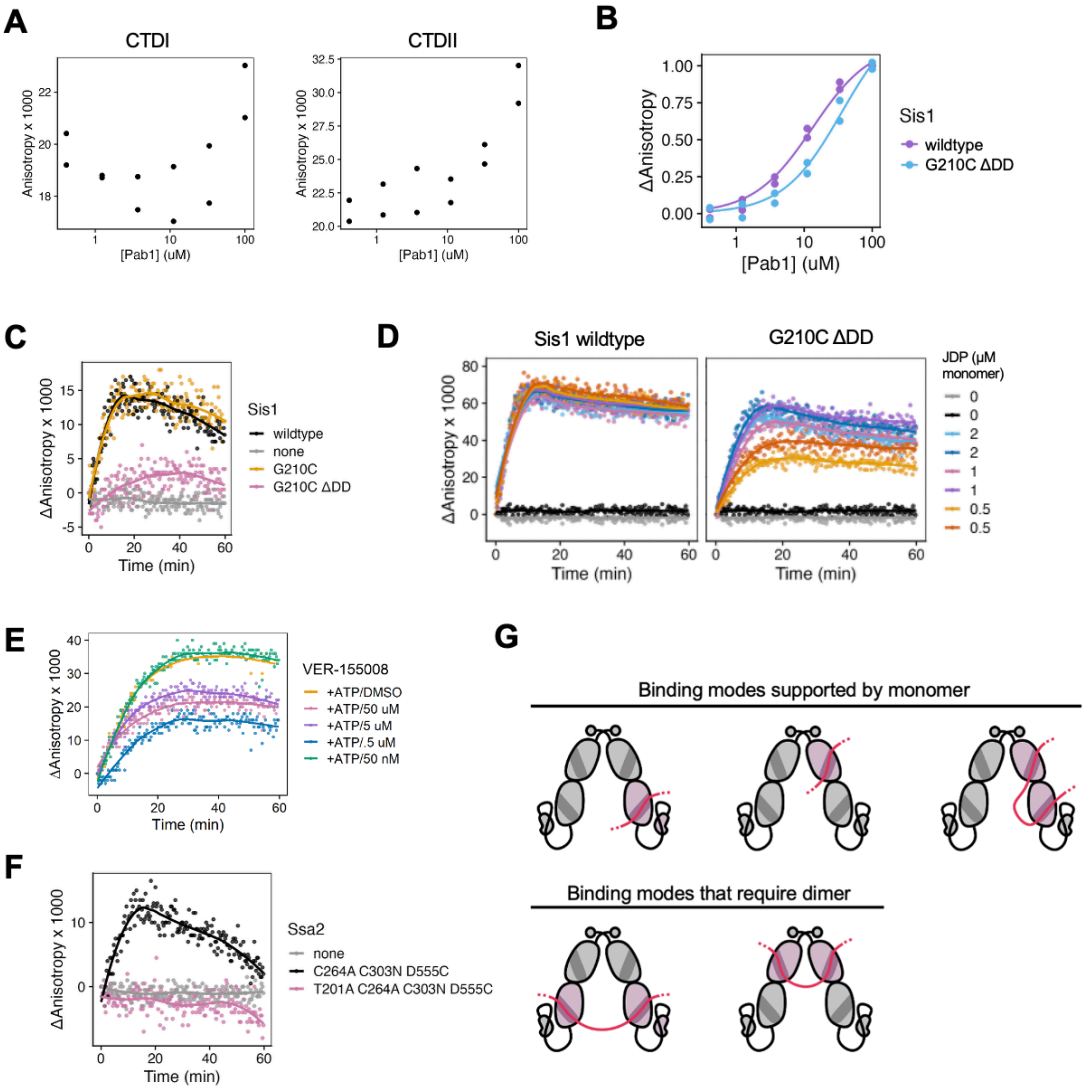

Figure 3.7, Interrogation of Sis1 function in dispersal.

(A) Binding assays of 200 nM CTDI-CF 488A or CTDII-CF 488A (by label concentration) to Pab1 heat shocked at 46 °C for 5 minutes at 125 μM, (B) Binding assay of 200 nM Sis1 ΔDD-CF 488A (by label concentration) to Pab1 heat shocked at 46 °C for 5 minutes at 125 μM, (C) Dispersal of Pab1 condensates by the specified Sis1 mutant (with 0.5 μM Ssa2, 100 nM Hsp104, 50 nM Sse1, 5 mM ATP). (D) Dispersal of Pab1 condensates with the specific concentration (by monomer) of Sis1 wildtype or G210C ΔDD (with 1 μM Ssa2, 100 nM Hsp104, 50 nM Sse1, 5 mM ATP). (E) Dispersal of Pab1 condensates in the presence of 1 μM Ssa2 and the specific concentration of VER-155008 (or DMSO vehicle), plus 100 nM Hsp104 hexamer, 50 nM Sse1, and 0.5 μM Sis1 dimer. (F) Dispersal of Pab1 condensates with 1 μM of the specified Ssa2 mutant, plus 100 nM Hsp104 hexamer, 50 nM Sse1, and 0.5 μM Sis1 dimer. (G) Cartoon representation of different hypothetical binding modes for Sis1, some of which are ruled out and/or tested in this work.

4 | Beyond Condensate Dispersal

In the preceding two chapters, I have described my two main research efforts: visualizing Pab1 condensates and their dispersal with quantitative single-molecule methods to understand how this process occurs, and interrogating the molecular basis of Sis1 and Ydj1's opposing behaviors in condensate dispersal to understand how these J-domain proteins work.

With the methods, reagents, and systems I established in my primary projects, I have also been positioned to make research contributions in several other areas. These other projects and collaborations are each distinct but unified by the broader goal of understanding how molecules in cells respond to physiological signals such as heat shock. They also expand the scope and impact of my primary research and offers exciting potential avenues for continued investigation.

4.1 Novel Technology for Multiplexed Biomolecule Detection

A major challenge in single-molecule imaging, as well as microscopy as a larger field, is how to investigate multiple molecular species at the same time. For example, chaperone-mediated dispersal of condensates—which in some ways, relative to other biological processes, is a well-behaved biochemical process of few components—involves the coordinated action of at least three chaperones (Sis1, Hsp70, and Hsp104) on a heterogeneous substrate composed of many molecules. To see all the molecular actors at once would require tracking at least four different species, which is to say four distinct imaging colors or channels.

Four-color imaging is possible with advanced conventional fluorescence microscopy, but further multiplexing runs into the problem of spectral overlap (i.e., the inability to determine if a particular photon originated from Species A or Species B, due to the overlap in the fluorescence emission of A and B). Surmounting this barrier has been the focus of ongoing research in the

single-molecule field, as well as in the Squires laboratory. A recent project in our lab, spearheaded by Drs. Jiachong Chu and Ayesha Ejaz, established a new technology to enable dozens of different biomolecular species to be identified in a single sample. This FRETfluor technology, described in Chu, Ejaz et al., requires only two fluorescence channels but uses Förster resonance energy transfer (FRET) and the precise arrangement and local environments of fluorophores on a DNA backbone to create many distinct spectroscopic signals.[95]

Given my work on purified protein systems and methods for protein labeling, I took on a role in this project to achieve proof-of-concept attachment of FRETfluors to biomolecular targets of interest. If we succeeded in this aim, we would open doors to a wide range of future applications, where FRETfluors could be deployed to study complex biological processes involving many actors or entities of highly heterogeneous and diverse composition (such as biomolecular condensates).

After experimenting with various samples and conditions, we accomplished this goal. I produced two classes of molecular targets for FRETfluors. Since a potential use of FRETfluors is to study mRNA transcripts and genetic targets, I generated a panel of 15 reverse-transcribed DNA targets amplified from the yeast transcriptome, selected from the most abundant mRNAs (Figure 4.1, A).[96] These genetic targets were successfully labeled via complementary base pairing.[95] I also used two of my single-accessible-cysteine protein mutants, Pab1 C70A C119A C368A A577C and Ydj1 C29A C370F, to pilot FRETfluor labeling of proteins. Our approach was to link a FRETfluor to a protein via a difunctionalized linker that had an NHS ester group and maleimide group (two chemical groups which react with free amines and cysteines, respectively, under appropriate chemical conditions). By reacting the FRETfluor with the NHS ester group and then reacting the protein with the maleimide of the linker, we could label a protein with a FRETfluor at a specific residue. I developed the biochemical conditions for this procedure, which contained three main

steps: FRETfluor-linker reaction, protein-linker reaction, and gel electrophoresis and extraction. The successful labeling of Pab1 and Ydj1 prior to gel extraction is shown in Figure 4.1, B.

This work is published in Chu, Ejaz et al., on which I am the author following the two co-first authors.[95] The FRETfluor technology continues to be an area of active investigation in the Squires laboratory, including using FRETfluor labeling of proteins for new biological studies and assay development.

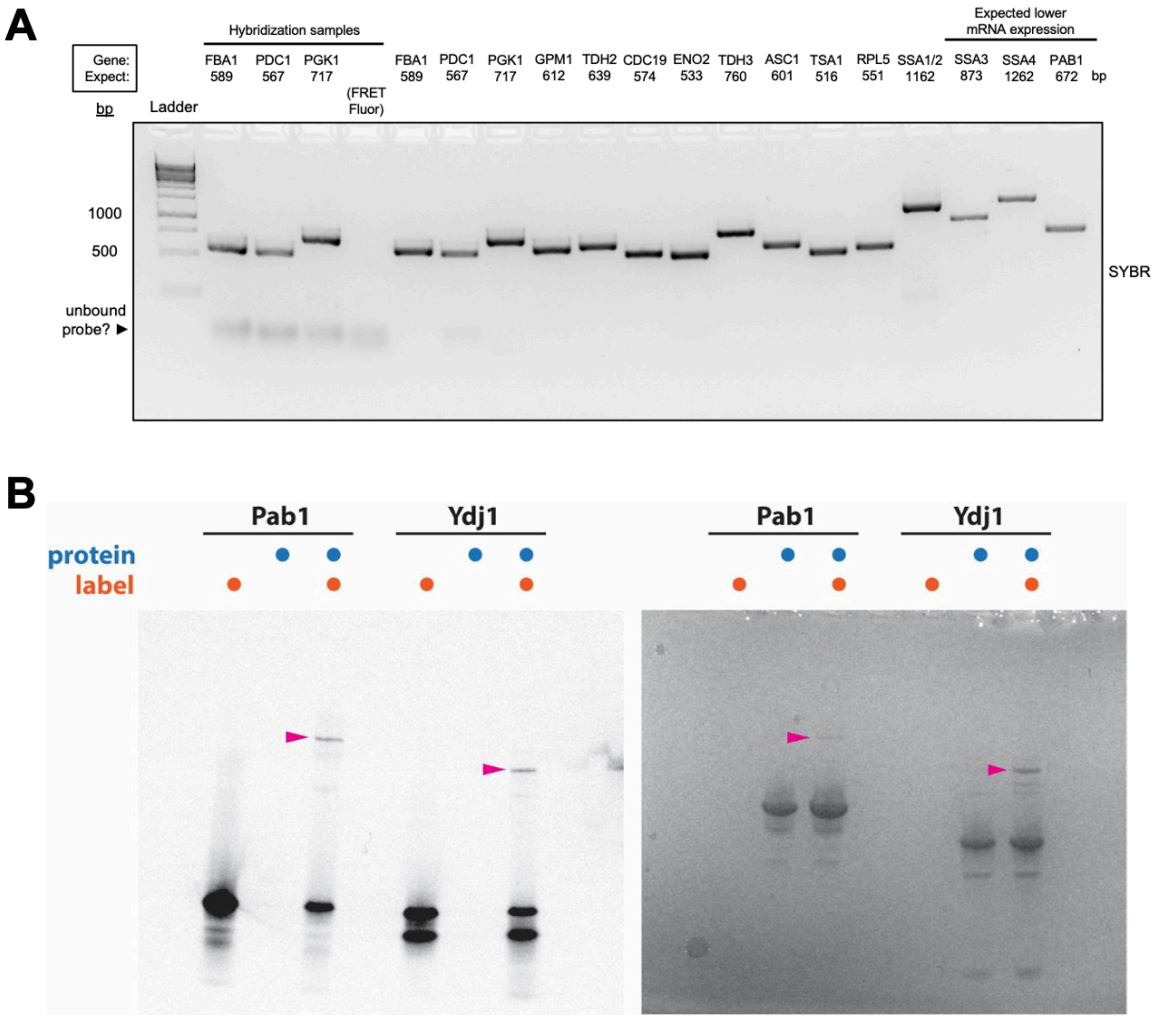

Figure 4.1, Molecular targets for FRETfluor labeling.

(A) Reverse transcriptase-PCR amplicons of 15 different transcript targets from yeast RNA. (B) SDS-PAGE gel on free FRETfluor, free protein, and the labeling reaction pre-gel extraction. Pink arrows indicate labeled product. Left image, red fluorescence; right image, whilte light image post-Coomassie stain. Panel B adapted from Chu, Ejaz et al.[95]

4.2 Visualizing Differential Condensation of Pab1 from Different Organisms

My main research focused on the dispersal of Pab1 condensates from the model organism *Saccharomyces cerevisiae*. From this research, we hoped to understand not only the budding yeast condensate dispersal process, but also to learn more general principles about chaperone action and condensate properties. Biomolecular condensation during stress, and specifically the condensation of Pab1, is a conserved response across many organisms. In the Drummond laboratory, a recent effort led by Dr. Samantha Keyport Kik shed light on the conservation of Pab1 condensation across three yeast species evolved to grow in different thermal environments.[66] This work demonstrated that Pab1 from different species condensed at different temperatures, tuned to the optimal growth temperatures of that organism.

My contribution to this project was to visualize directly the condensation of these proteins. I fluorescently labeled Pab1 from each species. Then, using an advanced on-stage heating device (VAHEAT, Interherence) and the microscope I designed and built, I performed temperature ramp experiments to reveal when each protein microscopically condensed. As expected, Pab1 from the three species condensed based on the species' preferred temperature regime and consistently with the biochemical findings (Figure 4.2). Condensation was drastic and nearly immediate, as the diffuse fluorescence signal clustered into bright objects within seconds (as expected for a phase separation process). The morphology of condensates (branched chains of clusters) was also similar and consistent with previous studies of *Saccharomyces cerevisiae* Pab1. From my microscopy, we gained a new window into what condensation of a well-established condensing protein looks like from different organisms adapted to different thermal environments, and how the qualities of this

molecular response might be conserved across species. This work is published in Keyport Kik et al., on which I am an author.[66]

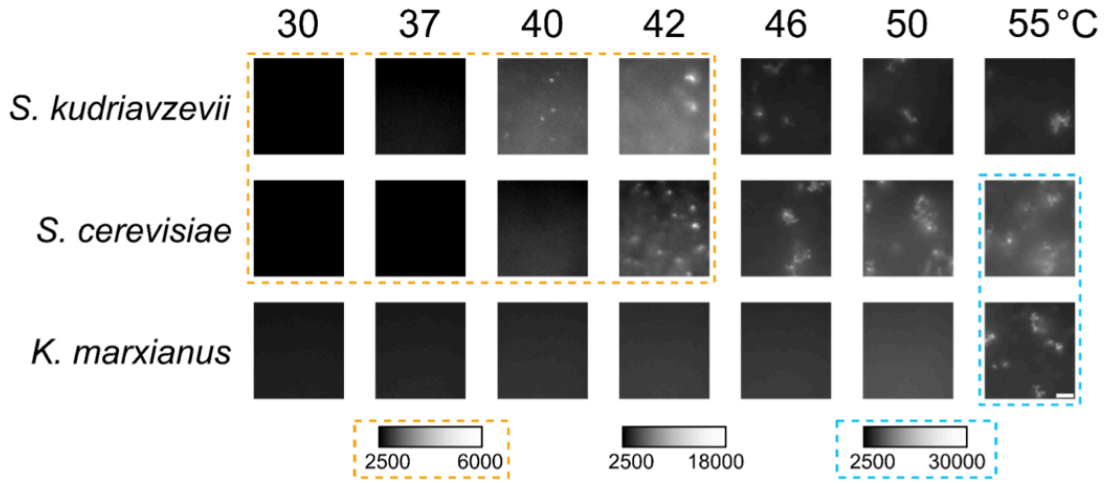

Figure 4.2, Imaging condensation of Pab1 from different species.

Adapted from Keyport Kik et al.[66] Fluorescently labeled Pab1 (10 μM total, 2% labeled) was held at 30 °C for four minutes, then incrementally heated to each higher temperature, using a VAHEAT on-stage heating device (Interherence). Three brightness scalings are shown to visualize condensates across the different conditions. Scale bar, 5 μm.

4.3 Human Chaperones and Human Cell Responses to Fever

Beyond fungal species, human and mammalian cells also have both protein condensation in response to stress and heat shock and the dispersal of those condensates during cellular recovery. We have gained considerable insight into the yeast system—the identities of proteins that condense at different severities of heat shock, and even the biochemical reconstitution of a particular model protein condensate (Pab1) and its dispersal—which does not exist in the human system.[47,56]

Although major advances have been made to understand mammalian condensate (stress granule) disassembly, whether mammalian chaperones directly disperse condensates induced by physiological stress has remained largely unsolved at a direct, biochemical level.[97–100] Mammalian cells lack Hsp104, which is required in the yeast system to achieve rapid Pab1 dispersal.[56] However, increasing evidence suggests that VCP/p97 (also an AAA+ protein) may fulfill an Hsp104-like disaggregation role in mammalian cells; also, Hsp104-independent disaggregation by chaperones (Hsp70, JDP, NEF) has been demonstrated in various systems.[53,56,57,72,77,99–103]

Using constructs generously provided by the laboratory of Bernd Bukau, I tested the ability of human Class B JDP and Hsp70 (single-accessible-cysteine mutants of DNAJB1 and HSPA8, which are homologs of yeast Sis1 and Ssa1/2) to substitute for yeast chaperones in yeast Pab1 dispersal.[72] Not only were DNAJB1 and HSPA8 highly active, but their activity was at least as robust as yeast Sis1 and Ssa2 (Figure 4.3, A). This experiment shows that human Hsp70 and Class B JDP can in principle act in the necessary ways to catalyze efficient condensate dispersal.

Whether and how human Hsp70 directly recognizes human condensates as substrates is an important scientific question, not just to understand how chaperones function, but also potentially to elucidate how cells sense and transduce elevated temperature. Immune cells respond to fever, a

self-induced physiological temperature signal, in part by activating the well-conserved heat shock response (upregulation of genes encoding chaperones).[39,40,104–109] The heat shock response is driven by Hsf1, which is basally repressed by Hsp70 and becomes active upon titration of Hsp70 to other substrates.[110–112] In the case of heat shock, what are these novel substrates which arise? In yeast, we now appreciate that condensed proteins, such as Pab1, are direct Hsp70 substrates induced by heat shock. Given the conservation of condensation responses and the heat shock response across organisms, we might predict that condensates to be molecular transducers of elevated temperature in human cells via recruitment of Hsp70 (Figure 4.3, B). Such hypothetical, fever-induced condensates have not been identified.

Moreover, the transcriptional responses of different human cell types to fever—which immune and/or non-immune cells sense fever and respond transcriptionally, with the heat shock response or other programs—has not been widely and systematically profiled. Testing how cells respond transcriptionally to fever (and to what degree they induce an Hsf1 heat shock response) would provide novel insight in human cell biology, as well as hint at whether an Hsp70 substrate-generating process such as protein condensation may be occurring in those cells.

In collaboration with Dr. Jared Bard and Joshua Melamed, I investigated transcriptional responses to fever temperature and chemical signaling in human cell lines. The monocytic immune cell line THP-1 induced a robust heat shock response in response to fever temperatures, consistent with the idea of immune cell fever sensing (Figure 4.3, C). Based on this result, we expanded our investigation to multiple cell lines and conditions. RNA degradation was an issue in many samples, but we proceeded with qPCR to identify the transcriptional effects of fever and lipopolysaccharide (LPS) treatment on cells (Figure 4.3, D). We observed that all cell lines induced the expression of Hsp70 (HSPA1A) in response to fever and independently induced the expression of IL-1β in

response to LPS (Figure 4.4). Confident in the validation of our cell treatments, I submitted RNA samples for sequencing. Once these data are analyzed, they may be a useful resource of human cell transcriptional responses to thermal (fever) and biochemical signals.

Even with our preliminary qPCR findings, we have observed that multiple cell types induce a heat shock response at fever temperature. We therefore hypothesize that in those cells, new Hsp70 substrates are emerging during fever, which may be protein condensates. An exciting area of future research is to profile condensation in these human cell lines at fever versus normal temperature. Protein condensation has been successfully profiled by sedimentation or filtration in yeast, cyanobacteria, *Xenopus* oocytes, and even mammalian cells.[47,113–115] Conducting such a study on human cells at fever temperature has the potential to unveil previously-unappreciated, physiological Hsp70 substrates involved in the transduction of temperature as a biophysical signal.

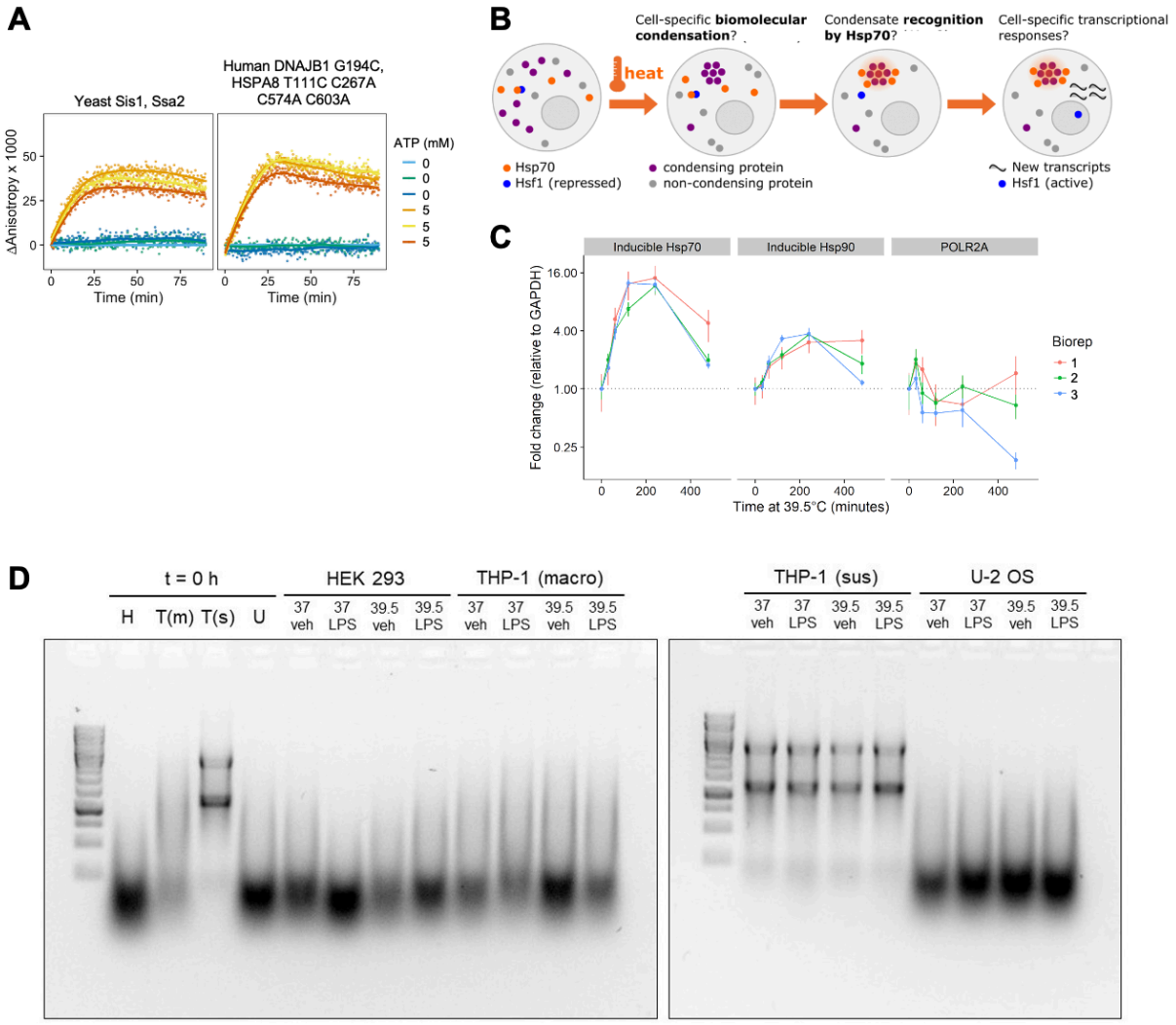

Figure 4.3, Human chaperones and cellular responses to heat shock.

(A) Yeast Pab1 condensate dispersal by yeast Hsp104 (100 nM), the indicated J-domain protein (0.5 μM dimer), and the indicated Hsp70 (1 μM). (B) Hypothetical model of how condensates could activate transcriptional responses (e.g., the Hsf1 heat shock response) in human cells during fever. (C) Expression of HSPA1A (inducible Hsp70), HSPC1 (inducible Hsp90), or RNA polymerase II subunit POLR2A, measured by qPCR, in THP-1 cells incubated at 39.5 °C at the specified timepoints. (D) Example of extracted RNA quality from different cell types.

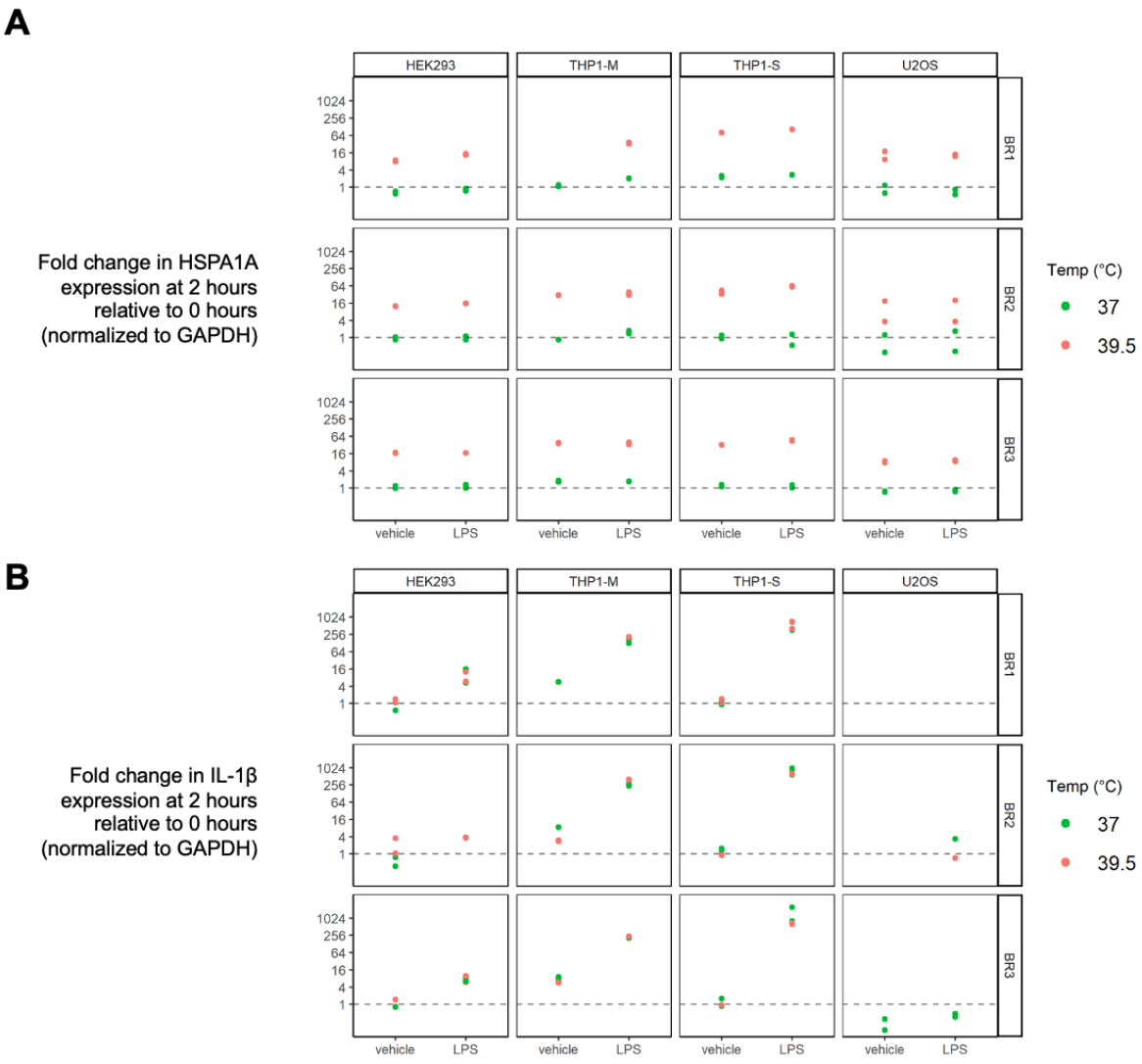

Figure 4.4, Transcriptional responses of human cells to fever.

HEK-293 cells, THP-1 cells differentiated into macrophages by phorbol 12-myristate 13-acetate treatment, THP-1 undifferentiated (suspension) cells, and U-2 OS cells were subjected to a 2 hour incubation at 37 °C or 39.5 °C with or without 100 ng/mL lipopolysaccharide (LPS) treatment. (A) Fold change in HSPA1A expression, measured by qPCR, normalized to GAPDH expression. (B) Fold change in IL-1β expression, measured by qPCR, normalized to GAPDH expression.

4.4 Conclusion

In this dissertation, I have made major advances in understanding both condensates and chaperones at the molecular scale. In my first research project, I provided new insight into the size and dispersal process of condensates with some of the first direct, single-molecule visualizations of their kind. In my second research project, I elucidated key features of the J-domain proteins Sis1 and Ydj1 which underlie their divergent behaviors in condensate dispersal, a process in which the molecular functions and specificities of J-domain proteins are not well understood. Finally, in my collaborations and other research, I have paved the way for new potential studies of biological systems (such as condensates and chaperones), by helping develop a technology for multiplexed molecular labeling and detection and by imaging condensates from different yeast species; and I have opened new areas of investigation into the actions of human chaperones on condensates and molecular-scale responses of human cells to fever and elevated temperature. This work helps build our scientific understanding of how cells respond to temperature at the molecular scale.

References

1. Davidson, S. C. *et al.* Ecological insights from three decades of animal movement tracking across a changing Arctic. *Science* **370**, 712–715 (2020).

2. Seebacher, F. Climate change impacts on animal migration. *Climate Change Responses* **2**, 1–2 (2015).

3. Yadlapalli, S. *et al.* Circadian clock neurons constantly monitor environmental temperature to set sleep timing. *Nature* **555**, 98–102 (2018).

4. Lahiri, K. *et al.* Temperature regulates transcription in the zebrafish circadian clock. *PLoS Biol.* **3**, e351 (2005).

5. Vallone, D. *et al.* Hypothermia modulates circadian clock gene expression in lizard peripheral tissues. *Am. J. Physiol. Regul. Integr. Comp. Physiol.* **292**, R160-6 (2007).

6. Brown, A. W. A. Factors in the attractiveness of bodies for mosquitoes. *Nature* **167**, 202 (1951).

7. Howlett, F. M. The Influence of Temperature upon the Biting of Mosquitoes. *Parasitology* **3**, 479–484 (1910).

8. Lockley, E. C. & Eizaguirre, C. Effects of global warming on species with temperature-dependent sex determination: Bridging the gap between empirical research and management. *Evol. Appl.* **14**, 2361–2377 (2021).

9. Haltenhof, T. *et al.* A Conserved Kinase-Based Body-Temperature Sensor Globally Controls Alternative Splicing and Gene Expression. *Mol. Cell* **78**, 57-69.e4 (2020).

10. Adams, O. A. *et al.* An unusually high upper thermal acclimation potential for rainbow trout. *Conserv Physiol* **10**, coab101 (2022).

11. FitzGerald, A. M. & Martin, B. T. Quantification of thermal impacts across freshwater life stages to improve temperature management for anadromous salmonids. *Conserv Physiol* **10**, coac013 (2022).

12. DuRant, S. E., Hopkins, W. A., Wilson, A. F. & Hepp, G. R. Incubation temperature affects the metabolic cost of thermoregulation in a young precocial bird. *Funct. Ecol.* **26**, 416–422 (2012).

13. Brewster, C. L., Sikes, R. S. & Gifford, M. E. Quantifying the cost of thermoregulation: thermal and energetic constraints on growth rates in hatchling lizards. *Funct. Ecol.* **27**, 490–497 (2013).

14. Ritossa, F. A new puffing pattern induced by temperature shock and DNP in drosophila. *Experientia* **18**, 571–573 (1962).

15. Ritossa, F. M. Experimental activation of specific loci in polytene chromosomes of Drosophila. *Exp. Cell Res.* **35**, 601–607 (1964).

16. Kluger, M. J., Kozak, W., Conn, C. A., Leon, L. R. & Soszynski, D. Role of fever in disease. *Ann. N. Y. Acad. Sci.* **856**, 224–233 (1998).

17. D'Alecy, L. G. & Kluger, M. J. Avian febrile response. *J. Physiol.* **253**, 223–232 (1975).

18. Hassan, I. A., Durdik, J. M., Satyajit, R., Renfro, Z. & Blake, H. Investigation on the role of temperature in macrophage responses. *The Journal of Immunology* **202**, 126.10-126.10 (2019).

19. Hassan, I. A., Renfro, Z., Blake, H., Rath, S. & Durdik, J. M. Effect of temperature on functional activity of macrophages in three different species. *The Journal of Immunology* **204**, 149.17-149.17 (2020).

20. Vaughn, L. K., Bernheim, H. A. & Kluger, M. J. Fever in the lizard Dipsosaurus dorsalis. *Nature* **252**, 473–474 (1974).

21. Bernheim, H. A. & Kluger, M. J. Fever: effect of drug-induced antipyresis on survival. *Science* **193**, 237–239 (1976).

22. Bernheim, H. A. & Kluger, M. J. Endogenous pyrogen-like substance produced by reptiles. *J. Physiol.* **267**, 659–666 (1977).

23. Myhre, K., Cabanac, M. & Myhre, G. Fever and behavioural temperature regulation in the frog Rana esculenta. *Acta Physiol. Scand.* **101**, 219–229 (1977).

24. Hutchison, V. H. & Erskine, D. J. Thermal Selection and Prostaglandin E_1 Fever in the Salamander Necturus maculosus. *Herpetologica* **37**, 195–198 (1981).

25. Covert, J. B. & Reynolds, W. W. Survival value of fever in fish. *Nature* **267**, 43–45 (1977).

26. Reynolds, W. W., Casterlin, M. E. & Covert, J. B. Behavioural fever in teleost fishes. *Nature* **259**, 41–42 (1976).

27. Gräns, A., Rosengren, M., Niklasson, L. & Axelsson, M. Behavioural fever boosts the inflammatory response in rainbow trout Oncorhynchus mykiss. *J. Fish Biol.* **81**, 1111–1117 (2012).

28. Boltaña, S. *et al.* Behavioural fever is a synergic signal amplifying the innate immune response. *Proc. Biol. Sci.* **280**, 20131381 (2013).

29. Rey, S., Moiche, V., Boltaña, S., Teles, M. & MacKenzie, S. Behavioural fever in zebrafish larvae. *Dev. Comp. Immunol.* **67**, 287–292 (2017).

30. Boltana, S. *et al.* Behavioral Fever Drives Epigenetic Modulation of the Immune Response in Fish. *Front. Immunol.* **9**, 1241 (2018).

31. Cabanac, M. & Le Guelte, L. Temperature regulation and prostaglandin E1 fever in scorpions. *J. Physiol.* **303**, 365–370 (1980).

32. Casadevall, A. Thermal Restriction as an Antimicrobial Function of Fever. *PLoS Pathog.* **12**, e1005577 (2016).

33. Tintó-Font, E. *et al.* A heat-shock response regulated by the PfAP2-HS transcription factor protects human malaria parasites from febrile temperatures. *Nat Microbiol* **6**, 1163–1174 (2021).

34. Muralidharan, V., Oksman, A., Pal, P., Lindquist, S. & Goldberg, D. E. Plasmodium falciparum heat shock protein 110 stabilizes the asparagine repeat-rich parasite proteome during malarial fevers. *Nat. Commun.* **3**, 1310 (2012).

35. Tintó-Font, E. & Cortés, A. Malaria parasites do respond to heat. *Trends Parasitol.* **38**, 435–449 (2022).

36. Kluger, M. J. & Vaughn, L. K. Fever and survival in rabbits infected with Pasteurella multocida. *J. Physiol.* **282**, 243–251 (1978).

37. Vaughn, L. K., Veale, W. L. & Cooper, K. E. Antipyresis: its effect on mortality rate of bacterially infected rabbits. *Brain Res. Bull.* **5**, 69–73 (1980).

38. Evans, S. S., Repasky, E. A. & Fisher, D. T. Fever and the thermal regulation of immunity: the immune system feels the heat. *Nat. Rev. Immunol.* **15**, 335–349 (2015).

39. Wang, X. *et al.* Febrile Temperature Critically Controls the Differentiation and Pathogenicity of T Helper 17 Cells. *Immunity* **52**, 328-341.e5 (2020).

40. Umar, D. *et al.* Febrile temperature change modulates CD4 T cell differentiation via a TRPV channel-regulated Notch-dependent pathway. *Proc. Natl. Acad. Sci. U. S. A.* **117**, 22357–22366 (2020).

41. O'Sullivan, D. *et al.* Fever supports CD8+ effector T cell responses by promoting mitochondrial translation. *Proc. Natl. Acad. Sci. U. S. A.* **118**, (2021).

42. Banani, S. F., Lee, H. O., Hyman, A. A. & Rosen, M. K. Biomolecular condensates: organizers of cellular biochemistry. *Nat. Rev. Mol. Cell Biol.* **18**, 285–298 (2017).

43. Cherkasov, V. *et al.* Coordination of translational control and protein homeostasis during severe heat stress. *Curr. Biol.* **23**, 2452–2462 (2013).

44. Kedersha, N. L., Gupta, M., Li, W., Miller, I. & Anderson, P. RNA-binding proteins TIA-1 and TIAR link the phosphorylation of eIF-2 alpha to the assembly of mammalian stress granules. *J. Cell Biol.* **147**, 1431–1442 (1999).

45. Riback, J. A. *et al.* Stress-Triggered Phase Separation Is an Adaptive, Evolutionarily Tuned Response. *Cell* **168**, 1028-1040.e19 (2017).

46. Chen, R. *et al.* HDX-MS finds that partial unfolding with sequential domain activation controls condensation of a cellular stress marker. *Proc. Natl. Acad. Sci. U. S. A.* **121**, e2321606121 (2024).

47. Wallace, E. W. J. *et al.* Reversible, Specific, Active Aggregates of Endogenous Proteins Assemble upon Heat Stress. *Cell* **162**, 1286–1298 (2015).

48. Mogk, A., Bukau, B. & Kampinga, H. H. Cellular Handling of Protein Aggregates by Disaggregation Machines. *Mol. Cell* **69**, 214–226 (2018).

49. Doyle, S. M., Genest, O. & Wickner, S. Protein rescue from aggregates by powerful molecular chaperone machines. *Nat. Rev. Mol. Cell Biol.* **14**, 617–629 (2013).

50. Saibil, H. Chaperone machines for protein folding, unfolding and disaggregation. *Nat. Rev. Mol. Cell Biol.* **14**, 630–642 (2013).

51. Walters, R. W., Muhlrad, D., Garcia, J. & Parker, R. Differential effects of Ydj1 and Sis1 on Hsp70-mediated clearance of stress granules in Saccharomyces cerevisiae. *RNA* **21**, 1660–1671 (2015).

52. Glover, J. R. & Lindquist, S. Hsp104, Hsp70, and Hsp40: a novel chaperone system that rescues previously aggregated proteins. *Cell* **94**, 73–82 (1998).

53. Nillegoda, N. B. *et al.* Evolution of an intricate J-protein network driving protein disaggregation in eukaryotes. *Elife* **6**, (2017).

54. Lu, Z. & Cyr, D. M. Protein Folding Activity of Hsp70 Is Modified Differentially by the Hsp40 Co-chaperones Sis1 and Ydj1 *. *J. Biol. Chem.* **273**, 27824–27830 (1998).

55. Clerico, E. M., Tilitsky, J. M., Meng, W. & Gierasch, L. M. How hsp70 molecular machines interact with their substrates to mediate diverse physiological functions. *J. Mol. Biol.* **427**, 1575–1588 (2015).

56. Yoo, H., Bard, J. A. M., Pilipenko, E. V. & Drummond, D. A. Chaperones directly and efficiently disperse stress-triggered biomolecular condensates. *Mol. Cell* **82**, 741-755.e11 (2022).

57. Nillegoda, N. B. *et al.* Crucial HSP70 co-chaperone complex unlocks metazoan protein disaggregation. *Nature* **524**, 247–251 (2015).

58. Keppler, A. *et al.* A general method for the covalent labeling of fusion proteins with small molecules in vivo. *Nat. Biotechnol.* **21**, 86–89 (2003).

59. Los, G. *et al.* Halotag interchangeable labeling technology for cell imaging and protein capture. *Cell Notes* (2005).

60. Yoo, H. & Drummond, D. A. Using fluorescence anisotropy to monitor chaperone dispersal of RNA-binding protein condensates. *STAR Protocols* **3**, 101409 (2022).

61. Ernst, O. & Zor, T. Linearization of the bradford protein assay. *J. Vis. Exp.* (2010) doi:10.3791/1918.

62. Gasteiger, E. *et al.* Protein identification and analysis tools on the ExPASy server. in *The Proteomics Protocols Handbook* 571–607 (Humana Press, Totowa, NJ, 2005). doi:10.1385/1-59259-890-0:571.

63. Paul, T. & Myong, S. Protocol for generation and regeneration of PEG-passivated slides for single-molecule measurements. *STAR Protoc* **3**, 101152 (2022).

64. Truong, C., Oudre, L. & Vayatis, N. Selective review of offline change point detection methods. *Signal Processing* **167**, 107299 (2020).

65. Yao, G. *et al.* PAB1 self-association precludes its binding to poly(A), thereby accelerating CCR4 deadenylation in vivo. *Mol. Cell. Biol.* **27**, 6243–6253 (2007).

66. Keyport Kik, S. *et al.* An adaptive biomolecular condensation response is conserved across environmentally divergent species. *Nat. Commun.* **15**, 3127 (2024).

67. Mühlhofer, M. *et al.* The heat shock response in yeast maintains protein homeostasis by chaperoning and replenishing proteins. *Cell Rep.* **29**, 4593-4607.e8 (2019).

68. Klinge, S., Voigts-Hoffmann, F., Leibundgut, M. & Ban, N. Atomic structures of the eukaryotic ribosome. *Trends Biochem. Sci.* **37**, 189–198 (2012).

69. Pietras, P. J. *et al.* Dynamic protein composition of Saccharomyces cerevisiae ribosomes in response to multiple stress conditions reflects alterations in translation activity. *Int. J. Biol. Macromol.* **268**, 132004 (2024).

70. Kaimal, J. M., Kandasamy, G., Gasser, F. & Andréasson, C. Coordinated Hsp110 and Hsp104 activities power protein disaggregation in Saccharomyces cerevisiae. *Mol. Cell. Biol.* **37**, e00027-17 (2017).

71. Sztangierska, W. *et al.* Early steps of protein disaggregation by Hsp70 chaperone and class B J-domain proteins are shaped by Hsp110. *Elife* **13**, (2024).

72. Wentink, A. S. *et al.* Molecular dissection of amyloid disaggregation by human HSP70. *Nature* **587**, 483–488 (2020).

73. Seyffer, F. *et al.* Hsp70 proteins bind Hsp100 regulatory M domains to activate AAA+ disaggregase at aggregate surfaces. *Nat. Struct. Mol. Biol.* **19**, 1347–1355 (2012).

74. Marzano, N. R., Paudel, B. P., van Oijen, A. M. & Ecroyd, H. Real-time single-molecule observation of chaperone-assisted protein folding. *Sci Adv* **8**, eadd0922 (2022).

75. Okuda, M., Niwa, T. & Taguchi, H. Single-molecule Analyses of the Dynamics of Heat Shock Protein 104 (Hsp104) and Protein Aggregates*. *J. Biol. Chem.* **290**, 7833–7840 (2015).

76. Ruger-Herreros, C., Svoboda, L., Mogk, A. & Bukau, B. Role of J-domain proteins in yeast physiology and protein quality control. *J. Mol. Biol.* 168484 (2024) doi:10.1016/j.jmb.2024.168484.

77. Faust, O. *et al.* HSP40 proteins use class-specific regulation to drive HSP70 functional diversity. *Nature* **587**, 489–494 (2020).

78. Wyszkowski, H. *et al.* Class-specific interactions between Sis1 J-domain protein and Hsp70 chaperone potentiate disaggregation of misfolded proteins. *Proc. Natl. Acad. Sci. U. S. A.* **118**, (2021).

79. Li, J., Wu, Y., Qian, X. & Sha, B. Crystal structure of yeast Sis1 peptide-binding fragment and Hsp70 Ssa1 C-terminal complex. *Biochem. J* **398**, 353–360 (2006).

80. Matos, C. O. *et al.* NMR studies on the structure of yeast Sis1 and the dynamics of its interaction with Ssa1-EEVD. *Molecules* **30**, 11 (2024).

81. Jiang, Y., Rossi, P. & Kalodimos, C. G. Structural basis for client recognition and activity of Hsp40 chaperones. *Science* **365**, 1313–1319 (2019).

82. Yu, H. Y. *et al.* Roles of intramolecular and intermolecular interactions in functional regulation of the Hsp70 J-protein co-chaperone Sis1. *J. Mol. Biol.* **427**, 1632–1643 (2015).

83. Kampinga, H. H. *et al.* Function, evolution, and structure of J-domain proteins. *Cell Stress Chaperones* **24**, 7–15 (2019).

84. Jarmoskaite, I., AlSadhan, I., Vaidyanathan, P. P. & Herschlag, D. How to measure and evaluate binding affinities. *Elife* **9**, (2020).

85. Mitchem, M. M., Shrader, C., Abedi, E. & Truman, A. W. Novel insights into the post-translational modifications of Ydj1/DNAJA1 co-chaperones. *Cell Stress Chaperones* **29**, 1–9 (2024).

86. Summers, D. W., Douglas, P. M., Ren, H.-Y. & Cyr, D. M. The Type I Hsp40 Ydj1 Utilizes a Farnesyl Moiety and Zinc Finger-like Region to Suppress Prion Toxicity*. *J. Biol. Chem.* **284**, 3628–3639 (2009).

87. Cho, H., Shim, W. J., Liu, Y. & Shan, S.-O. J-domain proteins promote client relay from Hsp70 during tail-anchored membrane protein targeting. *J. Biol. Chem.* **296**, 100546 (2021).

88. Li, J., Qian, X. & Sha, B. The crystal structure of the yeast Hsp40 Ydj1 complexed with its peptide substrate. *Structure* **11**, 1475–1483 (2003).

89. Sha, B., Lee, S. & Cyr, D. M. The crystal structure of the peptide-binding fragment from the yeast Hsp40 protein Sis1. *Structure* **8**, 799–807 (2000).

90. Klaips, C. L., Gropp, M. H. M., Hipp, M. S. & Hartl, F. U. Sis1 potentiates the stress response to protein aggregation and elevated temperature. *Nat. Commun.* **11**, 6271 (2020).

91. Schlecht, R. *et al.* Functional analysis of Hsp70 inhibitors. *PLoS One* **8**, e78443 (2013).

92. McCarty, J. S. & Walker, G. C. DnaK as a thermometer: threonine-199 is site of autophosphorylation and is critical for ATPase activity. *Proc. Natl. Acad. Sci. U. S. A.* **88**, 9513–9517 (1991).

93. Williamson, D. S. *et al.* Novel adenosine-derived inhibitors of 70 kDa heat shock protein, discovered through structure-based design. *J. Med. Chem.* **52**, 1510–1513 (2009).

94. Sakai, K. *et al.* Functional inhibition of heat shock protein 70 by VER-155008 suppresses pleural mesothelioma cell proliferation via an autophagy mechanism. *Thorac. Cancer* **12**, 491–503 (2021).

95. Chu, J. *et al.* Single-molecule fluorescence multiplexing by multi-parameter spectroscopic detection of nanostructured FRET labels. *Nat. Nanotechnol.* (2024) doi:10.1038/s41565-024-01672-8.

96. Csárdi, G., Franks, A., Choi, D. S., Airoldi, E. M. & Drummond, D. A. Accounting for experimental noise reveals that mRNA levels, amplified by post-transcriptional processes, largely determine steady-state protein levels in yeast. *PLoS Genet.* **11**, e1005206 (2015).

97. Gwon, Y. *et al.* Ubiquitination of G3BP1 mediates stress granule disassembly in a context-specific manner. *Science* **372**, eabf6548 (2021).

98. Maxwell, B. A. *et al.* Ubiquitination is essential for recovery of cellular activities after heat shock. *Science* **372**, eabc3593 (2021).

99. Saha, I. *et al.* The AAA+ chaperone VCP disaggregates Tau fibrils and generates aggregate seeds in a cellular system. *Nat. Commun.* **14**, 560 (2023).

100. Wang, B. *et al.* ULK1 and ULK2 Regulate Stress Granule Disassembly Through Phosphorylation and Activation of VCP/p97. *Mol. Cell* **74**, 742-757.e8 (2019).

101. Rampelt, H. *et al.* Metazoan Hsp70 machines use Hsp110 to power protein disaggregation: Disaggregation by animal Hsp110-Hsp70-Hsp40. *EMBO J.* **31**, 4221–4235 (2012).

102. Shorter, J. The mammalian disaggregase machinery: Hsp110 synergizes with Hsp70 and Hsp40 to catalyze protein disaggregation and reactivation in a cell-free system. *PLoS One* **6**, e26319 (2011).

103. Gao, X. *et al.* Human Hsp70 Disaggregase Reverses Parkinson's-Linked α-Synuclein Amyloid Fibrils. *Mol. Cell* **59**, 781–793 (2015).

104. Gothard, L. Q., Ruffner, M. E., Woodward, J. G., Park-Sarge, O.-K. & Sarge, K. D. Lowered temperature set point for activation of the cellular stress response in T-lymphocytes. *J. Biol. Chem.* **278**, 9322–9326 (2003).

105. Murapa, P., Gandhapudi, S., Skaggs, H. S., Sarge, K. D. & Woodward, J. G. Physiological fever temperature induces a protective stress response in T lymphocytes mediated by heat shock factor-1 (HSF1). *J. Immunol.* **179**, 8305–8312 (2007).

106. Pritchard, M. T., Li, Z. & Repasky, E. A. Nitric oxide production is regulated by fever-range thermal stimulation of murine macrophages. *J. Leukoc. Biol.* **78**, 630–638 (2005).

107. Tulapurkar, M. E., Ramarathnam, A., Hasday, J. D. & Singh, I. S. Bacterial lipopolysaccharide augments febrile-range hyperthermia-induced heat shock protein 70 expression and extracellular release in human THP1 cells. *PLoS One* **10**, e0118010 (2015).

108. Gupta, A. *et al.* Toll-like receptor agonists and febrile range hyperthermia synergize to induce heat shock protein 70 expression and extracellular release. *J. Biol. Chem.* **288**, 2756–2766 (2013).

109. Oehler, R. *et al.* Cell type-specific variations in the induction of hsp70 in human leukocytes by feverlike whole body hyperthermia. *Cell Stress Chaperones* **6**, 306–315 (2001).

110. Pincus, D. Regulation of Hsf1 and the Heat Shock Response. in *HSF1 and Molecular Chaperones in Biology and Cancer* (eds. Mendillo, M. L., Pincus, D. & Scherz-Shouval, R.) 41–50 (Springer International Publishing, Cham, 2020). doi:10.1007/978-3-030-40204-4_3.

111. Zheng, X. *et al.* Dynamic control of Hsf1 during heat shock by a chaperone switch and phosphorylation. *Elife* **5**, (2016).

112. Krakowiak, J. *et al.* Hsf1 and Hsp70 constitute a two-component feedback loop that regulates the yeast heat shock response. *Elife* **7**, (2018).

113. Pattanayak, G. K. *et al.* Daily Cycles of Reversible Protein Condensation in Cyanobacteria. *Cell Rep.* **32**, 108032 (2020).

114. Keber, F. C., Nguyen, T., Mariossi, A., Brangwynne, C. P. & Wühr, M. Evidence for widespread cytoplasmic structuring into mesoscale condensates. *Nat. Cell Biol.* **26**, 346–352 (2024).

115. Sui, X. *et al.* Widespread remodeling of proteome solubility in response to different protein homeostasis stresses. *Proc. Natl. Acad. Sci. U. S. A.* **117**, 2422–2431 (2020).